



ATLAS Note

ATL-COM-PHYS-2019-962

27th May 2021



Draft version 0.1

1

2 WZ + Heavy Flavor Production in pp collisions 3 at $\sqrt{s} = 13$ TeV

4

The ATLAS Collaboration¹, Aaron Webb^a, Peter Onyisi^a

5

^a*Univ. of Texas at Austin*

6

A measurement of the cross-section for production of WZ with an associated heavy flavor jet
7 is performed using 140 fb^{-1} of proton-proton collision data at $\sqrt{s} = 13$ TeV from the ATLAS
8 experiment at the LHC. A measurement of the fully leptonic decay mode, $WZ \rightarrow l\nu ll$, is
9 performed. The cross-section of $WZ + b$ and $WZ + \text{charm}$ in various fiducial regions is
10 measured.

11

© 2021 CERN for the benefit of the ATLAS Collaboration.

Reproduction of this article or parts of it is allowed as specified in the CC-BY-4.0 license.

12 **Contents**

13	1 Changes and outstanding items	4
14	1.1 Changelog	4
15	1.1.1 Changes relative to v8	4
16	1.1.2 Changes relative to v7	4
17	1.1.3 Changes relative to v5	5
18	1.1.4 Changes relative to v4	5
19	1.1.5 Changes relative to v3	5
20	1.1.6 Changes relative to v2	6
21	1.1.7 Changes relative to v1	6
22	1.2 Outstanding Items	6
23	2 Executive Summary	7
24	3 Data and Monte Carlo Samples	7
25	3.1 Data Samples	8
26	3.2 Monte Carlo Samples	8
27	4 Object Reconstruction	10
28	4.1 Trigger	10
29	4.2 Light leptons	11
30	4.3 Jets	12
31	4.4 B-tagged Jets	12
32	4.5 Missing transverse energy	13
33	4.6 Overlap removal	13
34	5 Event Selection and Signal Region Definitions	14
35	5.1 Event Preselection	14
36	5.2 Fit Regions	18
37	5.3 Non-Prompt Lepton Estimation	34
38	5.3.1 $t\bar{t}$ Validation	34
39	5.3.2 Z+jets Validation	37
40	6 tZ Separation Multivariate Analysis	41
41	6.1 Top Mass Reconstruction	42
42	6.2 tZ BDT	42
43	6.3 tZ Interference Studies	46
44	7 Systematic Uncertainties	48
45	8 Results	55
46	8.1 Fit Procedure	55
47	8.2 Results of the Simultaneous Fit	56
48	8.3 Inclusive 1+2 Jet Fit	67

49	8.4 Alternate tZ Inclusive Fit	71
50	8.4.1 tZ Inclusive Fit	71
51	8.4.2 Floating tZ	71
52	9 Conclusion	72
53	A Appendices	75
54	Appendices	75
55	A.1 Non-prompt lepton MVA	75
56	A.2 Non-prompt CR Modelling	77
57	A.3 DSID list	81

58 List of contributions

Aaron Webb	Main analyser. Responsible for ntuple production, fits, and note writing.
Peter Onyisi	Advisor to Aaron Webb. Analysis design and implementation strategy.

61 **1 Changes and outstanding items**

62 **1.1 Changelog**

63 This is version 9

64 **1.1.1 Changes relative to v8**

- 65 • Included more references to appendices in the text
- 66 • Expanded explanation of fiducial region definition
- 67 • Previous draft claimed that both standard and custom PLVs were used. Text is fixed to
68 state that a custom PLV is used for lepton iso, but standard lepton id is used
- 69 • Included plots of PLV output, included WPs used
- 70 • specified that non-prompt CR plots are post correction
- 71 • changed title of results section

72 **1.1.2 Changes relative to v7**

- 73 • Moved from LO to NLO tZ sample
- 74 • Add additional plots of Z+jets and ttbar CRs in Section ??
- 75 • Clarified CDI file used, MC ptag, PFlow jet algorithm
- 76 • Included overlap removal procedure
- 77 • Included details on PLV
- 78 • Added plots of missing tZ BDT input features for each fit region
- 79 • Changed reference on PLV to recent ttH/ttW note
- 80 • Included alternate fits with WZ+1-2 jet inclusive, tZ floating

81 **1.1.3 Changes relative to v5**

- 82 • added list of DSIDs to an appendix
 83 • included systematics on jet migrations
 84 • Updated results section to include simultaneous fit over 1-jet and 2-jet bins, describe
 85 unfolding procedure
 86 • Updated other sections to account for this change
 87 • Included info about migrations in Section 5.2

88 **1.1.4 Changes relative to v4**

- 89 • Fixed various typos, clarified wording
 90 • Expanded info about JER uncertainties, electron systematics, theory uncertainties
 91 • removed a table on lepton selection, included information in the text instead
 92 • Plotted lepton Pt Z and W for Zjet CR, rather than lep 1 and 2
 93 • fixed binning in kinematic plots
 94 • Included prefit and postfit yield tables
 95 • added signal modelling systematics
 96 • included alternate fit studies with tZ included in signal

97 **1.1.5 Changes relative to v3**

- 98 • Merged introduction into executive summary, including unblinding details and list of
 99 SRs/CRs used
 100 • listed ptag used (p4133), and release (AB 21.2.127)
 101 • Included table reftab:xsecUnc listing x-sec uncertainties used
 102 • Removed selection criteria listed in table ?? (QMisID, AmbiguityType) that were removed
 103 from the analysis
 104 • specified variable used to make truth jet flavor determination (HadronConeExclTruthLa-
 105 belIID)
 106 • fixed bug in MtLepMet calculation, updated selection/fits to account for this
 107 • Included plots of MtLepMet and PtZ, swapped lep 1 and 2 p_T plots for lep W and lep Z
 108 plots

- 109 • updated tZ BDT training to reduce overfitting, updated plots to include error bars, feature
110 importance
- 111 • updated table 3 to clarify selection, fix the tZ_BDT cut used
- 112 • replace a few broken ntuples which included large weight events
- 113 • include DL1r distribution for Z+jets and $t\bar{t}$ VRs
- 114 • Expanded section on fakes, included information on derived scale factors from VRs.
- 115 • Changed the kinematic plots to include $p_T(Z)$ and $m_T(W)$, list lepton p_T based on W and
116 Z candidates.

117 **1.1.6 Changes relative to v2**

- 118 • Added alternate VBS samples to include missing b-jet diagrams
- 119 • Included a section on tZ interference effects, ??.
- 120 • Updated to reflect changes for 2018, including the move to PFlow jets, DL1r, updated
121 trigger, and updated AnalysisBase version (now 21.2.127)
- 122 • Revised fit regions, using separate 1-jet and 2-jet fits, with all 2-j regions included
- 123 • updated plots for tZ BDT, added details about the model
- 124 • Included truth jet information

125 **1.1.7 Changes relative to v1**

- 126 • Added GRL list
- 127 • Fixed latex issue in line 92, typo in line 172
- 128 • Added tables ?? and ??, summarizing the event and object selection
- 129 • Added table ??, which includes the DSID of samples used
- 130 • Included reference to WZ inclusive paper in introduction

131 **1.2 Outstanding Items**

- 132 • Unblind, update plots and fits to include data
- 133 • Add cross-section, significance once unblinded

134 2 Executive Summary

135 The production of WZ in association with a heavy flavor jet represents an important background
 136 for many major analyses. This includes any process with leptons and b-jets in the final state,
 137 such as $t\bar{t}H$, $t\bar{t}W$, and $t\bar{t}Z$. While precise measurements have been made of WZ production
 138 [1], $WZ +$ heavy flavor remains poorly understood. This is largely because the QCD processes
 139 involved in the production of the b-jet make it difficult to simulate accurately. This introduces a
 140 large uncertainty for analyses that include this process as a background.

141 Motivated by its relevance to the $t\bar{t}H$ multilepton analysis, we perform a study of the fully
 142 leptonic decay mode of this channel; that is, events where both the W and Z decay leptonically.
 143 Because WZ has no associated jets at leading order, while the major backgrounds for this channel
 144 tend to have high jet multiplicity, events with more than two jets are rejected. This gives a final
 145 state signature of three leptons and one or two jets.

146 Events that meet this selection criteria are sorted into pseudo-continuous b-tagging regions based
 147 on the DL1r b-tag score of their associated jets. This is done to separate $WZ +$ b-jet events from
 148 $WZ +$ charm and $WZ +$ light jets. These regions are fit to data in order make a more accurate
 149 estimate of the contribution of $WZ +$ heavy-flavor, where heavy-flavor jets include b-jets and
 150 charm jets. The full Run-2 dataset collected by the ATLAS detector, representing 139 fb^{-1} of
 151 data from pp collisions at $\sqrt{s} = 13 \text{ TeV}$, is used for this study.

152 Section 3 details the data and Monte Carlo (MC) samples used in the analysis. The reconstruction
 153 of various physics objects is described in Section 4. Section 7 describes the event selection applied
 154 to these samples, along with the definitions of the various regions used in the fit. The multivariate
 155 analysis techniques used to separate the tZ background from $WZ +$ heavy flavor are described in
 156 Section 5. Section 8 describes the various sources of systematic uncertainties considered in the
 157 fit. Finally, the results of the analysis are summarized in Section 9, followed by a brief conclusion
 158 in Section 10.

159 **The current state of the analysis shows blinded results for the full Run-2 dataset. Regions
 160 containing >5% $WZ+b$ events are blinded, and results are from Asimov, MC only fits.**

161 3 Data and Monte Carlo Samples

162 Both data and Monte Carlo samples used in this analysis were prepared in the xAOD format,
 163 which was used to produce a Dx AOD sample in the HIGG8D1 derivation framework. The HIGG8D1
 164 framework is designed for the $t\bar{t}H$ multi-lepton analysis, which targets events with multiple
 165 leptons as well as tau hadrons. This framework skims the dataset to remove unneeded variables
 166 as well as entire events. Events are removed from the derivations that do not meet one of the
 167 following selections:

- 168 • at least two light leptons within a range $|\eta| < 2.6$, with leading lepton $p_T > 15 \text{ GeV}$ and
 169 subleading lepton $p_T > 5 \text{ GeV}$

- 170 • OR at least one light lepton with $p_T > 15$ GeV within a range $|\eta| < 2.6$, and at least two
 171 hadronic taus with $p_T > 15$ GeV.

172 Samples were then generated from these HIGG8D1 derivations with p-tag of p4134 for data
 173 and p4133 for Monte Carlo using AnalysisBase version 21.2.127 modified to include custom
 174 variables.

175 3.1 Data Samples

176 The study uses a sample of proton-proton collision data collected by the ATLAS detector from
 177 2015 through 2018 at an energy of $\sqrt{s} = 13$ TeV, which represents an integrated luminosity of
 178 139 fb^{-1} [2]. This data set was collected with a bunch crossing rate of 25 ns. All data used in
 179 this analysis was verified by data quality checks [3], having been included in the following Good
 180 Run Lists:

- 181 • data15_13TeV.periodAllYear_DetStatus-v79-repro20-02_DQDefects-00-02-02
 182 _PHYS_StandardGRL_All_Good_25ns.xml
- 183 • data16_13TeV.periodAllYear_DetStatus-v88-pro20-21_DQDefects-00-02-04
 184 _PHYS_StandardGRL_All_Good_25ns.xml
- 185 • data17_13TeV.periodAllYear_DetStatus-v97-pro21-13_Unknown_PHYS_StandardGRL
 186 _All_Good_25ns_Triggerno17e33prim.xml
- 187 • data18_13TeV.periodAllYear_DetStatus-v102-pro22-04_Unknown_PHYS_StandardGRL
 188 _All_Good_25ns_Triggerno17e33prim.xml

189 Runs included from the AllYear period containers are included.

190 3.2 Monte Carlo Samples

191 Several different generators were used to produce Monte Carlo simulations of the signal and
 192 background processes. For all samples, the response of the ATLAS detector is simulated using
 193 GEANT4 [4]. The WZ signal samples are simulated using Sherpa 2.2.2 [5]. Signal events are
 194 generated using NNPDF30NNLO PDF set with up to one parton at NLO and 2 to 3 partons at
 195 LO [**Butterworth:2015oua**].

196 The tZ background is simulated at NLO with **MADGRAPH5_AMC@NLO**, with **PYTHIA8** used to
 197 perform parton showering and fragmentation. The NNPDF30NNLO PDF set is used.

198 Specific information about the Monte Carlo samples being used can be found in Table 1. A list
 199 of the specific samples used by data set ID is shown in Table ??.

Table 1: The configurations used for event generation of signal and background processes, including the event generator, matrix element (ME) order, parton shower algorithm, and parton distribution function (PDF).

Process	Event generator	ME order	Parton Shower	PDF
WZ, VV	SHERPA 2.2.2	MEPS NLO	SHERPA	CT10 [6]
tZ	MG5_AMC [7]	NLO	PYTHIA 8	CTEQ6L1
t̄W	MG5_AMC (SHERPA 2.1.1)	NLO (LO multileg)	PYTHIA 8 (SHERPA)	NNPDF 3.0 NLO (NNPDF 3.0 NLO)
t̄(Z/γ* → ll)	MG5_AMC	NLO	PYTHIA 8	NNPDF 3.0 NLO
t̄H	MG5_AMC (MG5_AMC)	NLO (NLO)	PYTHIA 8 (HERWIG++) [9]	NNPDF 3.0 NLO [8] (CT10 [6])
tHqb	MG5_AMC	LO	PYTHIA 8	CT10
tHW	MG5_AMC (SHERPA 2.1.1)	NLO (LO multileg)	HERWIG++ (SHERPA)	CT10 (NNPDF 3.0 NLO)
tWZ	MG5_AMC	NLO	PYTHIA 8	NNPDF 2.3 LO
t̄t, t̄t̄t̄	MG5_AMC	LO	PYTHIA 8	NNPDF 2.3 LO [10]
t̄tW+W-	MG5_AMC	LO	PYTHIA 8	NNPDF 2.3 LO
t̄t	POWHEG-BOX v2 [11]	NLO	PYTHIA 8	NNPDF 3.0 NLO
t̄t̄γ	MG5_AMC	LO	PYTHIA 8	NNPDF 2.3 LO
s-, t-channel, Wt single top	POWHEG-BOX v1 [12]	NLO	PYTHIA 6	CT10
qqVV, VVV Z → l+l-	SHERPA 2.2.1	MEPS NLO	SHERPA	NNPDF 3.0 NLO

Sample	DSID
WZ	364253, 364739-42
VV	364250, 364254, 364255, 363355-60, 364890
t̄W	410155
t̄Z	410156, 410157, 410218-20
low mass t̄Z	410276-8
Rare Top	410397, 410398, 410399
single Top	410658-9, 410644-5
three Top	304014
four Top	410080
t̄WW	410081
Z + jets	364100-41
low mass Z + jets	364198-215
W + jets	364156-97
Vγ	364500-35
tZ	412063-5
tW	410013-4
WtZ	410408
VVV	364242-9
VH	342284-5
WtH	341998
t̄tγ	410389
t̄t	410470
t̄tH	345873-5, 346343-5

Table 2: List of Monte Carlo samples by data set ID used in the analysis.

200 4 Object Reconstruction

201 All regions defined in this analysis share a common lepton, jet, and overall event preselection.
 202 The selection applied to each physics object is detailed here; the event preselection, and the
 203 selection used to define the various fit regions, is described in Section 7.

204 4.1 Trigger

205 Events are required to be selected by dilepton triggers, as summarized in Table ??.

Dilepton triggers (2015)	
$\mu\mu$ (asymm.)	HLT_mu18_mu8noL1
ee (symm.)	HLT_2e12_lhloose_L12EM10VH
$e\mu, \mu e$ (\sim symm.)	HLT_e17_lhloose_mu14
Dilepton triggers (2016)	
$\mu\mu$ (asymm.)	HLT_mu22_mu8noL1
ee (symm.)	HLT_2e17_lhvloose_nod0
$e\mu, \mu e$ (\sim symm.)	HLT_e17_lhloose_nod0_mu14
Dilepton triggers (2017)	
$\mu\mu$ (asymm.)	HLT_mu22_mu8noL1
ee (symm.)	HLT_2e24_lhvloose_nod0
$e\mu, \mu e$ (\sim symm.)	HLT_e17_lhloose_nod0_mu14
Dilepton triggers (2018)	
$\mu\mu$ (asymm.)	HLT_mu22_mu8noL1
ee (symm.)	HLT_2e24_lhvloose_nod0
$e\mu, \mu e$ (\sim symm.)	HLT_e17_lhloose_nod0_mu14

Table 3: List of lowest p_T -threshold, un-prescaled dilepton triggers used for 2015-2018 data taking.

206 4.2 Light leptons

207 Electron candidates are reconstructed from energy clusters in the electromagnetic calorimeter
 208 that are associated with charged particle tracks reconstructed in the inner detector [13]. Electron
 209 candidates are required to have $p_T > 10$ GeV and $|\eta_{\text{cluster}}| < 2.47$. Muon candidates are
 210 reconstructed by combining inner detector tracks with track segments or full tracks in the muon
 211 spectrometer [14]. Muon candidates are required to have $p_T > 10$ GeV and $|\eta| < 2.5$. Candidates
 212 in the transition region between different electromagnetic calorimeter components, $1.37 <$
 213 $|\eta_{\text{cluster}}| < 1.52$, are rejected. A multivariate likelihood discriminant combining shower shape
 214 and track information is used to distinguish real electrons from hadronic showers (fake electrons).
 215 To further reduce the non-prompt electron contribution, the track is required to be consistent
 216 with originating from the primary vertex; requirements are imposed on the transverse impact
 217 parameter significance ($|d_0|/\sigma_{d_0} < 5$) and the longitudinal impact parameter ($|\Delta z_0 \sin \theta_\ell| < 0.5$
 218 mm). Electron candidates are required to pass TightLH identification.

219 Muon candidates are reconstructed by combining inner detector tracks with track segments or
 220 full tracks in the muon spectrometer [14]. Muon candidates are required to have $p_T > 10$ GeV
 221 and $|\eta| < 2.5$. The longitudinal impact parameter is the same for both electrons and muons, while
 222 muons are required to pass a slightly tighter transverse impact parameter, $|d_0|/\sigma_{d_0} < 3$. Muons
 223 are also required to pass Medium ID requirements.

224 Leptons are additionally required to pass a non-prompt BDT selection developed by the $t\bar{t}H$
225 multilepton/ $t\bar{t}W$ analysis group. This BDT and the WPs used are summarized in Appendix ??,
226 and described in detail in [15]. Optimized working points and scale factors for this BDT are
227 taken from that analysis.

228 4.3 Jets

229 Jets are reconstructed from calibrated topological clusters built from energy deposits in the
230 calorimeters [16], using the anti- k_t algorithm with a radius parameter $R = 0.4$. Particle Flow,
231 or PFlow, jets are used in the analysis. Jets with energy contributions likely arising from noise
232 or detector effects are removed from consideration [17], and only jets satisfying $p_T > 25$ GeV
233 and $|\eta| < 2.5$ are used in this analysis. For jets with $p_T < 60$ GeV and $|\eta| < 2.4$, a jet-track
234 association algorithm is used to confirm that the jet originates from the selected primary vertex,
235 in order to reject jets arising from pileup collisions [18].

236 4.4 B-tagged Jets

237 In order to make a measurement of $WZ +$ heavy flavor it is necessary to distinguish these events
238 from $WZ +$ light jets. For this purpose, the DL1r b-tagging algorithm is used to distinguish
239 heavy flavor jets from lighter ones. The DL1r algorithm uses jet kinematics, particularly jet
240 vertex information, as input for a neural network which assigns each jet a score designed to
241 reflect how likely that jet is to have originated from a b-quark.

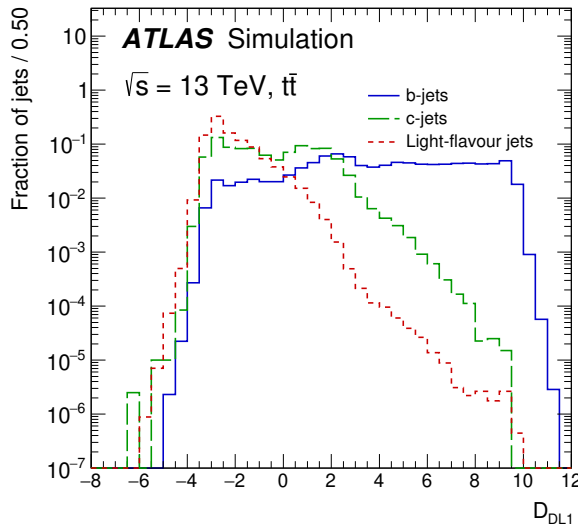


Figure 1: Output distribution of the DL1r algorithm for b-jets, charm jets, and light jets

242 From the output of the BDT, working points (WPs) are developed based on the efficiency of truth
 243 b-jets at particular values of the DL1r algorithm. These WPs are taken from the March 2020 CDI
 244 file, 2020-21-13TeV-MC16-CDI-2020-03-11_v2.root. The working points used in this analysis
 245 are summarized in Table 2.

WP	Rejection	
	b-jet eff.	c-jet
85%	2.6	29
77%	4.9	130
70%	9.4	390
60%	27	1300

Table 4: c-jet and light-flavor jet rejections corresponding to each b-tagging Working Point by b-jet efficiency, evaluated on $t\bar{t}$ events.

246 As shown in table 2, a tighter WP will accept fewer b-jets, but reject a higher fraction of charm
 247 and light jets. Generally, analyses that include b-jets will use a fixed working point, for example,
 248 requiring that a jet pass the 70% threshold. By instead treating these working point as bins, e.g.
 249 events with jets that fall between the 85% and 77% WPs fall into one bin, while events with jets
 250 passing the 60% WP fall into another, additional information can be gained. This analysis uses
 251 each of these working points to form orthogonal regions in order to provide separation between
 252 WZ + b, WZ + c, and WZ + light.

253 4.5 Missing transverse energy

254 Missing transverse momentum (E_T^{miss}) is used as part of the event selection. The missing
 255 transverse momentum vector is defined as the inverse of the sum of the transverse momenta of
 256 all reconstructed physics objects as well as remaining unclustered energy, the latter of which is
 257 estimated from low- p_T tracks associated with the primary vertex but not assigned to a hard object,
 258 with object definitions taken from [19]. Light leptons considered in the E_T^{miss} reconstruction are
 259 required to have $p_T > 10$ GeV, while jets are required to have $p_T > 20$ GeV.

260 4.6 Overlap removal

261 To avoid double counting objects and remove leptons originating from decays of hadrons, overlap
 262 removal is performed in the following order: any electron candidate within $\Delta R = 0.1$ of another
 263 electron candidate with higher p_T is removed; any electron candidate within $\Delta R = 0.1$ of a muon
 264 candidate is removed; any jet within $\Delta R = 0.3$ of an electron candidate is removed; if a muon
 265 candidate and a jet lie within $\Delta R = \min(0.4, 0.04 + 10[\text{GeV}] / p_T(\text{muon}))$ of each other, the jet
 266 is kept and the muon is removed.

267 This algorithm is applied to the preselected objects. The overlap removal procedure is summarized
 268 in Table ??.

Keep	Remove	Cone size (ΔR)
electron	electron (low p_T)	0.1
muon	electron	0.1
electron	jet	0.3
jet	muon	$\min(0.4, 0.04 + 10[\text{GeV}]/p_T(\text{muon}))$
electron	tau	0.2

Table 5: Summary of the overlap removal procedure between electrons, muons, and jets.

269 5 Event Selection and Signal Region Definitions

270 Event are required to pass a preselection described in Section 7.1 and summarized in Table ??.
 271 Those that pass this preselection are divided into various fit regions described in Section 7.2,
 272 based on the number of jets in the event, and the b-tag score of those jets.

273 5.1 Event Preselection

274 Events are required to include exactly three reconstructed light leptons passing the requirement
 275 described in ??, which have a total charge of ± 1 .

276 The leptons are ordered in the analysis code as 0, 1, and 2. Lepton 0 is the lepton whose charge
 277 is opposite the other two. Lepton 1 is the lepton closest to the opposite charge lepton, i.e. the
 278 smallest ΔR , leaving lepton 2 as the lepton further from the opposite charge lepton. Lepton 0
 279 is required to have $p_T > 10 \text{ GeV}$, while the same sign leptons, 1 and 2, are required to have
 280 $p_T > 20 \text{ GeV}$ to reduce the contribution of non-prompt leptons.

281 The invariant mass of at least one pair of opposite sign, same flavor leptons is required to fall
 282 within 10 GeV of the mass of the Z boson, 91.2 GeV. Events where one of the opposite sign pairs
 283 have an invariant mass less than 12 GeV are rejected in order to suppress low mass resonances.

284 An additional requirement is placed on the missing transverse energy, $E_T^{\text{miss}} > 20 \text{ GeV}$, and the
 285 transverse mass of the W candidate, $m(E_T^{\text{miss}} + l_{\text{other}}) > 30 \text{ GeV}$, defined as $\sqrt{2 p_T^{\text{lep}} E_T^{\text{miss}} * (1 - \cos(\phi_{\text{lep}} - \phi_{E_T^{\text{miss}}}))}$.
 286 Here E_T^{miss} is the missing transverse energy, and l_{other} is the lepton not included in the Z-
 287 candidate.

288 Events are required to have one or two reconstructed jets passing the selection described in
 289 Section ?? . Events with more than two jets are rejected in order to reduce the contribution of
 290 backgrounds such as $t\bar{t}Z$ and $t\bar{t}W$, which tend to have higher jet multiplicity.

Event Selection
Exactly three leptons with charge ± 1
Two same-charge leptons with $p_T > 20$ GeV
One opposite charge lepton with $p_T > 10$ GeV
$m(l^+l^-)$ within 10 GeV of 91.2 GeV
Transverse mass of W-candidate, $\sqrt{2p_T^{lep}E_T^{\text{miss}} * (1 - \cos(\phi_{lep} - \phi_{E_T^{\text{miss}}}))} > 30$ GeV
Missing transverse energy, $E_T^{\text{miss}} > 20$ GeV
One or two jets with $p_T > 25$ GeV

Table 6: Summary of the selection applied to events for inclusion in the fit

291 The event yields in the preselection region for both data and Monte Carlo are summarized in
 292 Table ??, which shows good agreement between data and Monte Carlo, and demonstrates that
 293 this region consists primarily of WZ events. The WZ events are split into WZ + b, WZ + c, and
 294 WZ + l based on the truth flavor of the associated jet in the event. Specifically, this determination
 295 is made based on the HadronConeExclTruthLabelID of the jet, as recommended by the b-
 296 tagging working group [20]. In this ordering b-jet supersedes charm, which supersedes light. That
 297 is, WZ + l events contain no charm and no b jets at truth level, WZ + c contain at least one truth
 298 charm and no b-jets, and WZ + b contains at least one truth b-jet.

Process	Events
WZ + b	167.6 ± 6.5
WZ + c	1080 ± 40
WZ + l	7220 ± 310
Other VV	850 ± 140
t̄tW	16.8 ± 2.3
t̄tZ	115 ± 17
rare Top	2.2 ± 0.1
Single top	0.10 ± 0.45
Three top	0.01 ± 0.01
Four top	0.02 ± 0.01
t̄tWW	0.23 ± 0.05
Z + jets	600 ± 260
V + γ	37 ± 54
tZ	190 ± 70
tW	5.5 ± 1.2
WtZ	25.8 ± 1.1
VVV	26.2 ± 0.9
VH	94 ± 7
t̄t	108.68 ± 8
t̄tH	4.3 ± 0.5
Total	10600 ± 530
Data	10574

Table 7: Event yields in the preselection region at 139.0 fb^{-1}

²⁹⁹ Here Other VV represents diboson processes other than WZ, and consists predominantly of
³⁰⁰ $ZZ \rightarrow ll\bar{l}\bar{l}$ events where one of the leptons is not reconstructed.

³⁰¹ Simulations are further validated by comparing the kinematic distributions of the Monte Carlo
³⁰² with data, which are shown in Figure ???. Here, bins with 5% or more WZ+b are blinded.

WZ Fit Region - Inclusive

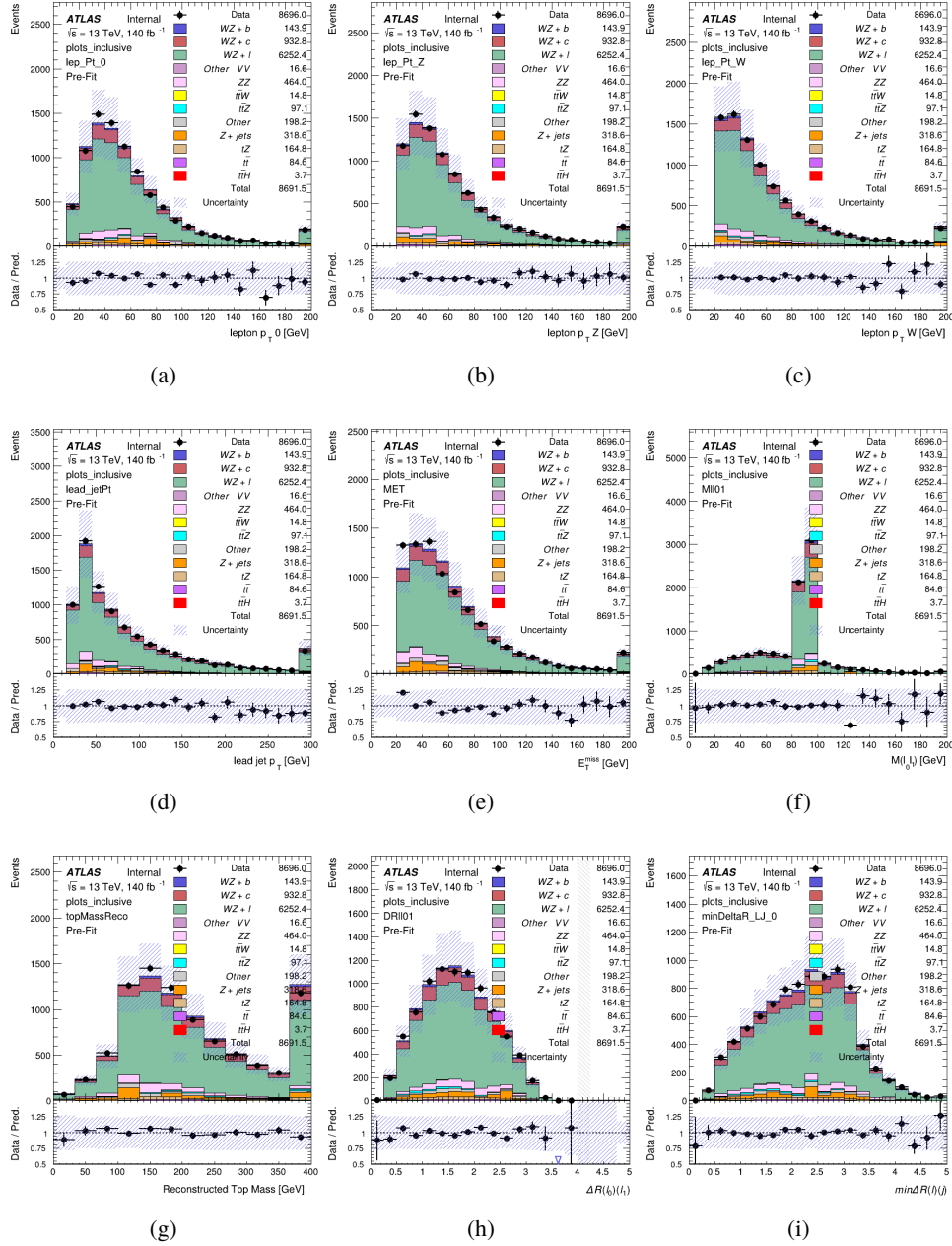


Figure 2: Comparisons between the data and MC distributions in the preselection region for (a) the p_T of the opposite sign lepton, (b) the p_T of the other lepton from the Z candidate, (c) the p_T of the lepton from the W candidate, (d) the leading jet p_T , (e) the E_T^{miss} , and (f) the invariant mass of leptons 0 and 1, (g) the reconstructed top mass, (h) $\Delta(R)$ between lepton 0 and 1, (i) the $\Delta(R)$ between the closest lepton and jet.

303 **5.2 Fit Regions**

304 Once preselection has been applied, the remaining events are categorized into one of twelve
 305 orthogonal regions. The regions used in the fit are summarized in Table 3.

Table 8: A list of the regions used in the fit and the selection used for each.

Region	Selection
1j, <85%	$N_{\text{jets}} = 1, n_{\text{Jets_DL1r_85}} = 0$
1j, 85%-77%	$N_{\text{jets}} = 1, n_{\text{Jets_DL1r_85}} = 1, n_{\text{Jets_DL1r_77}} = 0$
1j, 77%-70%	$N_{\text{jets}} = 1, n_{\text{Jets_DL1r_77}} = 1, n_{\text{Jets_DL1r_70}} = 0$
1j, 70%-60%	$N_{\text{jets}} = 1, n_{\text{Jets_DL1r_70}} = 1, n_{\text{Jets_DL1r_60}} = 0$
1j, >60%	$N_{\text{jets}} = 1, n_{\text{Jets_DL1r_60}} = 1, tZ \text{ BDT} > 0.12$
1j tZ CR	$N_{\text{jets}} = 1, n_{\text{Jets_DL1r_60}} = 1, tZ \text{ BDT} < 0.12$
2j, <85%	$N_{\text{jets}} = 2, n_{\text{Jets_DL1r_85}} = 0$
2j, 85%-77%	$N_{\text{jets}} = 2, n_{\text{Jets_DL1r_85}} \geq 1, n_{\text{Jets_DL1r_77}} = 0$
2j, 77%-70%	$N_{\text{jets}} = 2, n_{\text{Jets_DL1r_77}} \geq 1, n_{\text{Jets_DL1r_70}} = 0$
2j, 70%-60%	$N_{\text{jets}} = 2, n_{\text{Jets_DL1r_70}} \geq 1, n_{\text{Jets_DL1r_60}} = 0$
2j, >60%	$N_{\text{jets}} = 2, n_{\text{Jets_DL1r_60}} \geq 1, tZ \text{ BDT} > 0.12$
2j tZ CR	$N_{\text{jets}} = 2, n_{\text{Jets_DL1r_60}} \geq 1, tZ \text{ BDT} < 0.12$

306 The working points discussed in Section ?? are used to separate events into fit regions based on
 307 the highest working point reached by a jet in each event. Because the background composition
 308 differs significantly based on the number of b-jets, events are further subdivided into 1-jet and
 309 2-jet regions in order to minimize the impact of background uncertainties.

310 An unfolding procedure is performed to account for differences in the number of reconstructed
 311 jets compared to the number of truth jets in each event. The `AntiKt4TruthDressedWZJets`
 312 truth jet collection is used to make this determination. In order to account for migration of
 313 WZ+1-jet and WZ+2-jet events between the 1-jet and 2-jet bins at reco level, the signal samples
 314 are separated based on the number of truth jets. Events with 0 jets or more than 3 jets at truth
 315 level, yet fall within one of the categories listed in Table 3, are categorized as WZ + other, and
 316 treated as a background. The migration matrix in the number of jets at truth level versus reco
 317 level is shown in Figure ?? . The composition of the number of truth jets in each reco jet bin is
 318 taken from MC, with uncertainties in these estimates described in detail in Section 8.

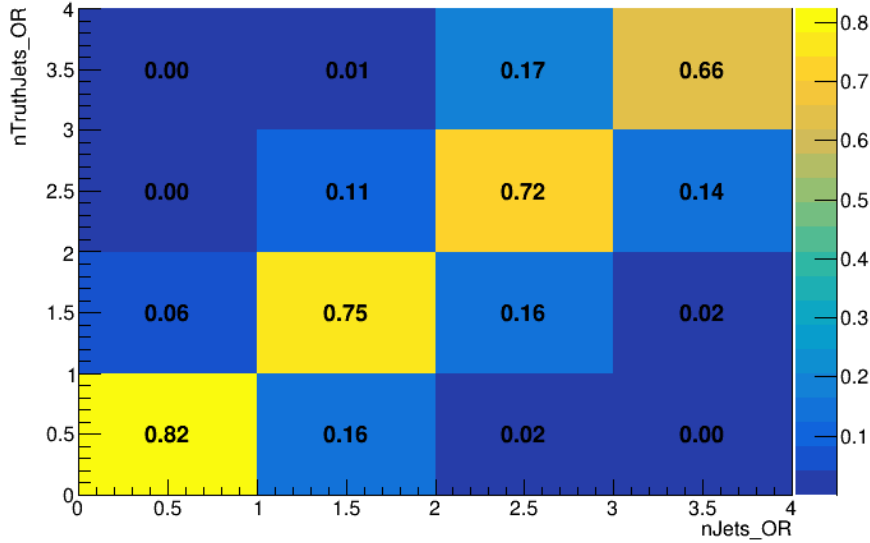


Figure 3: Number of truth jets compared to the number of reconstructed jets in each WZ event falling in the preselection region. Each row is normalized to unity.

319 An additional tZ control region is created based on the BDT described in Section 5. The region
 320 with 1-jet passing the 60% working point is split in two - a signal enriched region of events with
 321 a BDT score greater than 0.12, and a tZ control region including events with less than 0.12. This
 322 cutoff is arrived at by performing an Asimov fit with a variety of cutoffs, and selecting the value
 323 that produces the highest significance for the measurement of WZ + b.

324 The modeling in each region is validated by comparing data and MC predictions for various
 325 kinematic distributions. These plot are shown in Figures ??-??.

WZ Fit Region - 1j Inclusive

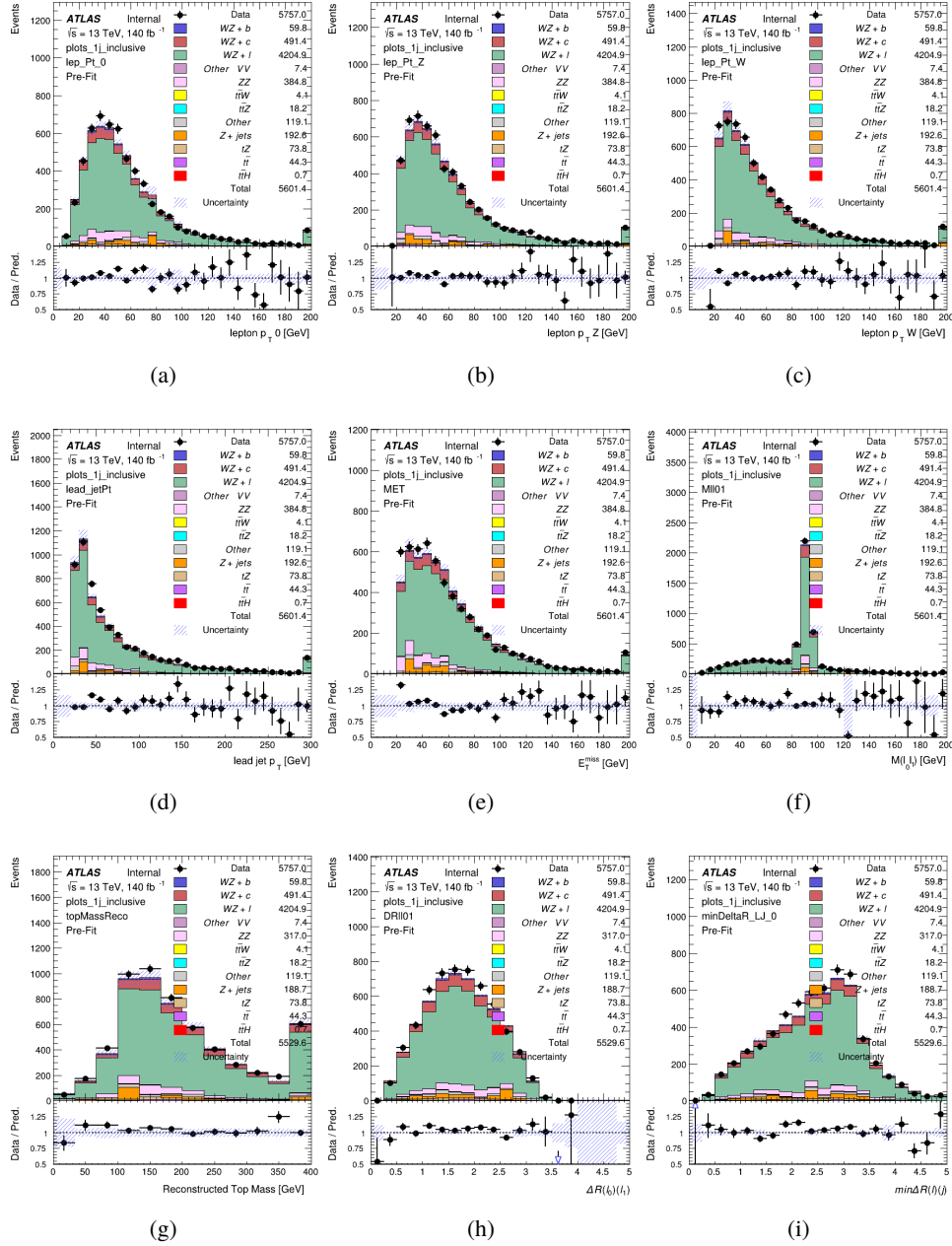


Figure 4: Comparisons between the data and MC distributions in the preselection region for (a) the p_T of the opposite sign lepton, (b) the p_T of the other lepton from the Z candidate, (c) the p_T of the lepton from the W candidate, (d) the leading jet p_T , (e) the E_T^{miss} , and (f) the invariant mass of leptons 0 and 1, (g) the reconstructed top mass, (h) $\Delta(R)$ between lepton 0 and 1, (i) the $\Delta(R)$ between the closest lepton and jet.

WZ Fit Region - 1j < 85% WP

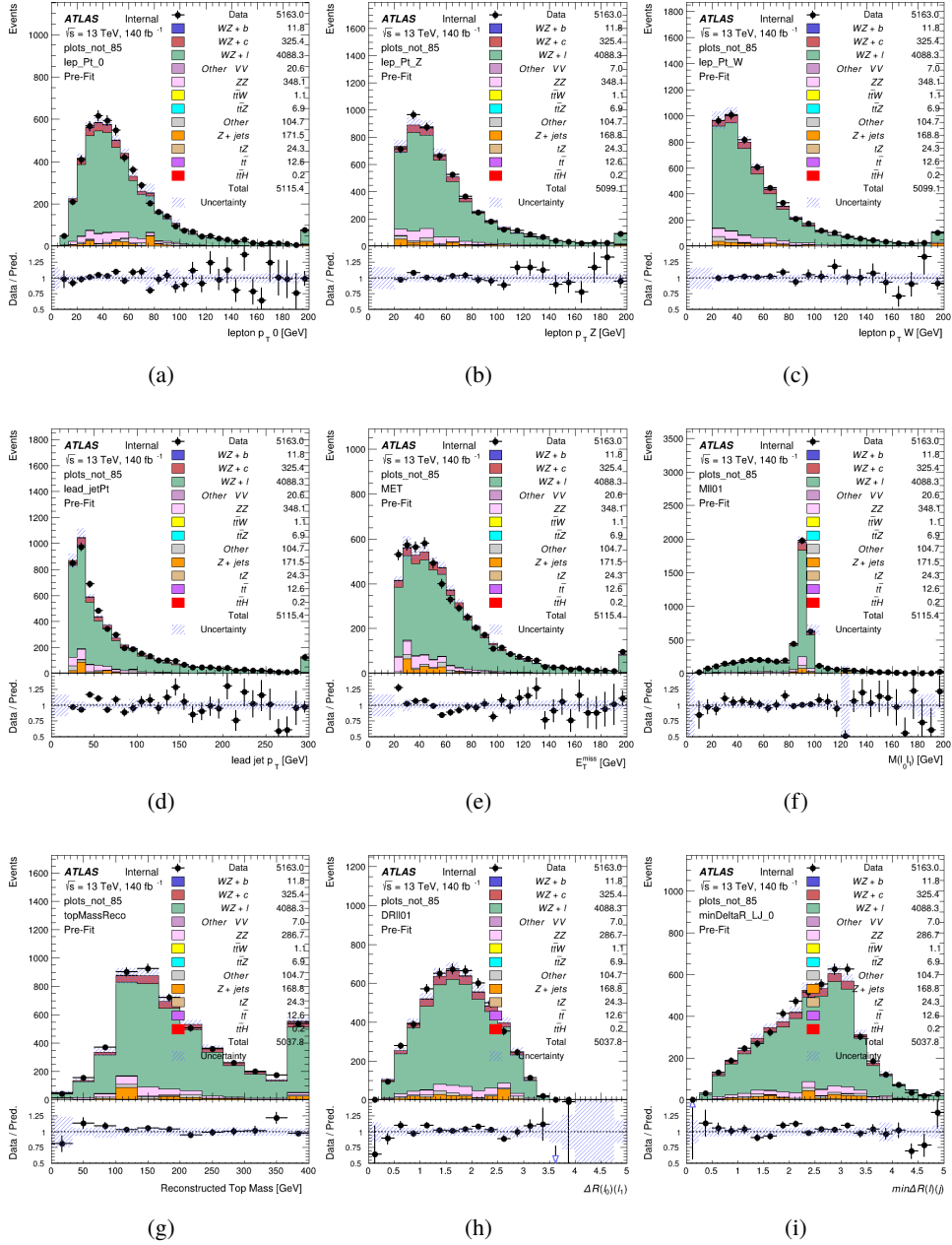


Figure 5: Comparisons between the data and MC distributions in the preselection region for (a) the p_T of the opposite sign lepton, (b) the p_T of the other lepton from the Z candidate, (c) the p_T of the lepton from the W candidate, (d) the leading jet p_T , (e) the E_T^{miss} , and (f) the invariant mass of leptons 0 and 1, (g) the reconstructed top mass, (h) $\Delta(R)$ between lepton 0 and 1, (i) the $\Delta(R)$ between the closest lepton and jet.

WZ Fit Region - 1j 77-85% WP

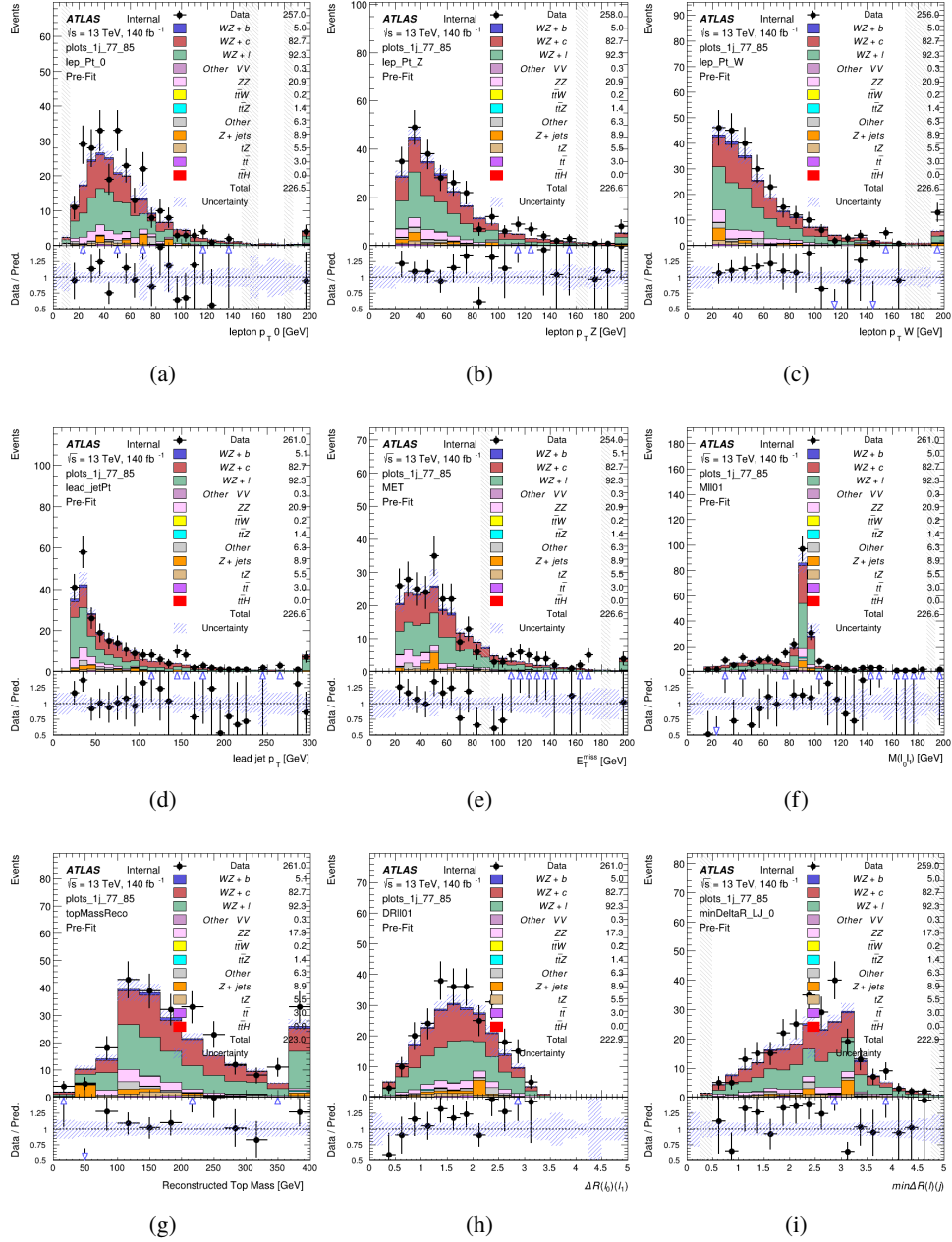


Figure 6: Comparisons between the data and MC distributions in the preselection region for (a) the p_T of the opposite sign lepton, (b) the p_T of the other lepton from the Z candidate, (c) the p_T of the lepton from the W candidate, (d) the leading jet p_T , (e) the E_T^{miss} , and (f) the invariant mass of leptons 0 and 1, (g) the reconstructed top mass, (h) $\Delta(R)$ between lepton 0 and 1, (i) the $\Delta(R)$ between the closest lepton and jet.

WZ Fit Region - 1j 70-77% WP

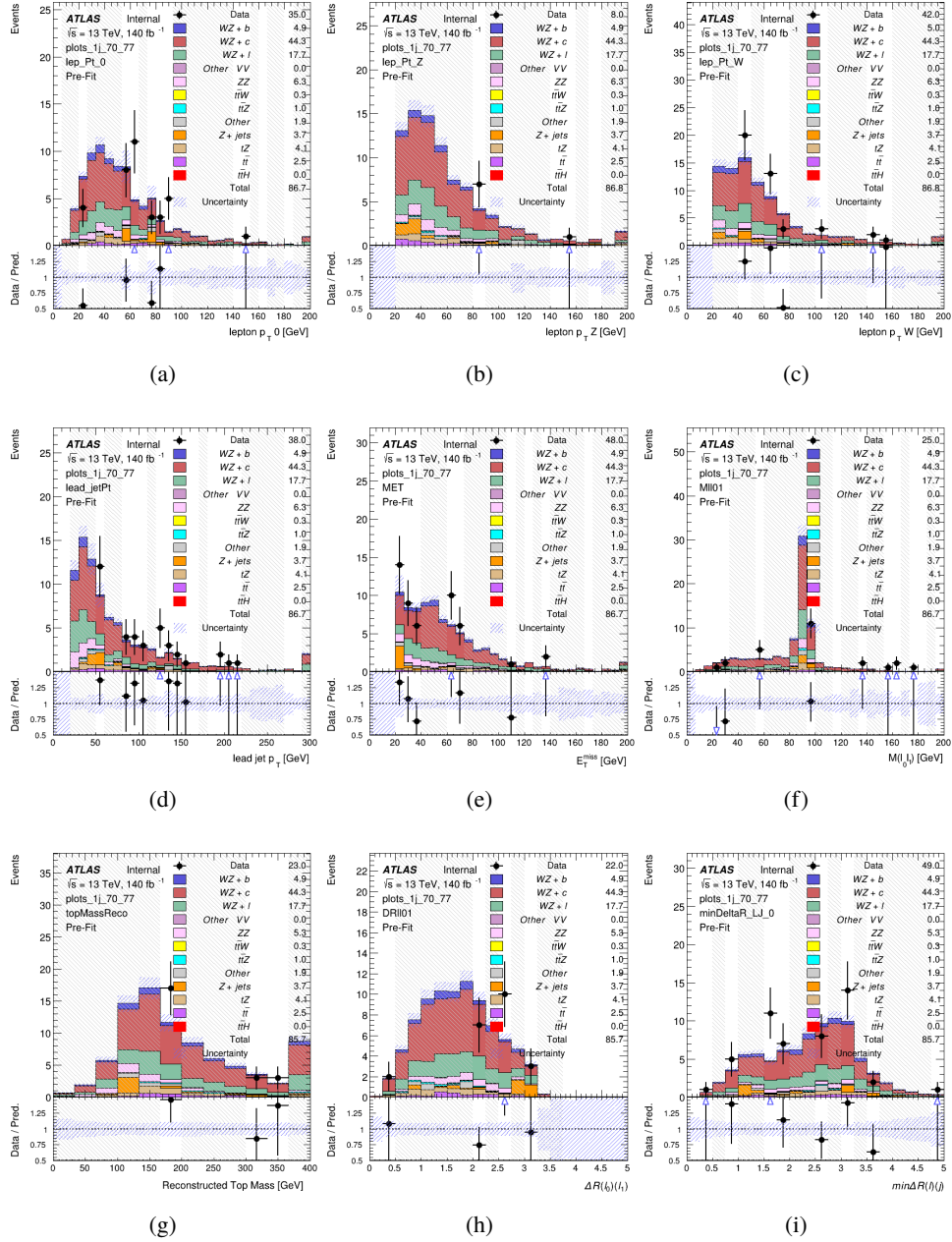


Figure 7: Comparisons between the data and MC distributions in the preselection region for (a) the p_T of the opposite sign lepton, (b) the p_T of the other lepton from the Z candidate, (c) the p_T of the lepton from the W candidate, (d) the leading jet p_T , (e) the E_T^{miss} , and (f) the invariant mass of leptons 0 and 1, (g) the reconstructed top mass, (h) $\Delta(R)$ between lepton 0 and 1, (i) the $\Delta(R)$ between the closest lepton and jet.

WZ Fit Region - 1j 60-70% WP

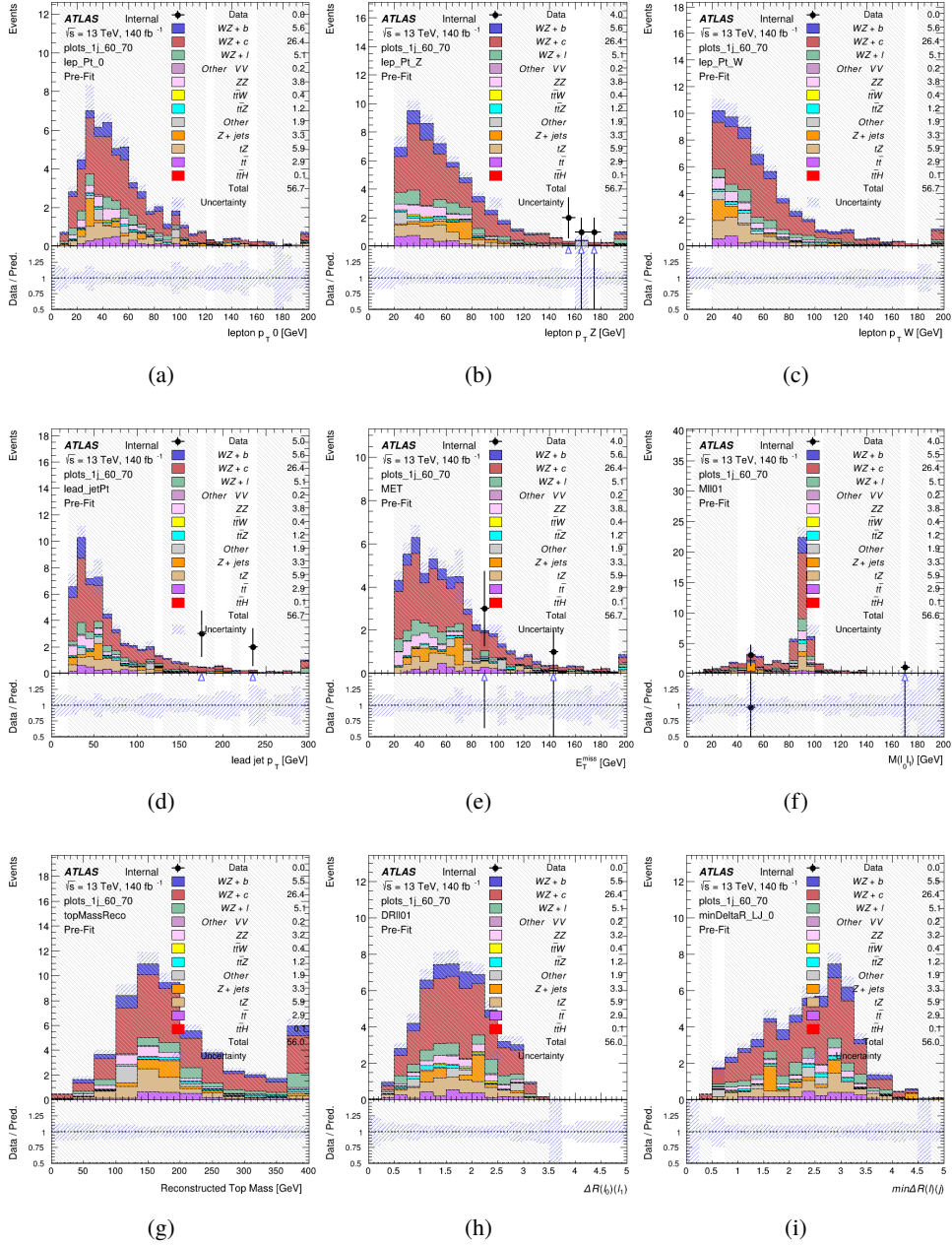


Figure 8: Comparisons between the data and MC distributions in the preselection region for (a) the p_T of the opposite sign lepton, (b) the p_T of the other lepton from the Z candidate, (c) the p_T of the lepton from the W candidate, (d) the leading jet p_T , (e) the E_T^{miss} , and (f) the invariant mass of leptons 0 and 1, (g) the reconstructed top mass, (h) $\Delta(R)$ between lepton 0 and 1, (i) the $\Delta(R)$ between the closest lepton and jet.

WZ Fit Region - 1j 60% WP

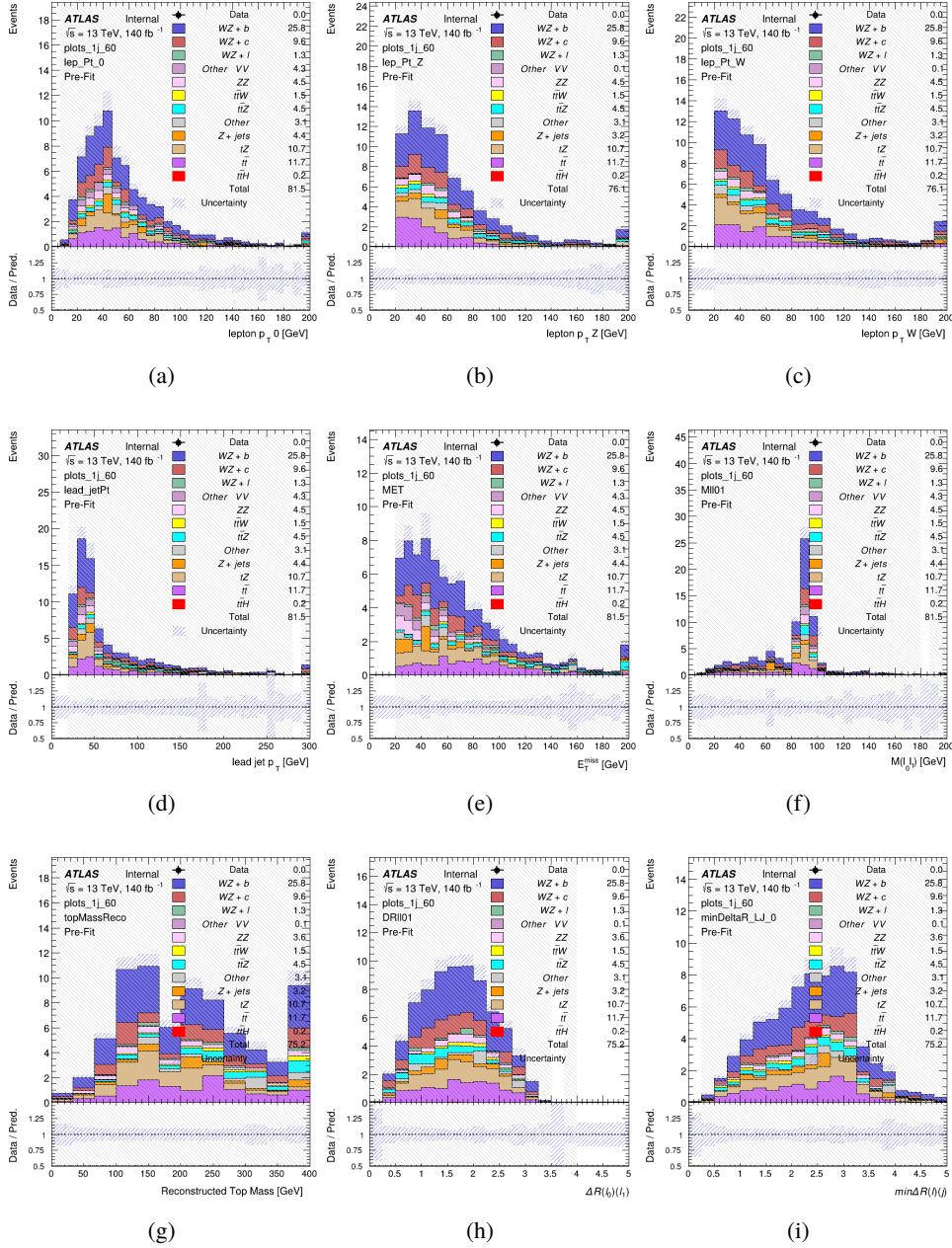


Figure 9: Comparisons between the data and MC distributions in the preselection region for (a) the p_T of the opposite sign lepton, (b) the p_T of the other lepton from the Z candidate, (c) the p_T of the lepton from the W candidate, (d) the leading jet p_T , (e) the E_T^{miss} , and (f) the invariant mass of leptons 0 and 1, (g) the reconstructed top mass, (h) $\Delta(R)$ between lepton 0 and 1, (i) the $\Delta(R)$ between the closest lepton and jet.

WZ Fit Region - tZ-CR

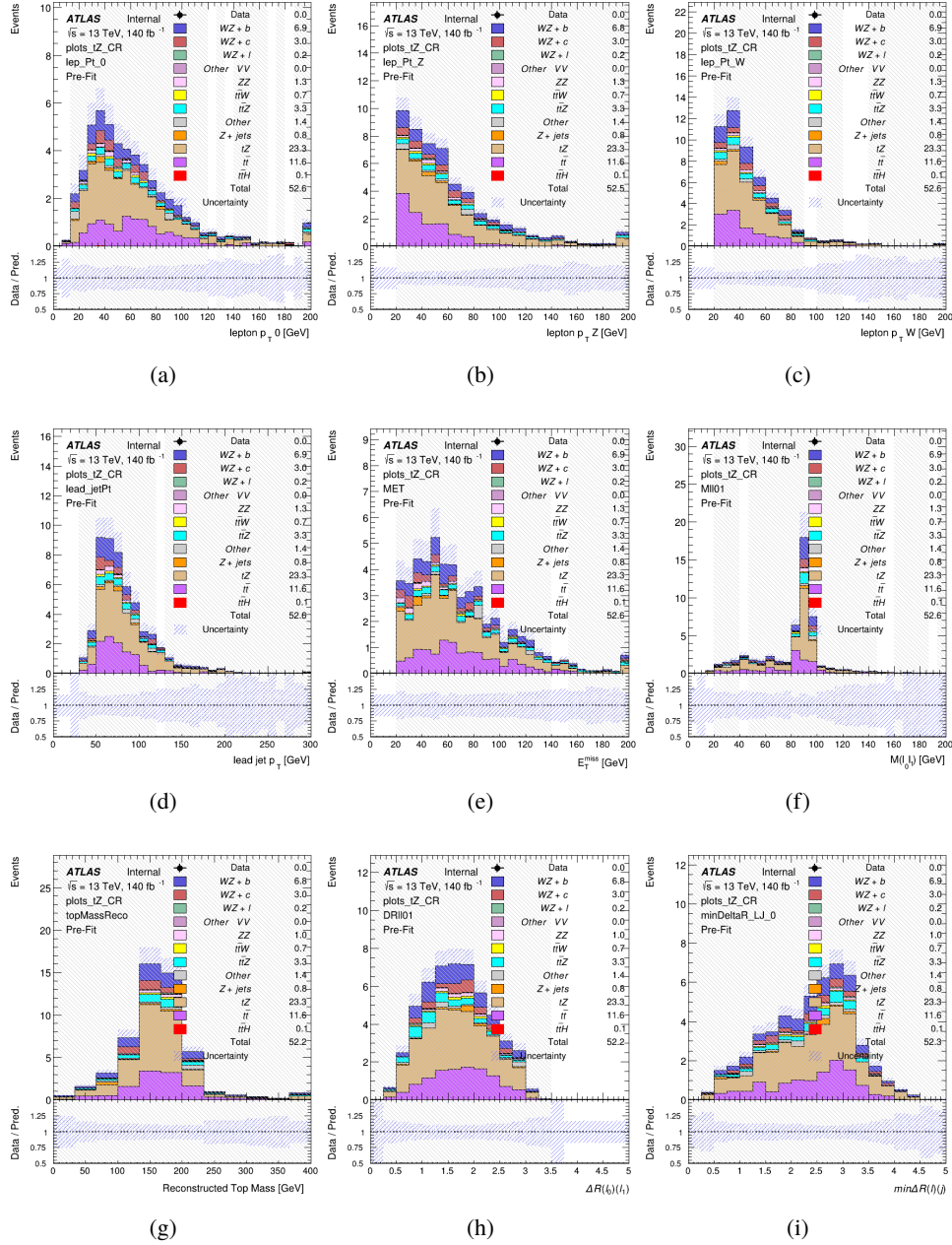


Figure 10: Comparisons between the data and MC distributions in the preselection region for (a) the p_T of the opposite sign lepton, (b) the p_T of the other lepton from the Z candidate, (c) the p_T of the lepton from the W candidate, (d) the leading jet p_T , (e) the E_T^{miss} , and (f) the invariant mass of leptons 0 and 1, (g) the reconstructed top mass, (h) $\Delta(R)$ between lepton 0 and 1, (i) the $\Delta(R)$ between the closest lepton and jet.

WZ Fit Region - 2j Inclusive

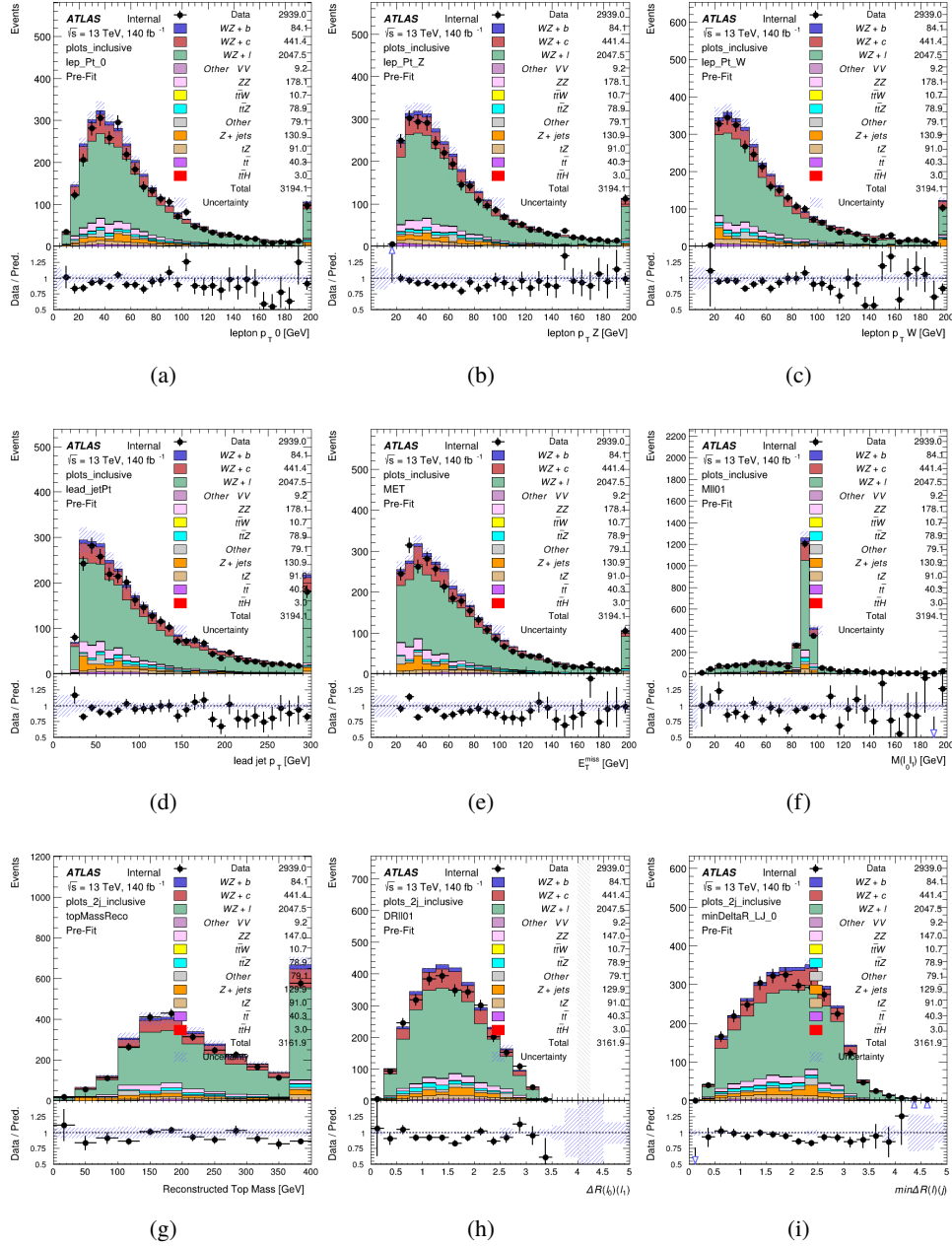


Figure 11: Comparisons between the data and MC distributions in the preselection region for (a) the p_T of the opposite sign lepton, (b) the p_T of the other lepton from the Z candidate, (c) the p_T of the lepton from the W candidate, (d) the leading jet p_T , (e) the E_T^{miss} , and (f) the invariant mass of leptons 0 and 1, (g) the reconstructed top mass, (h) $\Delta(R)$ between lepton 0 and 1, (i) the $\Delta(R)$ between the closest lepton and jet.

WZ Fit Region - 2j < 85% WP

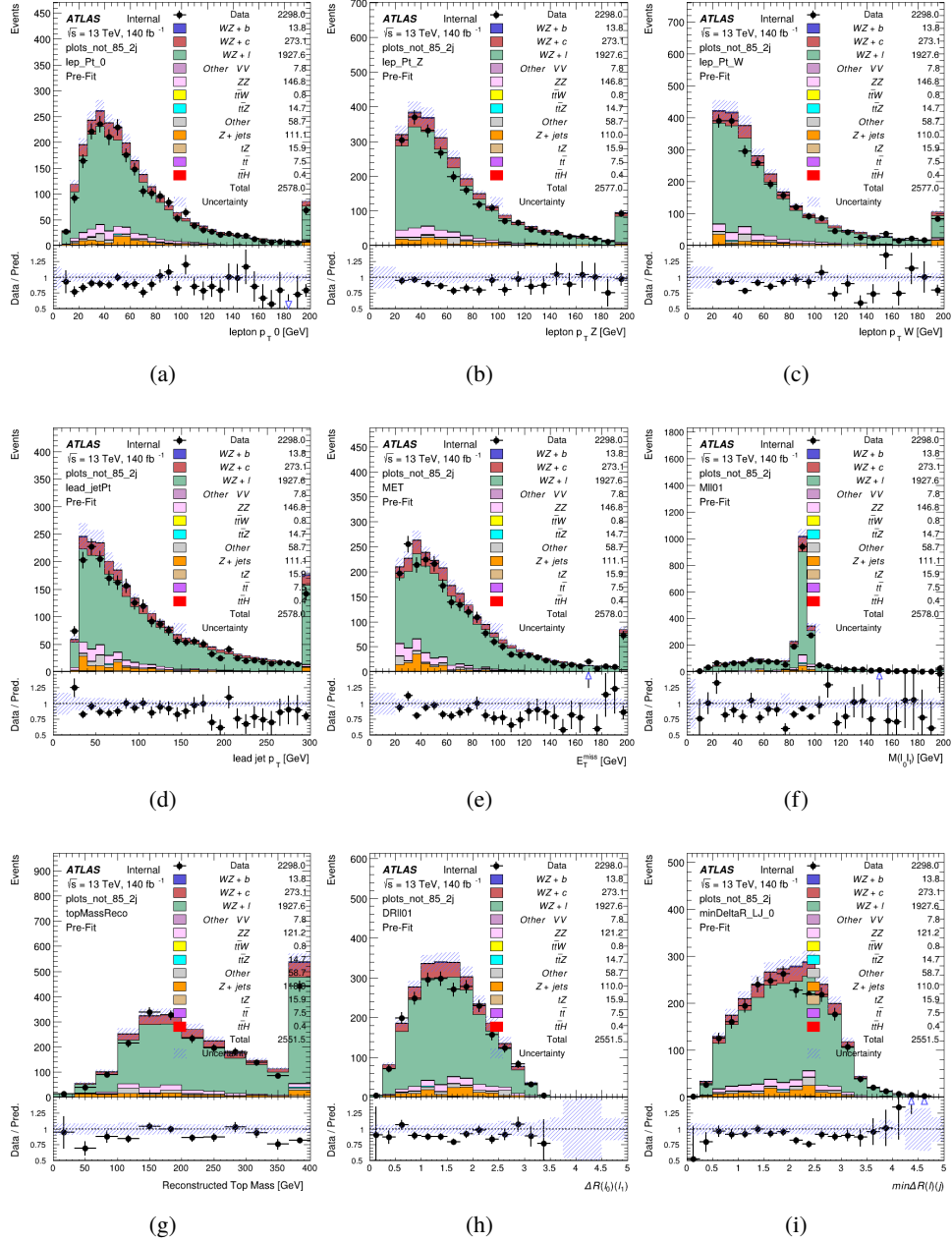


Figure 12: Comparisons between the data and MC distributions in the preselection region for (a) the p_T of the opposite sign lepton, (b) the p_T of the other lepton from the Z candidate, (c) the p_T of the lepton from the W candidate, (d) the leading jet p_T , (e) the E_T^{miss} , and (f) the invariant mass of leptons 0 and 1, (g) the reconstructed top mass, (h) $\Delta(R)$ between lepton 0 and 1, (i) the $\Delta(R)$ between the closest lepton and jet.

WZ Fit Region - 2j 77-85% WP

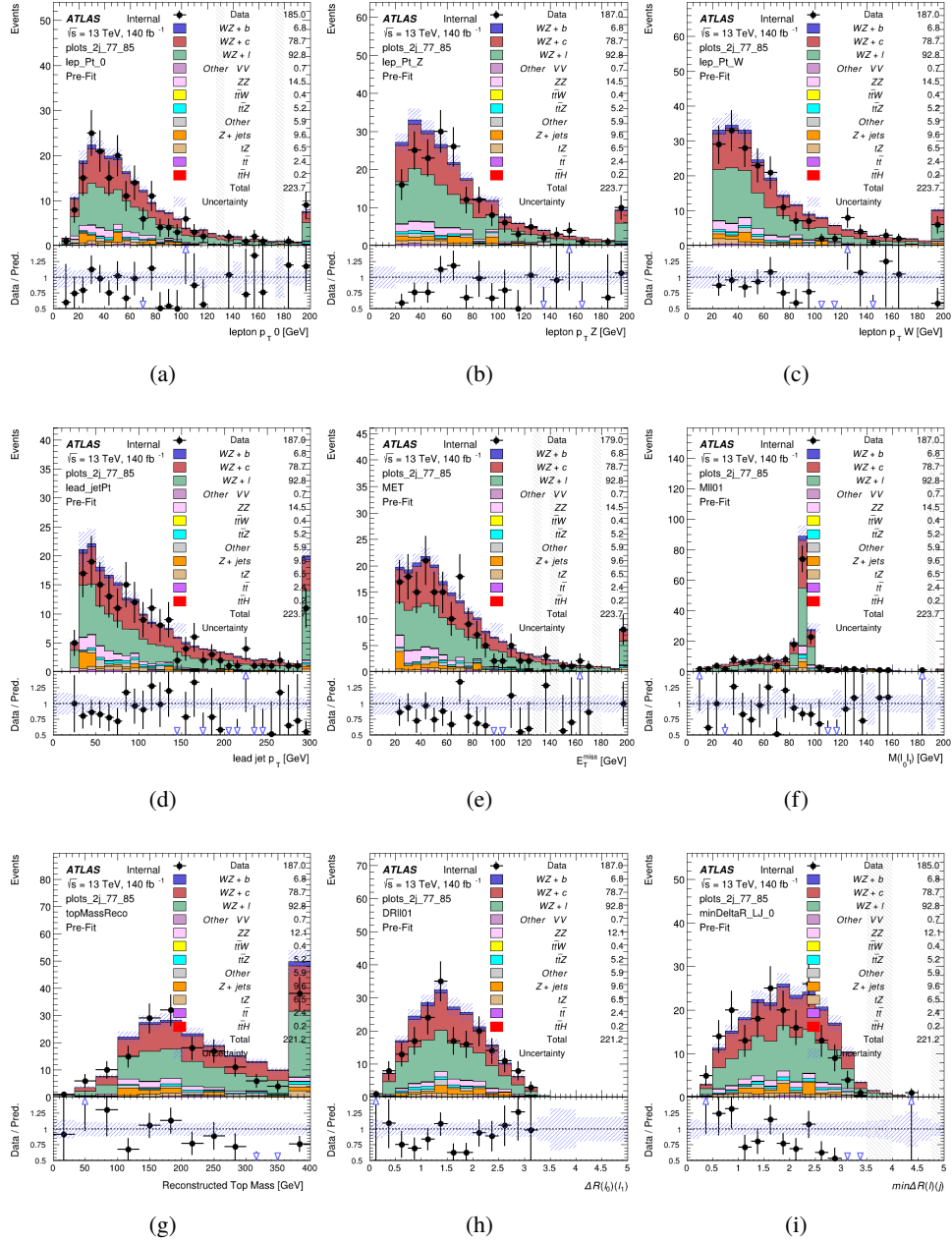


Figure 13: Comparisons between the data and MC distributions in the preselection region for (a) the p_T of the opposite sign lepton, (b) the p_T of the other lepton from the Z candidate, (c) the p_T of the lepton from the W candidate, (d) the leading jet p_T , (e) the E_T^{miss} , and (f) the invariant mass of leptons 0 and 1, (g) the reconstructed top mass, (h) $\Delta(R)$ between lepton 0 and 1, (i) the $\Delta(R)$ between the closest lepton and jet.

WZ Fit Region - 2j 70-77% WP

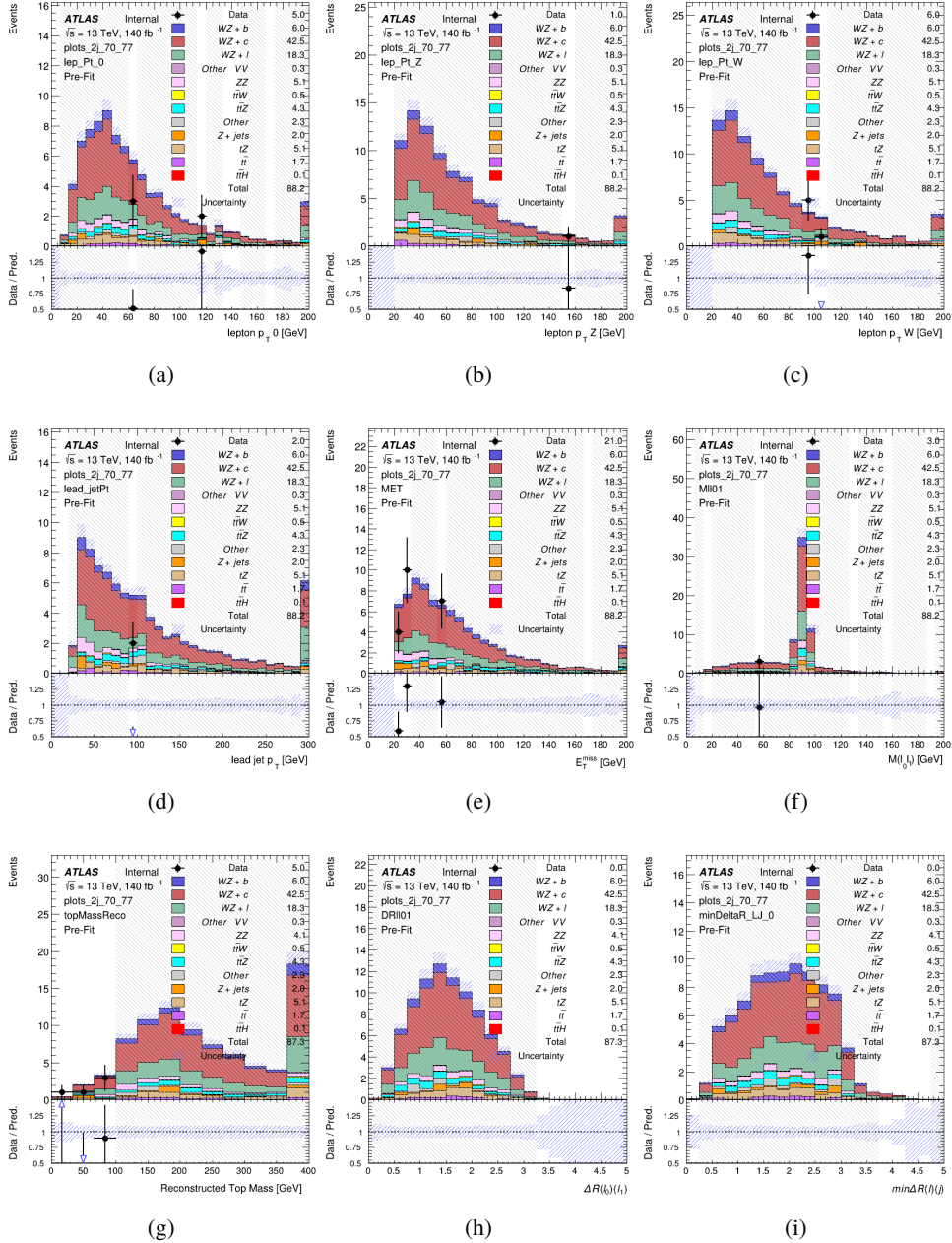


Figure 14: Comparisons between the data and MC distributions in the preselection region for (a) the p_T of the opposite sign lepton, (b) the p_T of the other lepton from the Z candidate, (c) the p_T of the lepton from the W candidate, (d) the leading jet p_T , (e) the E_T^{miss} , and (f) the invariant mass of leptons 0 and 1, (g) the reconstructed top mass, (h) $\Delta(R)$ between lepton 0 and 1, (i) the $\Delta(R)$ between the closest lepton and jet.

WZ Fit Region - 2j 60-70% WP

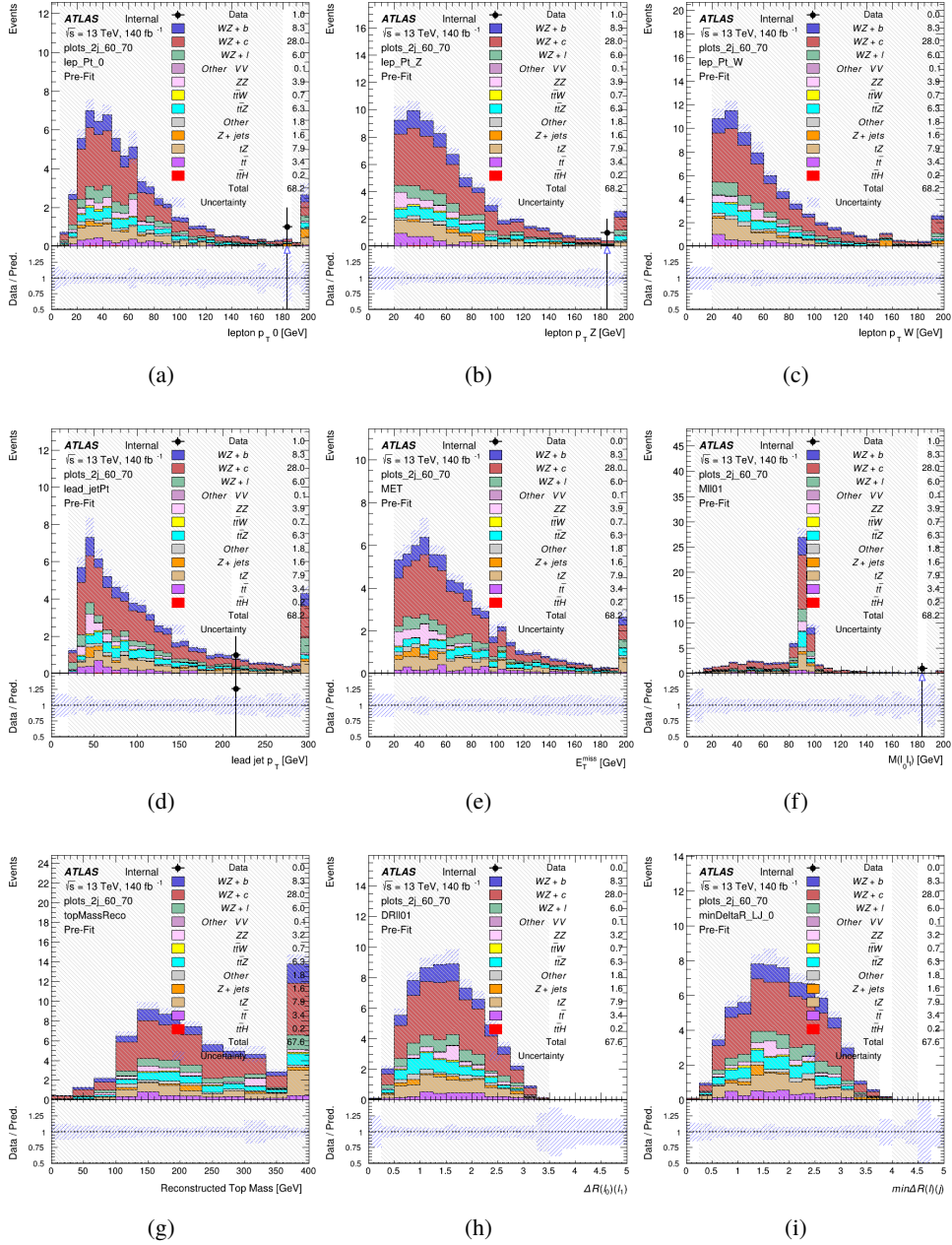


Figure 15: Comparisons between the data and MC distributions in the preselection region for (a) the p_T of the opposite sign lepton, (b) the p_T of the other lepton from the Z candidate, (c) the p_T of the lepton from the W candidate, (d) the leading jet p_T , (e) the E_T^{miss} , and (f) the invariant mass of leptons 0 and 1, (g) the reconstructed top mass, (h) $\Delta(R)$ between lepton 0 and 1, (i) the $\Delta(R)$ between the closest lepton and jet.

WZ Fit Region - 2j 60% WP

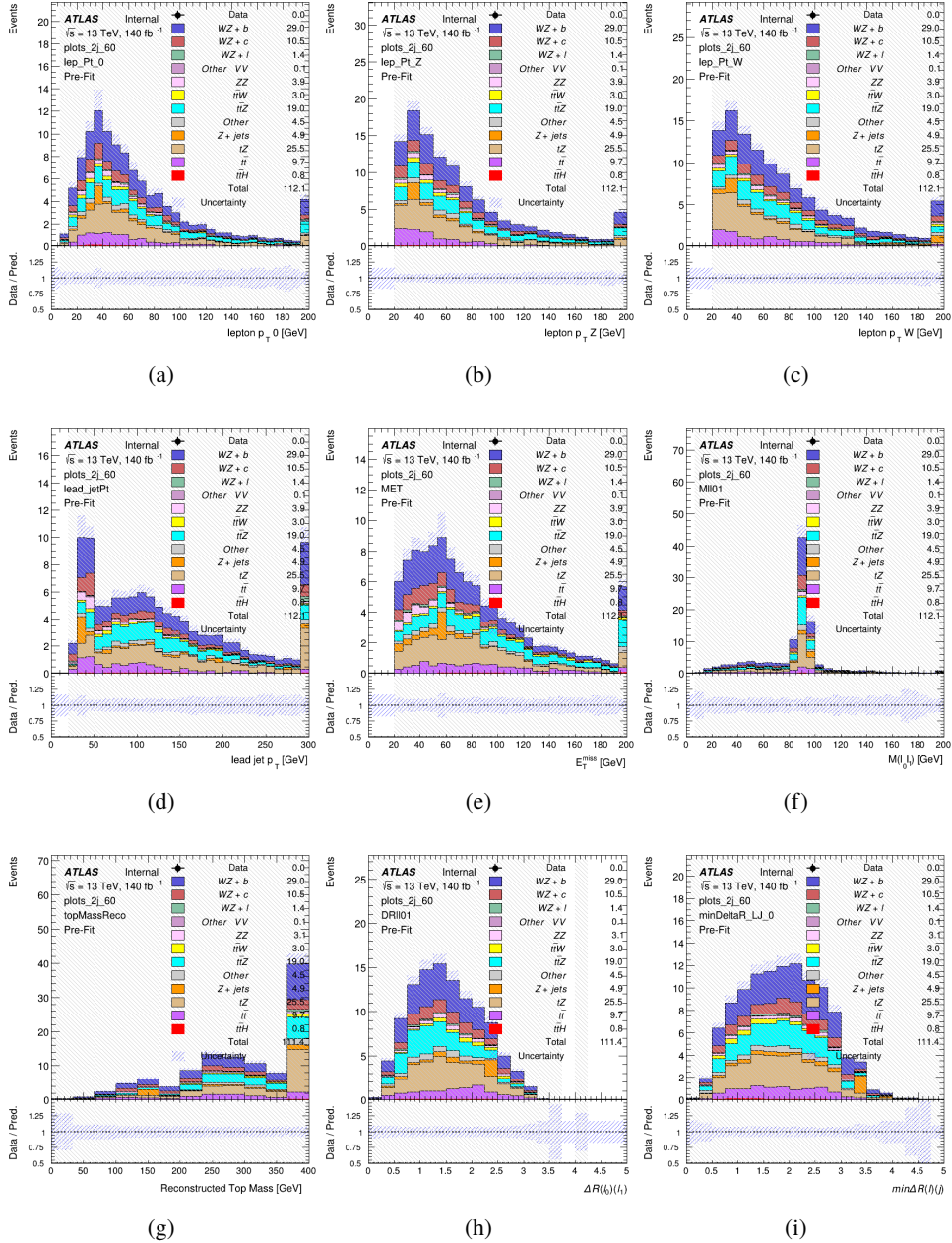


Figure 16: Comparisons between the data and MC distributions in the preselection region for (a) the p_T of the opposite sign lepton, (b) the p_T of the other lepton from the Z candidate, (c) the p_T of the lepton from the W candidate, (d) the leading jet p_T , (e) the E_T^{miss} , and (f) the invariant mass of leptons 0 and 1, (g) the reconstructed top mass, (h) $\Delta(R)$ between lepton 0 and 1, (i) the $\Delta(R)$ between the closest lepton and jet.

WZ Fit Region - tZ-CR-2j

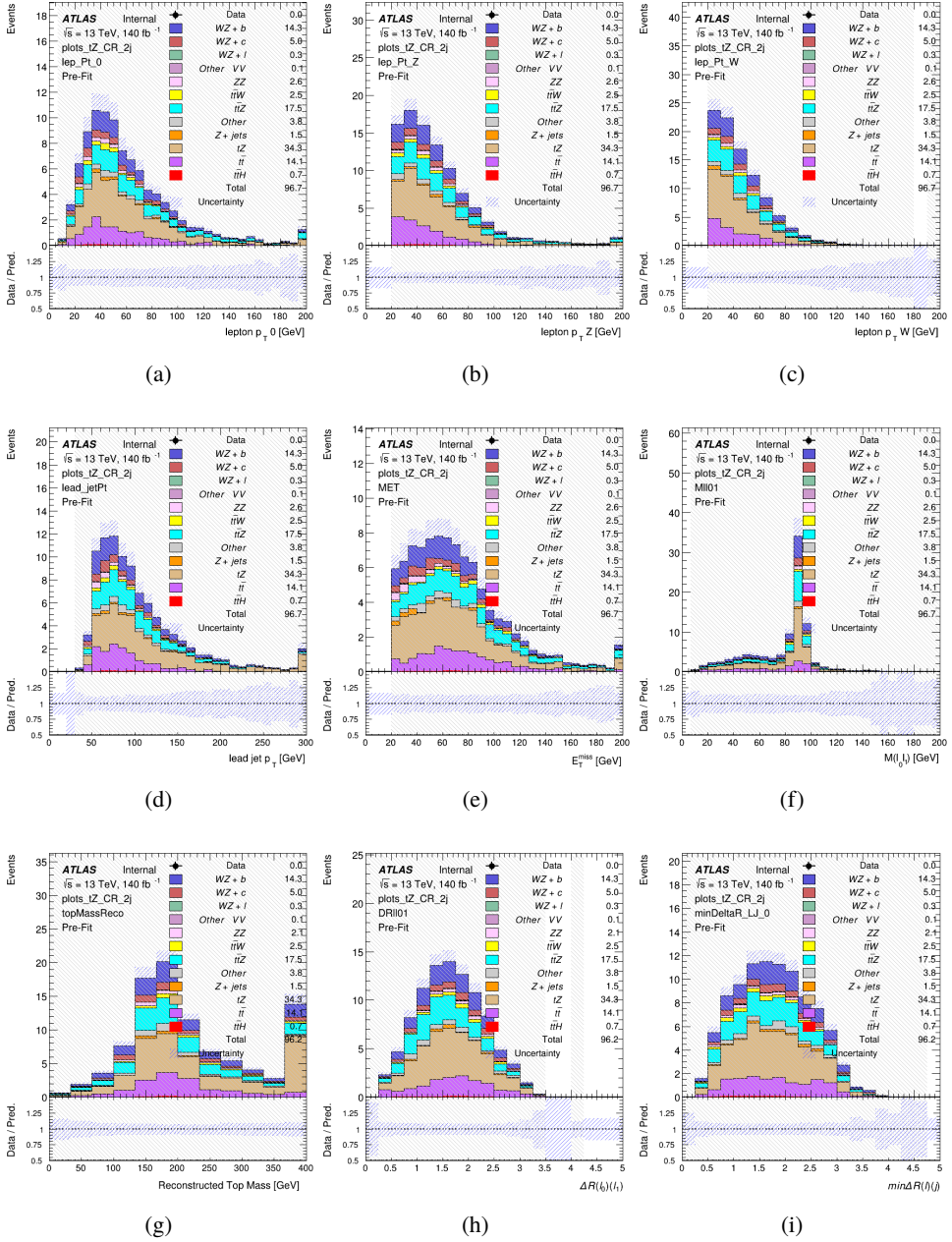


Figure 17: Comparisons between the data and MC distributions in the preselection region for (a) the p_T of the opposite sign lepton, (b) the p_T of the other lepton from the Z candidate, (c) the p_T of the lepton from the W candidate, (d) the leading jet p_T , (e) the E_T^{miss} , and (f) the invariant mass of leptons 0 and 1, (g) the reconstructed top mass, (h) $\Delta(R)$ between lepton 0 and 1, (i) the $\Delta(R)$ between the closest lepton and jet.

326 **5.3 Non-Prompt Lepton Estimation**

327 Two processes act as sources of non-prompt leptons appear in the analysis: $t\bar{t}$ and $Z+jet$
328 production both produce two prompt leptons, and each contribute to the 31 region when an
329 additional non-prompt lepton appears in the event. The contribution of these processes is
330 estimated with Monte Carlo simulations, which are validated using enriched validation regions.

331 The modelling in the $Z+jets$ and $t\bar{t}$ CRs is further validated for each of the pseudo-continuous
332 b-tag regions used in the analysis. The relevant lepton p_T spectrum in each b-tag region is shown
333 in Appendix ?? for these CRs after the correction factors derived below have been applied.

334 **5.3.1 $t\bar{t}$ Validation**

335 $t\bar{t}$ events can produce two prompt leptons from the decay of each of the tops. These top decays
336 produce two b-quarks, the decay of which can produce additional non-prompt leptons, which
337 occasionally pass the event preselection. In order to validate that the Monte Carlo accurately
338 simulates this process accurately, the MC prediction in a non-prompt $t\bar{t}$ enriched validation
339 region is compared to data.

340 The $t\bar{t}$ validation region is similar to the preselection region - three leptons meeting the criteria
341 described in Section 7 are required, and the requirements on E_T^{miss} remain the same. However,
342 the selection requiring a lepton pair form a Z -candidate are reversed. Events where the invariant
343 mass of any two opposite sign, same flavor leptons falls within 10 GeV of 91.2 GeV are rejected.
344 This ensures the $t\bar{t}$ validation region is orthogonal to the preselection region.

345 Further, because the jet multiplicity of $t\bar{t}$ events tends to be higher than WZ , the number of jets
346 in each event is required to be greater than 1. As b-jets are almost invariably produced from top
347 decays, at least one b-tagged jet passing the 70% DL1r WP in each event is required. Various
348 kinematic plots of this region are shown in Figure ??.

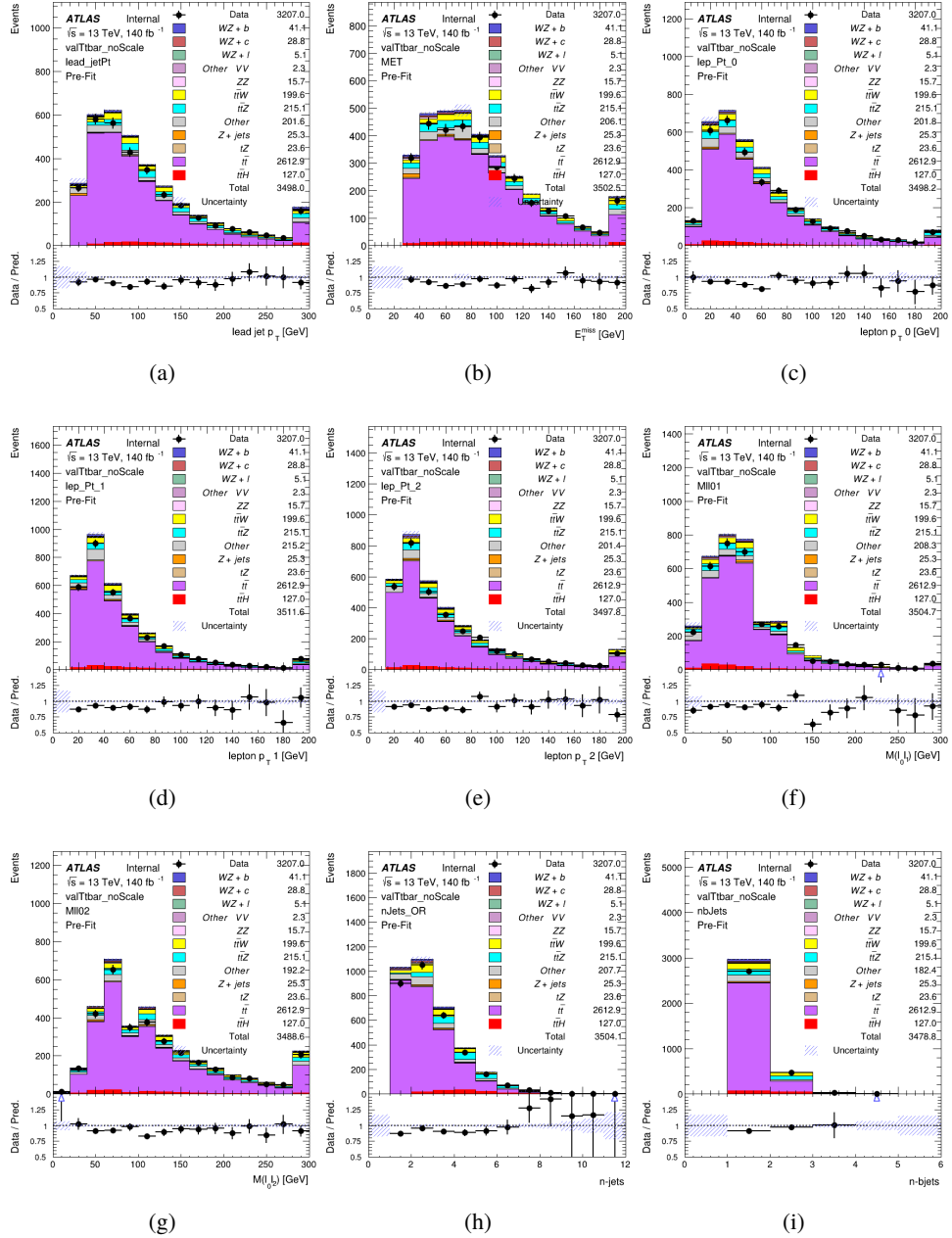


Figure 18: Comparisons between the data and MC distributions in the $t\bar{t}$ validation region for (a) the p_T of the leading jet, (b) the missing transverse energy, (c) the p_T of lepton 0, (d) p_T of lepton 1, (e) p_T of lepton 2, (f) the invariant mass of leptons 0 and 1, (g) the invariant mass of leptons 0 and 2, (h) the number of jets, (i) the number of b-tagged jets.

349 The shape of each distribution agrees quite well between data and MC, with a constant offset
 350 between the two. This is accounted for by applying a constant correction factor of 0.9 to the $t\bar{t}$

351 MC prediction. Plots showing the kinematics of the $t\bar{t}$ VR after this correction factor has been
 352 applied are shown in Figure ??.

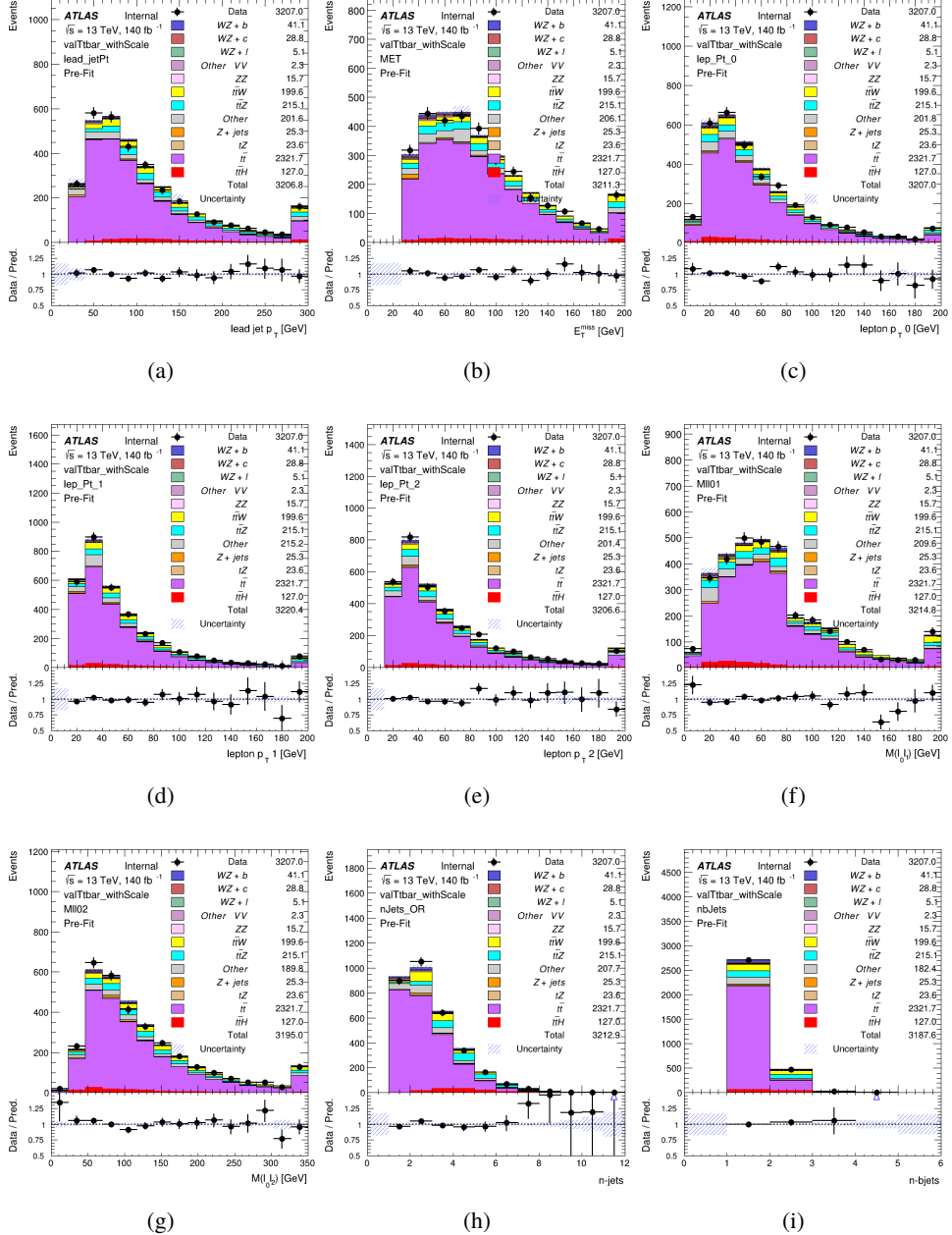


Figure 19: Comparisons between the data and MC distributions in the $t\bar{t}$ validation region after the correction factor has been applied for (a) the p_T of the leading jet, (b) the missing transverse energy, (c) the p_T of lepton 0, (d) p_T of lepton 1, (e) p_T of lepton 2, (f) the invariant mass of leptons 0 and 1, (g) the invariant mass of leptons 0 and 2, (h) the number of jets, (i) the number of b-tagged jets.

353 The modeling is further validated by looking at the yield in the $t\bar{t}$ VR for each DL1r WP, giving
 354 a clearer correspondence to the signal regions used in the fit. For these plots, the requirement
 355 that each event contain at least one b-tagged jet is removed. Each region shown in Figure ??
 356 requires one or more jets pass the listed WP, with no jets passing the next highest WP.

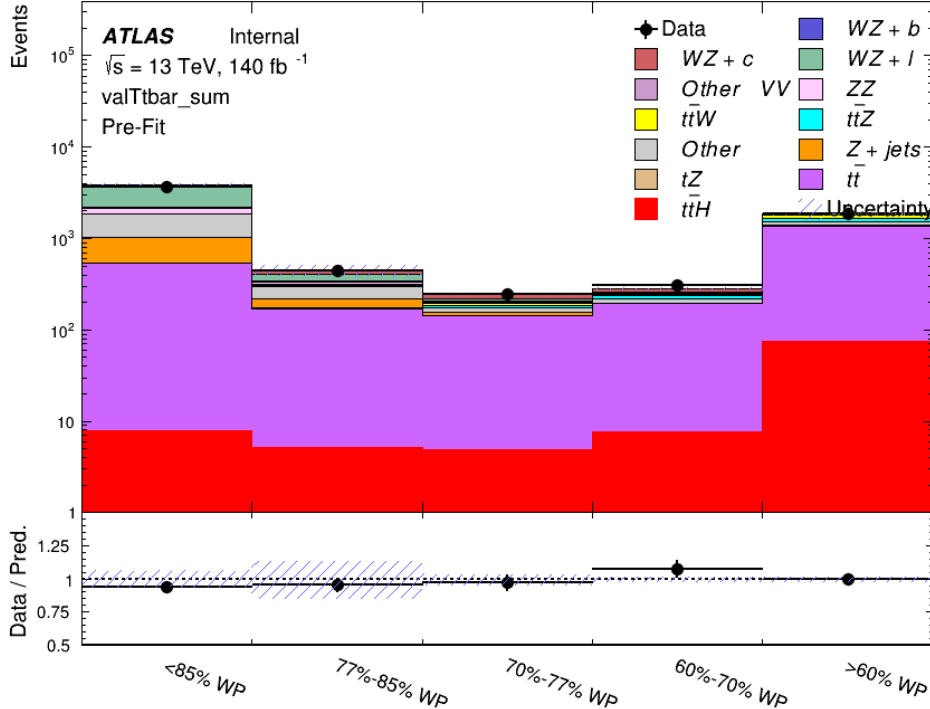


Figure 20: Data and MC comparisons for each DL1r WP for both 1-jet and 2-jet regions, after the $t\bar{t}$ VR selection and correction factor have been applied

357 As data and MC are found to agree within 20% for each of these working points, a 20% systematic
 358 uncertainty on the $t\bar{t}$ prediction is included for the analysis.

359 5.3.2 Z+jets Validation

360 Similar to $t\bar{t}$, a non-prompt Z+jets validation region is produced in order to validate the MC
 361 predictions. The lepton requirements remain the same as the preselection region. Because no
 362 neutrinos are present for this process, the E_T^{miss} cut is reversed, requiring $E_T^{\text{miss}} < 30$ GeV. This
 363 also ensures this validation region is orthogonal to the preselection region. Further, the number
 364 of jets in each event is required to be greater than or equal to one. Various kinematic plots of this
 365 region are shown below. The general agreement between data and MC in each of these suggests
 366 that the non-prompt contribution of Z+jets is well modeled by Monte Carlo.

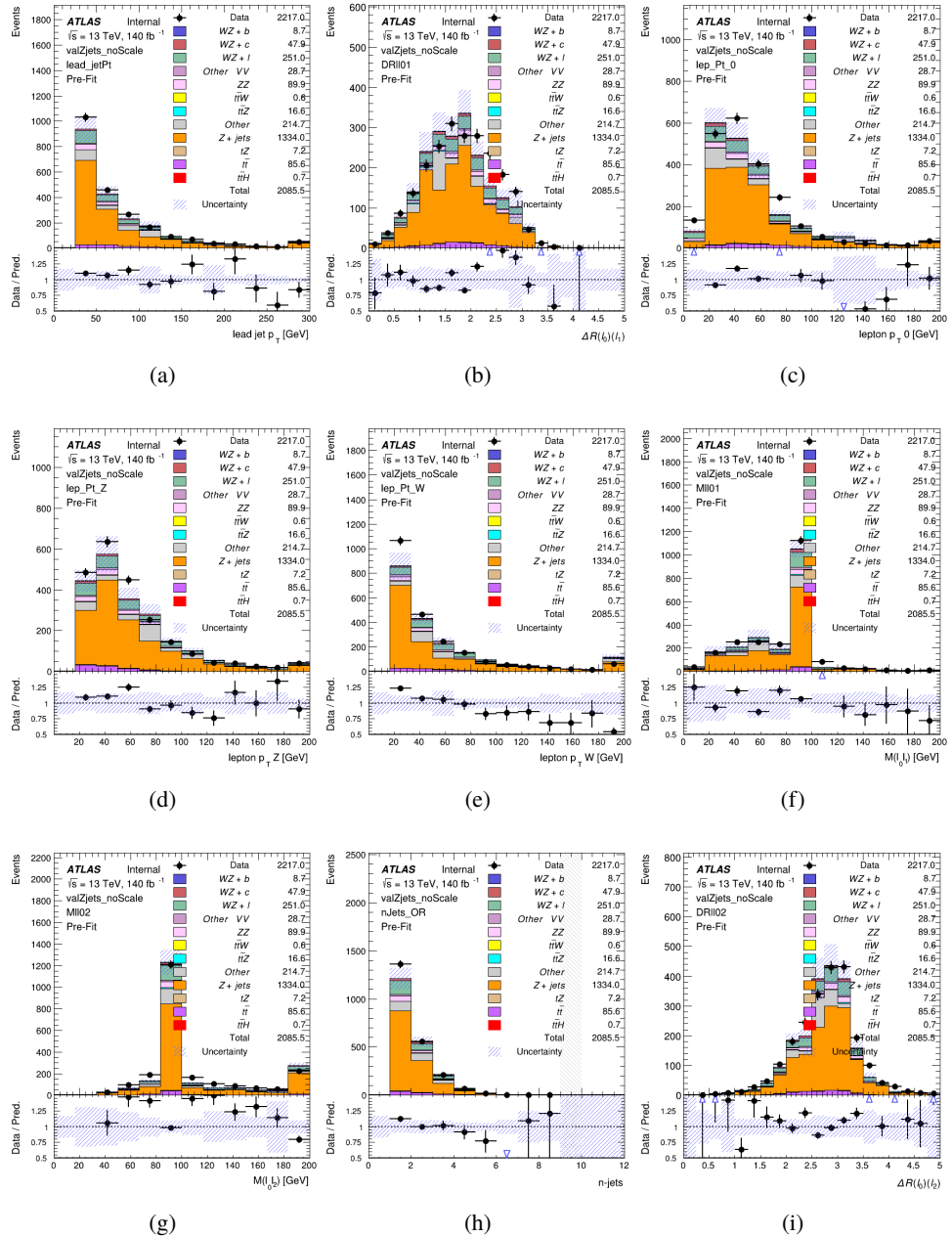


Figure 21: Comparisons between the data and MC distributions in the Z+jets validation region for (a) the p_T of the leading jet, (b) ΔR between leptons 0 and 1, (c) the p_T of lepton 0, (d) p_T of SS lepton from the Z candidate, (e) p_T of the SS lepton from the W candidate, (f) the invariant mass of leptons 0 and 1, (g) the invariant mass of leptons 0 and 2, (h) the number of jets, (i) ΔR between leptons 0 and 2. Includes only statistical uncertainties

367 While there is general agreement between data and MC within statistical uncertainty, the shape

of the p_T spectrum of the lepton from the W candidate is found to differ. As this is the lepton not included in the Z-candidate, in the case of Z+jets, this lepton is most often the non-prompt lepton. A similar effect is seen for both non-prompt muons and electrons in the Z+jets validation region, as shown in Figure ??.

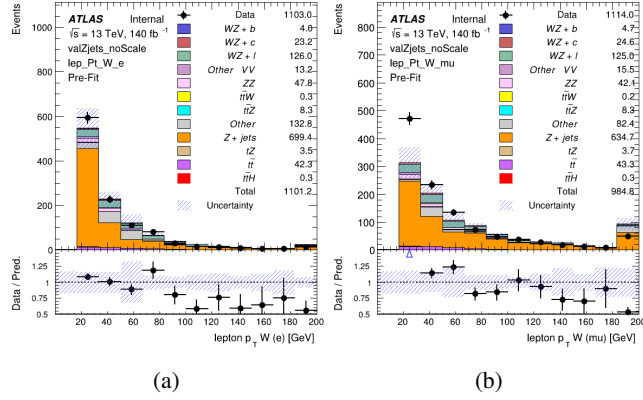


Figure 22: p_T spectrum of the lepton from the W candidate for (a) electrons and (b) muons

To account for this discrepancy, a variable correction factor is applied to Z+jets. χ^2 minimization of the W lepton p_T spectrum is performed to derive a correction factor as a function of this p_T . Kinematic plots of the Z + jets validation region after this correction factor has been applied are shown in Figure ??.

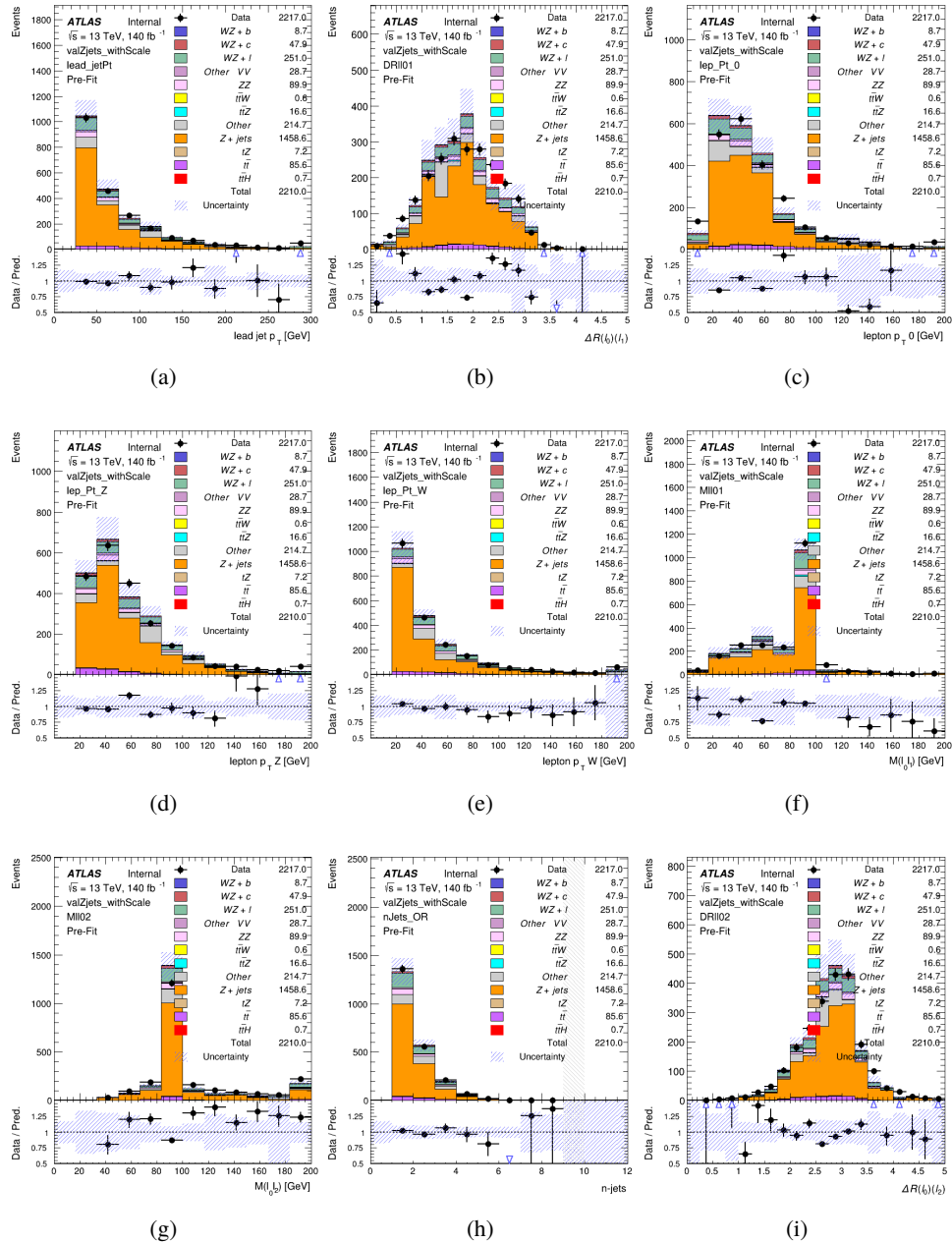


Figure 23: Comparisons between the data and MC distributions in the $Z+jets$ validation region after the correction factor has been applied for (a) the p_T of the leading jet, (b) ΔR between leptons 0 and 1, (c) the p_T of lepton 0, (d) p_T of SS lepton from the Z candidate, (e) p_T of the SS lepton from the W candidate, (f) the invariant mass of leptons 0 and 1, (g) the invariant mass of leptons 0 and 2, (h) the number of jets, (i) ΔR between leptons 0 and 2

376 The modeling is further validated by looking at the yield in the $Z+jets$ VR for each DL1r WP,

377 giving a clearer correspondence to the signal regions used in the fit. Each region shown in Figure
 378 ?? requires one or more jets pass the listed WP, with no jets passing the next highest WP.

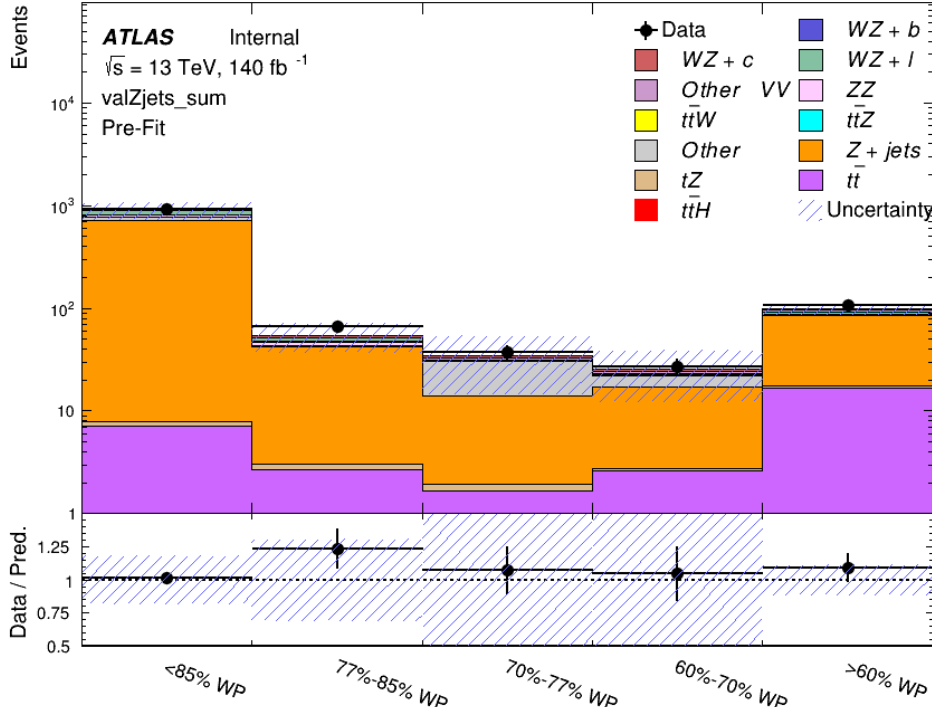


Figure 24: Data and MC comparisons for each DL1r WP for both 1-jet and 2-jet regions, after the Z+jets VR selection and correction factor have been applied

379 For each of the b-tagging working points considered, the data falls within 25% of the MC
 380 prediction once this correction factor has been applied. Therefore, a 25% systematic uncertainty
 381 is applied to Z + jets in the analysis.

382 6 tZ Separation Multivariate Analysis

383 Because tZ produces a final state identical to signal, it represents a predominant background in
 384 the most signal enriched regions. That is, the region with one jet passing the 60% DL1r WP.
 385 Therefore, a boosted decision tree (BDT) algorithm is trained to separate WZ + heavy flavor
 386 from tZ.

387 Separation between tZ and WZ + heavy flavor is achieved in part by reconstructing the invariant
 388 mass of the top candidate, which clusters more closely to the top mass for tZ than WZ + heavy
 389 flavor. The result of this BDT is used to create a tZ enriched region in the fit, reducing its impact
 390 on the measurement of WZ + heavy flavor.

391 **6.1 Top Mass Reconstruction**

392 The reconstruction of the top mass follows the procedure described in detail in section 6.1 of
 393 [21]. The mass of the top quark candidate is reconstructed from the jet, the lepton not included
 394 in the Z-candidate, and a reconstructed neutrino. In the case that there is one jet in the event,
 395 there is only possible b-jet candidate. For events with two jets, the jet with the highest DL1r
 396 score is used.

397 The neutrino from the W decay is expected to be the only source of E_T^{miss} . Therefore, the E_T
 398 and ϕ of the neutrino are taken from the E_T^{miss} measurement. This leaves the z-component of
 399 the neutrino momentum, $p_{\nu z}$ as the only unknown.

400 This unknown is solved for by taking the combined invariant mass of the lepton and neutrino to
 401 give the invariant mass of the W boson:

$$402 \quad (p_l + p_\nu)^2 = m_W^2$$

403 Expanding this out into components, this equation gives:

$$404 \quad \sqrt{p_{T\nu}^2 + p_{z\nu}^2} E_l = \frac{m_w^2 - m_l^2}{2} + p_{T\nu}(p_{lx}\cos\phi_\nu + p_{ly}\sin\phi_\nu) + p_{lz}p_{\nu z}$$

405 This equation gives two solutions for $p_{\nu z}$. For cases where only one of these solutions is real,
 406 that is taken as the value of $p_{\nu z}$. For instances with two real solutions, the one which is shown
 407 to be correct in the largest fraction of simulations is taken. For cases when no real solution is
 408 found, often because of detector effects, the value of E_T^{miss} is varied in decreasing increments of
 409 100 MeV until a real solution is found.

410 The reconstructed top mass distribution for tZ and WZ + b can be seen in figure ??.

411 **6.2 tZ BDT**

412 A Boosted Decision Tree (BDT), specifically XGBoost [22], is used to provide separation between
 413 tZ and WZ+b. The following kinematic variables are used as inputs:

- 414 • The invariant mass of the reconstructed top candidate
- 415 • p_T of each of the leptons, jet
- 416 • The invariant mass of each combination of lepton pairs, $M(l\bar{l})$
- 417 • E_T^{miss}
- 418 • Distance between each combination of leptons, $\Delta R(l\bar{l})$
- 419 • Distance between each lepton and the jet, $\Delta R(lj)$

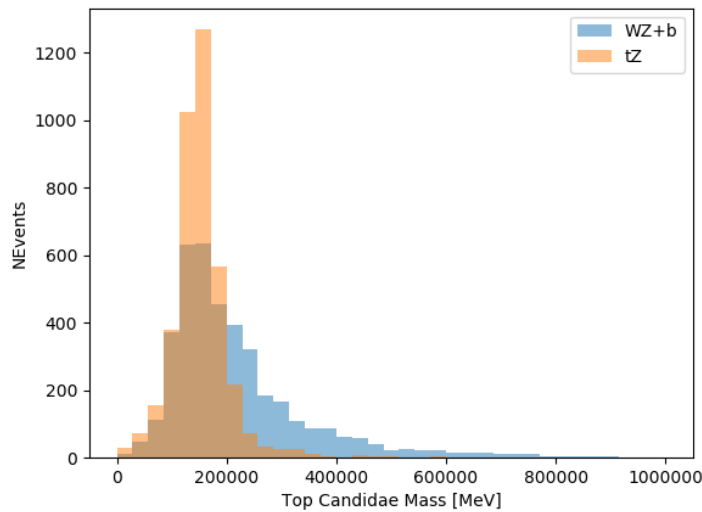


Figure 25: Reconstructed top mass distributions for tZ and WZ + b, measured in MeV.

420 The training samples included only events meeting the requirements of the 1-jet, >60% region,
 421 i.e. passing all the selection described in section 7 and having exactly one jet which passes the
 422 tightest (60%) DL1r working point.

423 The distributions of a few of these features for both signal and background is shown in figure
 424 ??.

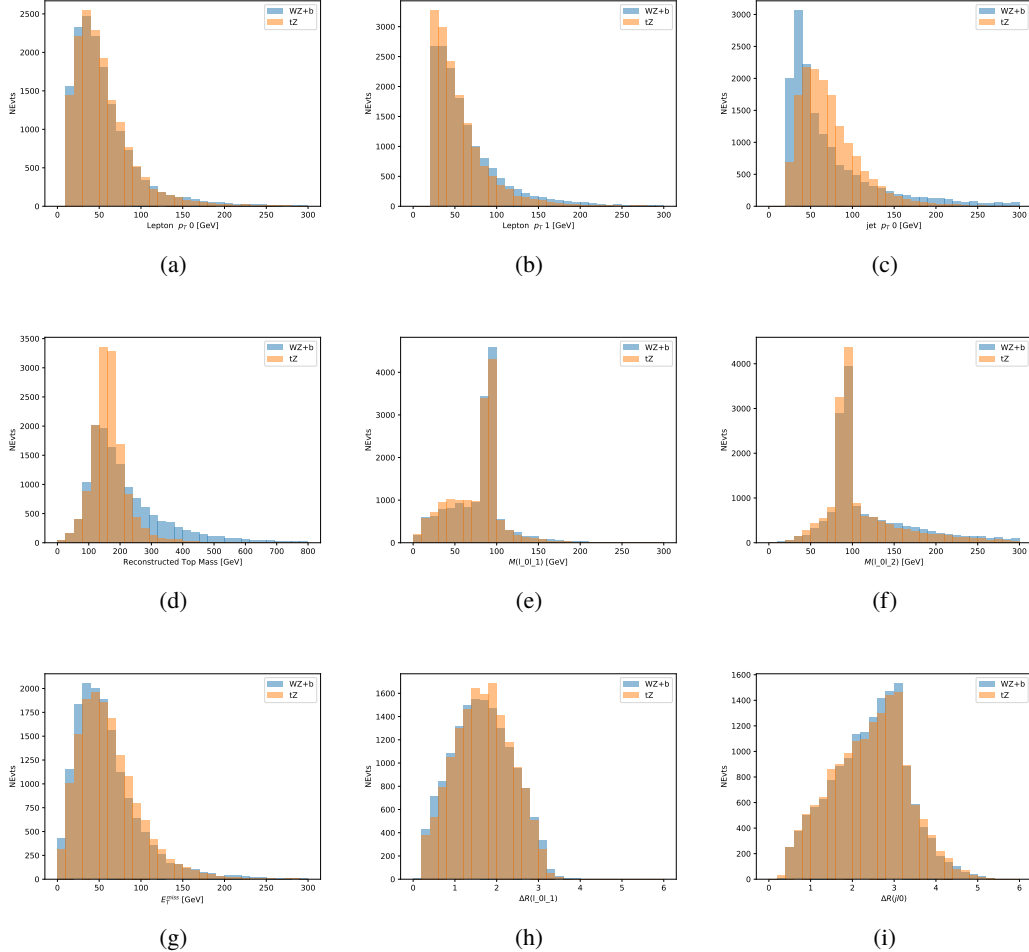


Figure 26: Distribution of input features of the BDT for signal (WZ) and background (tZ). Both are scaled to an equal number of events. (a), (b) and (c) show the p_T of lepton 0, lepton 1, and the jet, (d) show the reconstructed top mass, (e) and (f) show the invariant mass of leptons 0 and 1, leptons 0 and 2. (g) shows the E_T^{miss} of each event. (h) and (i) show the ΔR between lepton 0 and lepton 1, and the jet.

425 A sample of 20,000 background (tZ) and signal (WZ+b) Monte Carlo events are used to train
 426 the BDT. And additional 5,000 events are reserved for testing the model, in order to prevent
 427 over-fitting. A total of 750 decision trees with a maximum depth of 6 branches are used to build
 428 the model. These parameters are chosen empirically, by training several models with different
 429 parameters and selecting the one that gave the best separation for the test sample.

430 The results of the BDT training are shown in figure 1. The output scores for both signal and
 431 background events is shown on the left. The right shows the receiving operating characteristic
 432 (ROC) curve that results from the MVA. The ROC curve represents the background rejection
 433 as a function of signal efficiency, where each point on the curve represents a different response

434 score.

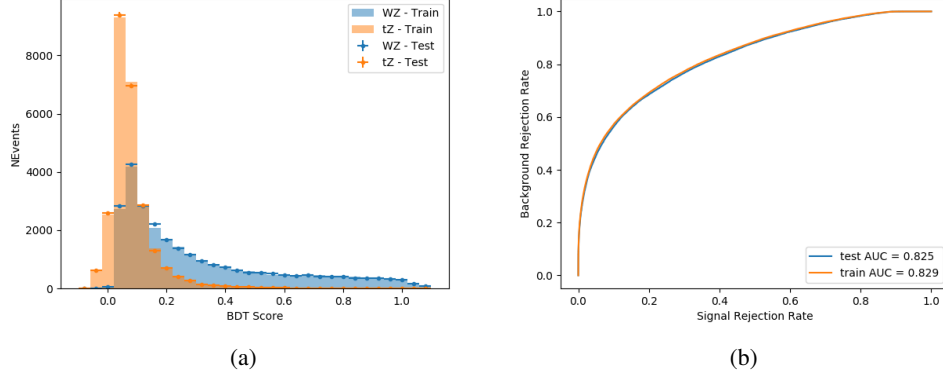


Figure 27: Distribution of the BDT response for signal and background events on the left, the ROC curve for the BDT on the right.

435 The relative important of each input feature in the model, measured by how often they appeared
436 in the decision trees, is shown in figure ??.

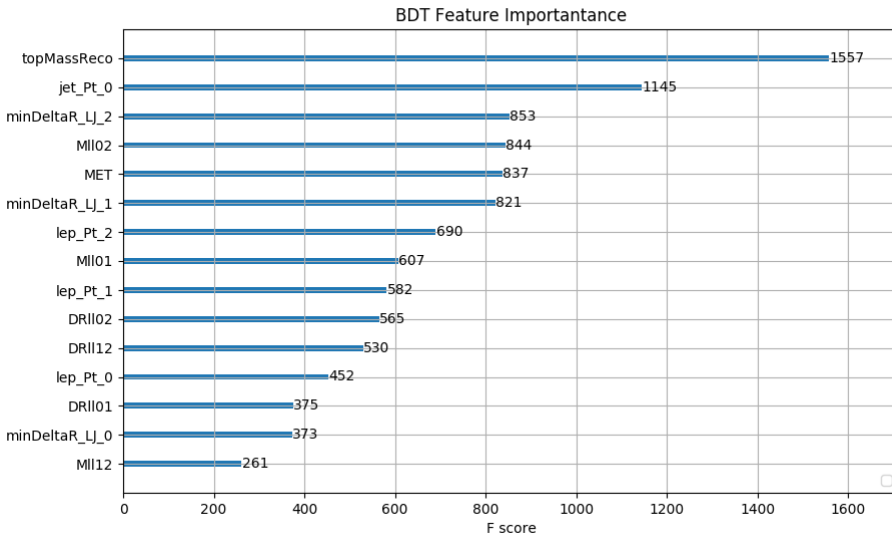


Figure 28: Relative importance of each input feature in the model.

437 These results suggest that some amount of separation can be achieved between these two pro-
438 cesses, with a high BDT score selecting a set of events that is pure in WZ + b. A BDT score

439 of 0.725 is selected as a cutoff, where events with scores higher than this form a signal enriched
440 region, and events with scores lower than this form a tZ control region. This cutoff is selected by
441 varying the value of this cutoff in stat-only Asimov fits, and selecting the value that minimizes
442 the statistical uncertainty on WZ + b.

443 **6.3 tZ Interference Studies**

444 Because it includes an on-shell Z boson as well as a b-jet and W from the top decay, tZ
445 production represents an identical final state to WZ + b-jet. This implies the possibility of matrix
446 level interference between these two processes not accounted for in the Monte Carlo simulations,
447 which consider the two processes independently. Truth level studies are performed in order to
448 estimate the impact of these interference effects.

449 In order to estimate the matrix level interference effects between tZ and WZ + b-jet, two different
450 sets of simulations are produced using MadGraph 5 [Madgraph] - one which simulates these
451 two processes independently, and another where they are produced simultaneously, such that
452 interference effects are present. These two sets of samples are then compared, and the difference
453 between them can be taken to represent any interference effects.

454 MadGraph simulations of 10,000 tZ and 10,000 WZ + b-jet events are produced, along with
455 20,000 events where both are present, in the fiducial region where three leptons and at least one
456 jet are produced.

457 A selection mimicking the preselection used in the main analysis is applied to the samples: The
458 SS leptons are required to have $p_T > 20$ GeV, and > 10 GeV is required for the OS lepton. The
459 associated b-jet is required to have $p_T > 25$ GeV, and all physics objects are required to fall in a
460 range of $|\eta| < 2.5$.

461 The kinematics of these samples after the selection has been applied are shown below:

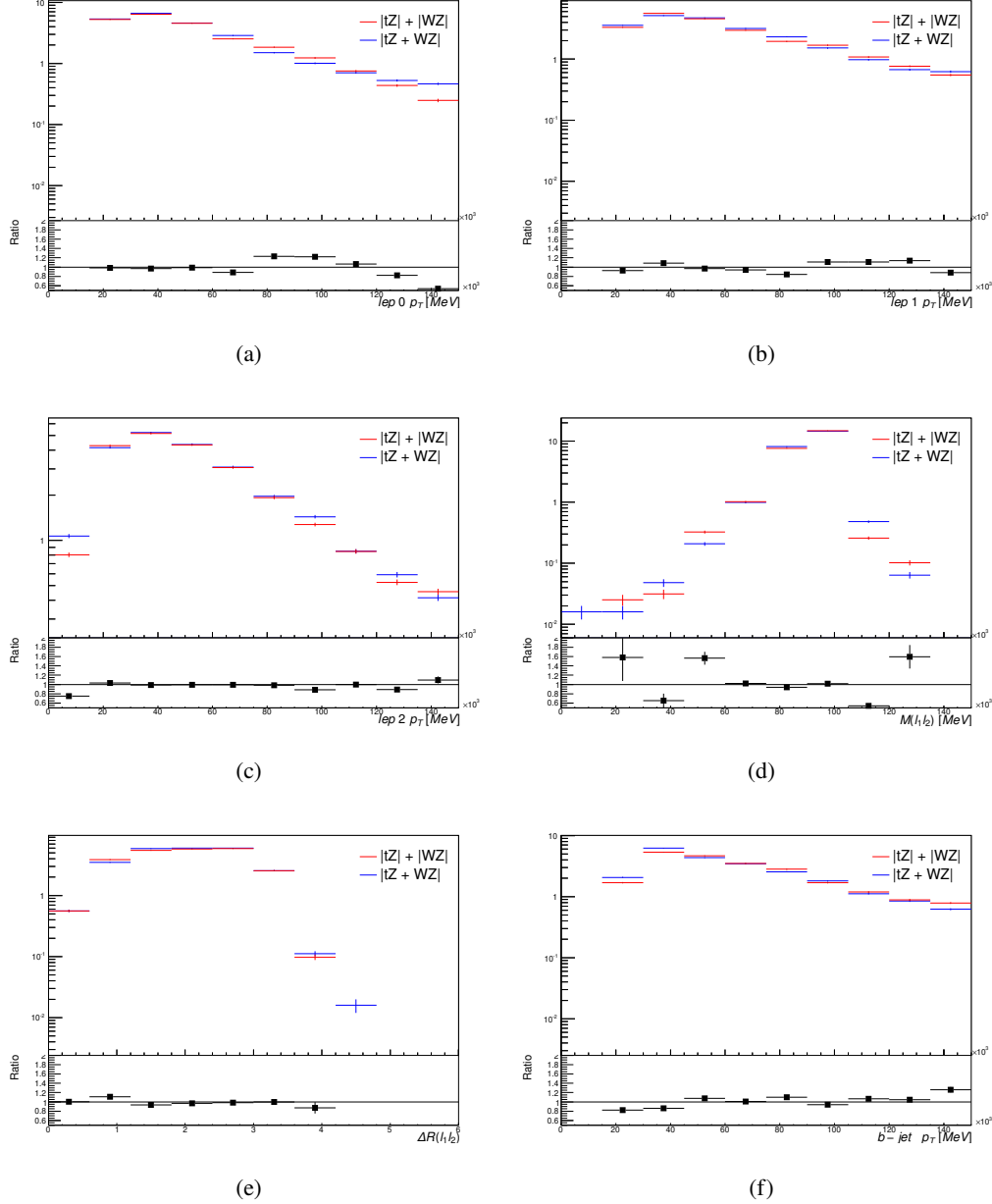


Figure 29: Comparisons between (a) the p_T of the lepton from the W, (b) and (c) show the p_T of the lepton from the Z, (d) the invariant mass of the Z-candidate, (e) ΔR of the leptons from the Z, and (f) the p_T of the b-jet, for WZ and tZ events generated with interference effects (blue) and without interference effects (red).

462 The overall cross-section of the two methods agree within error, and no significant differences
463 in the kinematic distributions are seen. It is therefore concluded that interference effects do not

⁴⁶⁴ significantly impact the results.

⁴⁶⁵ 7 Systematic Uncertainties

⁴⁶⁶ The systematic uncertainties that are considered are summarized in Table 4. These are imple-
⁴⁶⁷ mented in the fit either as a normalization factors or as a shape variation or both in the signal
⁴⁶⁸ and background estimations. The numerical impact of each of these uncertainties is outlined in
⁴⁶⁹ Section 9.

Table 9: Sources of systematic uncertainty considered in the analysis.

Systematic uncertainty	Components
Luminosity	1
Pileup reweighting	1
Physics Objects	
Electron	6
Muon	15
Jet energy scale	28
Jet energy resolution	8
Jet vertex fraction	1
Jet flavor tagging	131
E_T^{miss}	3
Total (Experimental)	194
Signal Modeling	
Shape modelling	3
Renormalization and factorization scales	5
nJet Migration	5
Background Modeling	
Cross section	15
Renormalization and factorization scales	12
Parton shower and hadronization model	2
Shower tune	4
Total (Signal and background modeling)	41
Total (Overall)	236

⁴⁷⁰ The uncertainty in the combined 2015–2018 integrated luminosity is 1.7% [23], obtained using
⁴⁷¹ the LUCID-2 detector [24] for the primary luminosity measurements.

⁴⁷² The experimental uncertainties are related to the reconstruction and identification of light
⁴⁷³ leptons and b-tagging of jets, and to the reconstruction of E_T^{miss} . The TOTAL electron ID

474 correlation model is used, corresponding to 1 electron ID systematic. Electron ID is found to be
475 a subleading systematic that is unconstrained by the fit, making it an appropriate choice for this
476 analysis.

477 The sources which contribute to the uncertainty in the jet energy scale (JES) [25] are decom-
478 posed into uncorrelated components and treated as independent sources in the analysis. The
479 CategoryReduction model is used to account for JES uncertainties, which decomposes the uncer-
480 tainties into 30 nuisance parameters included in the fit. The SimpleJER model is used to account
481 for jet energy resolution (JER) uncertainties, and 8 JER uncertainty components included as NPs
482 in the fit.

483 The uncertainties in the b-tagging efficiencies measured in dedicated calibration analyses
484 [26] are also decomposed into uncorrelated components. The large number of components for
485 b-tagging is due to the calibration of the distribution of the MVA discriminant.

486 The full list of systematic uncertainties considered in the analysis is summarized in Tables ??,
487 ?? and ??.

488

Experimental Systematics on Leptons and E_T^{miss}			
Type	Description	Systematics Name	Application
Trigger			
Scale Factors	Trigger Efficiency	lepSFTrigTight_MU(EL)_SF_Trigger_STAT(SYST)	Event Weight
Muons			
Efficiencies	Reconstruction and Identification	lepSFObjTight_MU_SF_ID_STAT(SYST)	Event Weight
	Isolation	lepSFObjTight_MU_SF_Isol_STAT(SYST)	Event Weight
	Track To Vertex Association	lepSFObjTight_MU_SF_TTVA_STAT(SYST)	Event Weight
p_T Scale	p_T Scale	MUONS_SCALE	p_T Correction
Resolution	Inner Detector Energy Resolution	MUONS_ID	p_T Correction
	Muon Spectrometer Energy Resolution	MUONS_MS	p_T Correction
Electrons			
Efficiencies	Reconstruction	lepSFObjTight_EL_SF_ID	Event Weight
	Identification	lepSFObjTight_EL_SF_Reco	Event Weight
	Isolation	lepSFObjTight_EL_SF_Isol	Event Weight
Scale Factor	Energy Scale	EG_SCALE_ALL	Energy Correction
Resolution	Energy Resolution	EG_RESOLUTION_ALL	Energy Correction
E_T^{miss}			
Soft Tracks Terms	Resolution	MET_SoftTrk_ResoPerp	p_T Correction
	Resolution	MET_SoftTrk_ResoPara	p_T Correction
	Scale	MET_SoftTrk_ScaleUp	p_T Correction
	Scale	MET_SoftTrk_ScaleDown	p_T Correction

Table 10: Summary of experimental systematics considered for leptons and E_T^{miss} . Includes type, description, name of systematic as used in the fit, and mode of application. The mode of application indicates the systematic evaluation, e.g. as an overall event re-weighting (Event Weight) or rescaling (p_T Correction).

Experimental Systematics on Jets			
Type	Origin	Systematics Name	Application
Jet Vertex Tagger		JVT	Event Weight
Energy Scale	Calibration Method	JET_21NP_ JET_EffectiveNP_1-19	p_T Correction p_T Correction
	η inter-calibration	JET_EtaIntercalibration_Modelling JET_EtaIntercalibration_NonClosure JET_EtaIntercalibration_TotalStat	p_T Correction p_T Correction p_T Correction
	High p_T jets	JET_SingleParticle_HighPt	p_T Correction
	Pile-Up	JET_Pileup_OffsetNPV JET_Pileup_OffsetMu JET_Pileup_PtTerm JET_Pileup_RhoTopology	p_T Correction p_T Correction p_T Correction p_T Correction
	Non Closure	JET_PunchThrough_MC15	p_T Correction
	Flavour	JET_Flavor_Response JET_BJES_Response JET_Flavor_Composition	p_T Correction p_T Correction p_T Correction
Resolution		JET_JER_SINGLE_NP	Event Weight

Table 11: Jet systematics take into account effects of jets calibration method, η inter-calibration, high p_T jets, pile-up, and flavor response. They are all diagonalised into effective parameters.

Experimental Systematics on b-tagging		
Type	Origin	Systematic Name
Scale Factors	DL1r b-tagger efficiency on b originated jets in bins of η	DL1r_Continuous_EventWeight_B0-29
	DL1r b-tagger efficiency on c originated jets in bins of η	DL1r_Continuous_EventWeight_C0-19
	DL1r b-tagger efficiency on light flavoured originated jets in bins of η and p_T	DL1r_Continuous_EventWeight_Light0-79
	DL1r b-tagger extrapolation efficiency	DL1r_Continuous_EventWeight_extrapolation DL1r_Continuous_EventWeight_extrapolation_from_charm

Table 12: Summary of experimental systematics to be included for b-tagging of jets in the analysis, using the continuous DL1r tagging algorithm. All of the b-tagging related systematics are applied as event weights. From left: type, description, and the name of systematic used in the fit.

489 Theoretical uncertainties applied to MC predictions, including cross section, PDF, and scale
 490 uncertainties are taken from theory calculations, with the exception of non-prompt and diboson
 491 backgrounds. The cross-section uncertainty on tZ is taken from [27]. Derivation of the non-
 492 prompt background uncertainties, Z+jets and tt}, are explained in detail in Section 7.3. These
 493 normalization uncertainties are chosen so as to account for the complete uncertainty in the
 494 non-prompt contribution, and therefore no additional modelling uncertainties are considered for
 495 Z+jets and tt}.

496 The other VV + heavy flavor processes (namely VV+b and VV+charm, which primarily consist
 497 of ZZ events) are also poorly understood, because these processes involve the same physics as
 498 WZ + heavy flavor, and have also not been measured. Therefore, a conservative 50% uncertainty
 499 is applied to those samples. While this uncertainty is large, it is found to have little impact on
 500 the significance of the final result.

501 The theory uncertainties applied to the predominate background estimates are summarized in
 502 Table 5.

Process	X-section [%]
tZ	X-sec: ± 15.2 QCD Scale: $^{+5.2}_{-1.3}$ PDF($+\alpha_S$): ± 1.2
t̄t H (aMC@NLO+Pythia8)	QCD Scale: $^{+5.8}_{-9.2}$ PDF($+\alpha_S$): ± 3.6
t̄t Z (aMC@NLO+Pythia8)	QCD Scale: $^{+9.6}_{-11.3}$ PDF($+\alpha_S$): ± 4
t̄t W (aMC@NLO+Pythia8)	QCD Scale: $^{+12.9}_{-11.5}$ PDF($+\alpha_S$): ± 3.4
VV + b/charm (Sherpa 2.2.1)	± 50
VV + light (Sherpa 2.2.1)	± 6
t̄t	± 20
Z + jets	± 25
Others	± 50

Table 13: Summary of theoretical uncertainties for MC predictions in the analysis.

The fit involves varying the overall normalization of signal templates over the regions described in Section 7.2, which are defined by the flavor and number of associated jets at truth-level. The modelling of these template shapes therefore significantly impacts the final result. Additional signal uncertainties, probing the shape of the signal templates as well as the rate of migrations between the number of truth-jets and reconstructed jets, are estimated by comparing estimates from the nominal Sherpa WZ samples with alternative WZ samples generated with POWHEG+PYTHIA8 (DSID 361601). Separate systematics are included in the fit for WZ + b, WZ + c and WZ + light, where the distribution among each of the fit regions is varied based on the prediction of the Powheg sample.

The variations in the signal templates are shown in Figures ?? and ???. Each of these plots are normalized to unity in order to capture the relevant differences in shape.

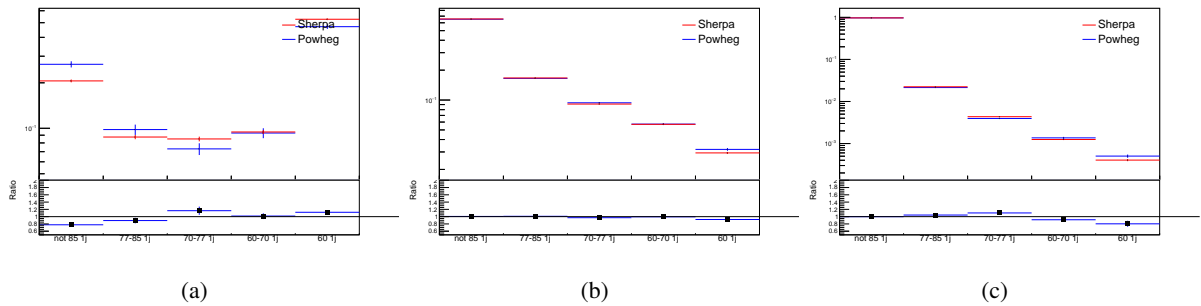


Figure 30: Comparison between Sherpa and Powheg predictions of the distribution of (a) WZ + b, (b) WZ + charm, and (c) WZ + light among the various b-tag WPs used in the 1-jet fit.

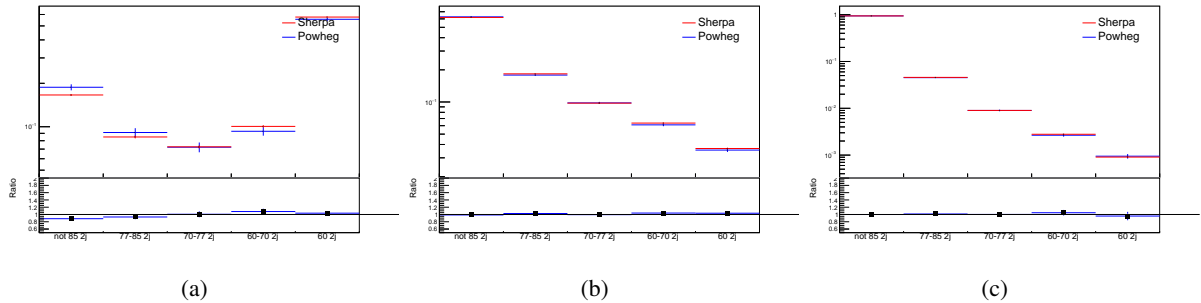


Figure 31: Comparison between Sherpa and Powheg predictions of the distribution of (a) WZ + b, (b) WZ + charm, and (c) WZ + light among the various b-tag WPs used in the 2-jet fit.

514 Separate systematics are included in the fit for WZ + b, WZ + charm and WZ + light, where
515 the distribution among each of the fit regions is varied based on the prediction of the Powheg
516 sample.

517 A similar approach is taken to account for uncertainties in migrations between the number of
 518 reco and truth jets. The fraction of events with 1 truth jet which fall into the 1 jet bin versus the
 519 2 jet bin at reco level is compared for Sherpa and Powheg. The same is done for events with 2
 520 truth jets. This comparison is shown in figure ??.

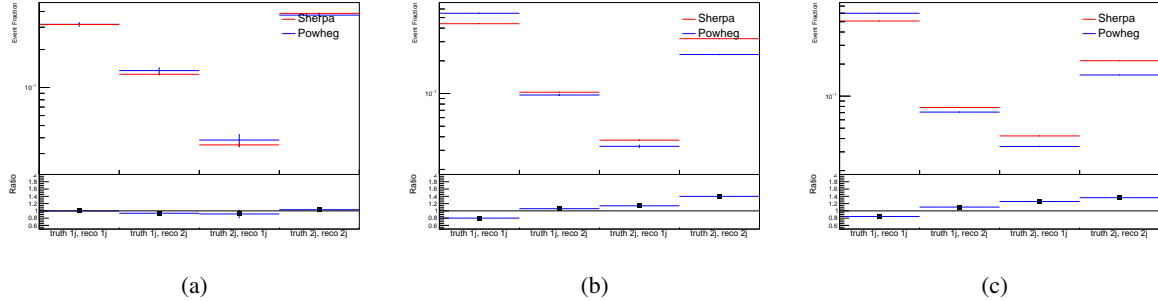


Figure 32: Comparison between Sherpa and Powheg predictions for truth jet migrations between the 1 and 2 jet reco bins for (a) WZ + b, (b) WZ + charm, and (c) WZ + light

521 A systematic is included where events are shifted between the 1-jet and 2-jet regions based on
522 the differences between these two shapes. This is done independently for each of the WZ + b,
523 WZ + charm, and WZ + light templates.

Additional systematics are included to account for the uncertainty in the contamination of 0 jet and 3 or more jet events (at truth level) in the 1 and 2 reco jet bins. Because these events fall

526 outside the scope of this measurement, these events are included as a background. As such, a
 527 normalization, rather than a shape, uncertainty is applied for this background.

528 The number of WZ events with 0-jets and $>=3$ -jets in the reconstructed 1-jet and 2-jet regions
 529 are compared for Sherpa and Powheg, as seen in figure ???. These differences are taken as separate
 530 normalization systematics on the yield of WZ+0-jet and WZ+ $>=3$ -jet events.

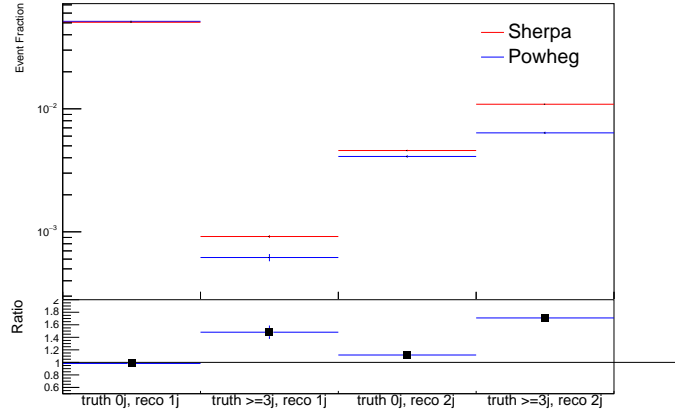


Figure 33: Comparison between Sherpa and Powheg predictions for 0 and $>=3$ truth jet contributions in the 1 and 2 jet reco bins

531 8 Results

532 8.1 Fit Procedure

533 A maximum-likelihood fit is performed over the various fit regions described in Section 7 in
 534 order to extract the best-fit value of the WZ + b-jet and WZ + charm jet contributions for events
 535 with both 1 and 2 associated jets.

536 Because the fit regions are defined by the number of associated jets at reco-level, an unfolding
 537 procedure is applied to the signal in order to account for differences in the number of truth jets
 538 compared to the number of reco-jets. The WZ + b, WZ + charm and WZ + light contributions
 539 are separated into independent samples based on the number of truth jets in each event. WZ + 1
 540 truth-jet and WZ + 2 truth-jets are treated as signal samples, while WZ + 0 truth-jets and WZ +
 541 $>=3$ truth-jets are treated as an additional background.

542 A maximum likelihood fit to data is performed simultaneously in the regions described in Section
 543 7, summarized in figure 2. The six signal templates, which include WZ+b 1-jet, WZ+c 1-jet,
 544 WZ+l 1-jet, WZ+b 2-jets, WZ+c 2-jets, WZ+l 2-jets, are allowed to float, while the remaining
 545 background contributions are held fixed. The parameters $\mu_{WZ+b-1-jet}$, $\mu_{WZ+charm1-jet}$,

546 $\mu_{WZ+\text{light}-1\text{-jet}}$, $\mu_{WZ+b-2\text{-jet}}$, $\mu_{WZ+\text{charm}2\text{-jet}}$, $\mu_{WZ+\text{light}-2\text{-jet}}$, where $\mu = \sigma_{\text{observed}}/\sigma_{\text{SM}}$,
 547 are extracted from the fit. A simultaneous fit is performed over all 1-jet and 2-jet regions.

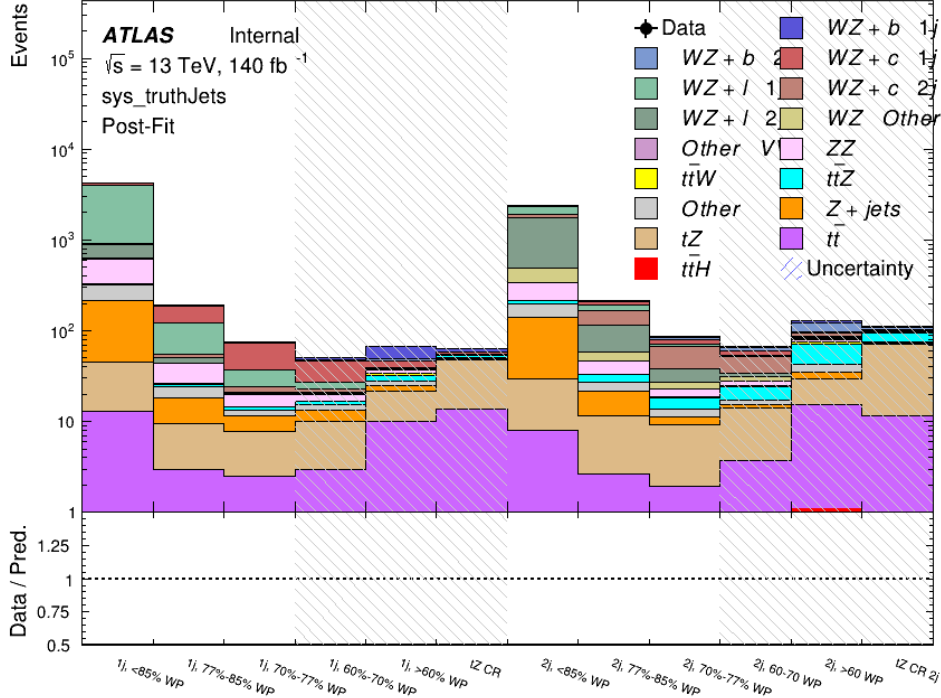


Figure 34: Post-fit summary of the fit regions.

548 As described in Section 8, there are 230 systematic uncertainties that are considered as NPs in
 549 the fit. These NPs are constrained by Gaussian or log-normal probability density functions. The
 550 latter are used for normalisation factors to ensure that they are always positive. The expected
 551 number of signal and background events are functions of the likelihood. The prior for each NP
 552 is added as a penalty term, decreasing the likelihood as it is shifted away from its nominal value.
 553 The correlations between these nuisance parameters are summarized in Figure ??.

554 Several alternative fit strategies are documented in Appendices 9.3-9.4.1. These include a
 555 measurement of $WZ + 1$ or 2 jets inclusively, a fit where tZ is allowed to float, and a case where
 556 tZ is included as part of the signal.

557 8.2 Results of the Simultaneous Fit

558 The Asimov fit for 1-jet events gives an expected μ value of $1.00^{+0.47}_{-0.43}(\text{stat})^{+0.30}_{-0.27}(\text{sys})$ for WZ
 559 + b . The fitted cross-section modifiers for $WZ + \text{charm}$ and $WZ + \text{light}$ are $1.00 \pm 0.17 \pm 0.17$
 560 and $1.00 \pm 0.06 \pm 0.14$, respectively.

561 The expected cross-section of WZ+b with 1-jet is $1.74^{+0.82}_{-0.75}(\text{stat})^{+0.53}_{-0.48}(\text{sys})$ fb, and $14.6 \pm$
 562 $2.5(\text{stat}) \pm 2.3(\text{sys})$ fb for WZ + charm, with a correlation of -0.15 between them. An expected
 563 significance of 2.0 is observed for WZ + b in this region.

564 For 2-jet events, the fit gives an expected μ value of $1.00^{+0.53}_{-0.51}(\text{stat})^{+0.39}_{-0.34}(\text{sys})$ for WZ + b.
 565 The fitted cross-section modifiers for WZ + charm and WZ + light are $1.00 \pm 0.25 \pm 0.21$ and
 566 $1.00 \pm 0.06 \pm 0.16$, respectively.

567 The expected WZ + b cross-section in the 2-jet region is $2.5^{+1.3}_{-1.3}(\text{stat})^{+0.95}_{-0.83}(\text{sys})$ fb with an
 568 expected significance of 1.7σ . The 2-jet expected cross-section of WZ + charm is $12.7 \pm$
 569 $3.2(\text{stat}) \pm 2.7(\text{sys})$ fb, and the correlation between WZ + charm and WZ + b is -0.22.

570 A summary of the correlation between the various WZ components is summarized in Table ??.

571

	WZ + b - 1-jet	WZ + c - 1-jet	WZ + l - 1-jet	WZ + b - 2-jet	WZ + c - 2-jet	WZ + l - 2-jet
WZ + b - 1-jet	1.00	-0.15	0.28	-0.13	-0.22	0.17
WZ + c - 1-jet	-	1.00	0.36	0.13	-0.14	-0.16
WZ + l - 1-jet	-	-	1.00	0.10	-0.20	-0.39
WZ + b - 2-jet	-	-	-	1.00	-0.22	0.17
WZ + c - 2-jet	-	-	-	-	1.00	0.23
WZ + l - 2-jet	-	-	-	-	-	1.00

Table 14: Correlations between the various components of WZ

572 The correlations between the all of the nuisance parameters considered in the fit are summarized
 573 in Figure ??.[a](#)

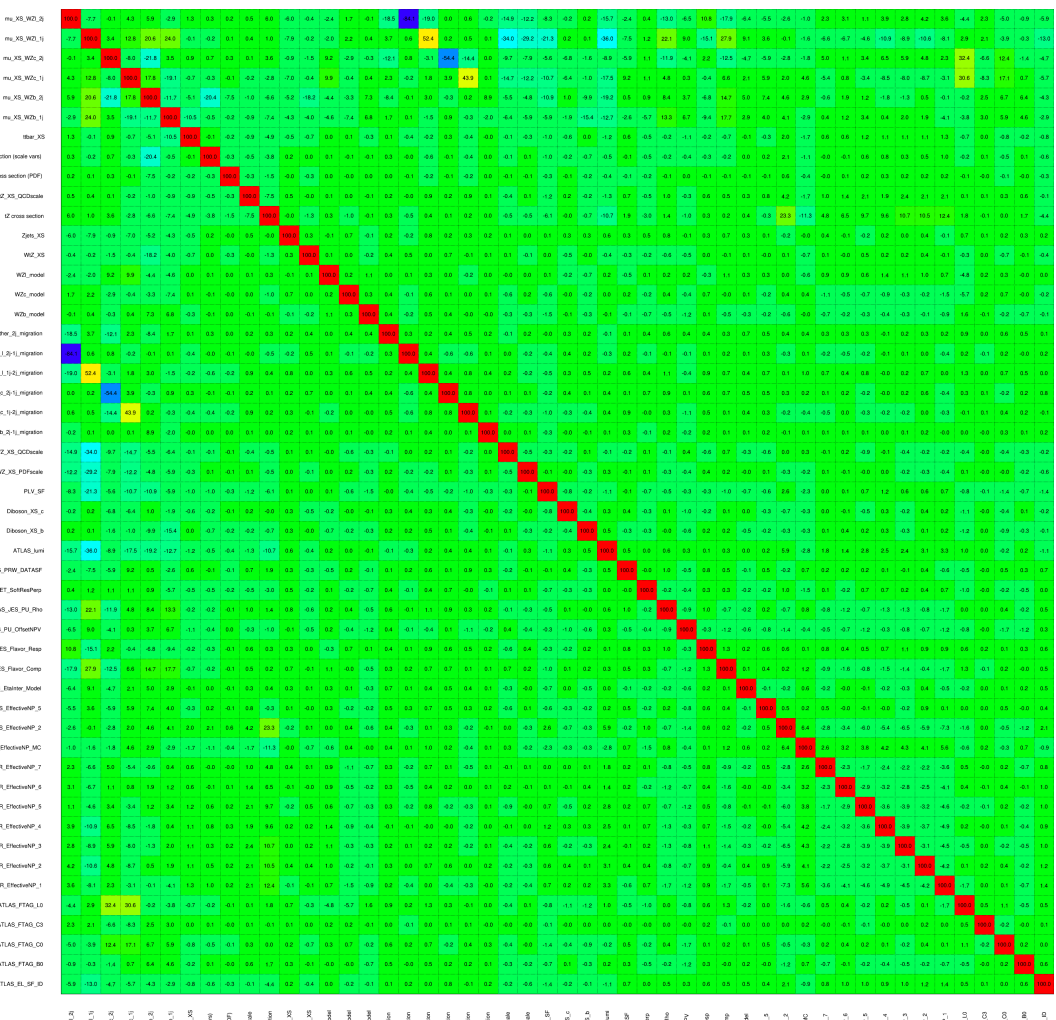


Figure 35: Correlations between nuisance parameters

⁵⁷⁴ The pre-fit yields in each of the 1-jet regions used in the fit are shown in Table ??.

Sample	1j, <85% WP	1j, 77%-85% WP	1j, 70%-77% WP	1j, 60%-70% WP	1j, >60% WP	tZ CR
WZ + b – 1j	8.1 ± 1.6	4.7 ± 0.5	4.6 ± 0.4	5.1 ± 0.4	18.1 ± 2.4	5.0 ± 0.6
WZ + c – 1j	260 ± 22	81 ± 6	43.1 ± 3.6	25.8 ± 2.6	9.4 ± 1.8	2.9 ± 0.6
WZ + l – 1j	3090 ± 250	91 ± 13	17 ± 3	4.9 ± 1.6	1.3 ± 0.4	0.2 ± 0.1
WZ + b – 2j	1.10 ± 0.37	0.44 ± 0.11	0.39 ± 0.06	0.62 ± 0.14	2.1 ± 0.5	0.59 ± 0.14
WZ + c – 2j	21 ± 5	5.6 ± 1.2	3.0 ± 0.7	2.0 ± 0.5	0.70 ± 0.20	0.30 ± 0.08
WZ + l – 2j	250 ± 60	5.7 ± 1.6	0.73 ± 0.53	0.31 ± 0.15	0.07 ± 0.06	0.01 ± 0.01
WZ – Other	13 ± 5	1.4 ± 0.4	0.42 ± 0.08	0.2 ± 0.01	0.30 ± 0.05	0.67 ± 0.15
Other VV	6.2 ± 0.6	0.2 ± 0.4	0.2 ± 0.04	0.07 ± 0.1	0.1 ± 0.1	0.1 ± 0.2
ZZ	336 ± 26	17.8 ± 2.1	4.3 ± 0.6	1.7 ± 0.5	0.36 ± 0.08	0.10 ± 0.03
t <bar>t>W</bar>	1.1 ± 0.2	0.2 ± 0.1	0.3 ± 0.1	0.4 ± 0.1	1.5 ± 0.3	0.7 ± 0.2
t <bar>t>Z</bar>	6.8 ± 1.2	1.4 ± 0.3	1.0 ± 0.2	1.2 ± 0.2	4.4 ± 0.8	3.2 ± 0.6
Z + jets	169 ± 38	8.9 ± 1.9	3.7 ± 0.8	3.3 ± 0.7	3.2 ± 0.7	0.8 ± 0.17
V + γ	45 ± 28	1.9 ± 2.4	0.1 ± 0.1	0.02 ± 0.01	1.0 ± 0.9	0.02 ± 0.03
tZ	31.8 ± 4.3	6.4 ± 1.1	5.3 ± 0.8	7.2 ± 1.1	11.8 ± 2.0	33.9 ± 4.5
tW	1.4 ± 0.8	0.2 ± 0.5	0.0 ± 0.2	0.7 ± 0.6	0.26 ± 0.42	0.39 ± 0.41
WtZ	2.3 ± 1.2	0.6 ± 0.3	0.3 ± 0.21	0.27 ± 0.2	1.1 ± 0.7	0.6 ± 0.5
VVV	12.4 ± 0.5	0.93 ± 0.06	0.35 ± 0.03	0.13 ± 0.02	0.14 ± 0.03	0.02 ± 0.01
VH	40 ± 6	2.6 ± 1.4	0.9 ± 0.8	0.7 ± 0.8	0.5 ± 0.6	0.0 ± 0.0
t <bar>t></bar>	12.1 ± 1.6	2.9 ± 0.6	2.5 ± 0.5	2.8 ± 0.5	11.2 ± 1.4	10.9 ± 1.5
t <bar>t>H</bar>	0.24 ± 0.03	0.05 ± 0.01	0.04 ± 0.01	0.06 ± 0.01	0.20 ± 0.03	0.13 ± 0.02
Total	5010 ± 260	227 ± 24	88 ± 12	57 ± 8	76 ± 16	53 ± 8

Table 15: Pre-fit yields in each of the 1-jet regions.

⁵⁷⁶ The post-fit yields in each region are summarized in Figure ??.

⁵⁷⁷

	1j, <85% WP	1j, 77%-85% WP	1j, 70%-77% WP	1j, 60%-70% WP	1j, >60% WP	tZ CR
WZ + b - 1j	8.1 ± 4.9	4.7 ± 2.0	4.6 ± 2.0	5.1 ± 2.1	18 ± 10	5.0 ± 2.5
WZ + c - 1j	260 ± 60	80 ± 14	43 ± 7	26 ± 5	7.4 ± 2.3	2.1 ± 0.7
WZ + l - 1j	3090 ± 130	90 ± 11	17.3 ± 2.8	4.9 ± 1.6	1.3 ± 0.4	0.23 ± 0.13
WZ + b - 2j	1.10 ± 0.37	0.44 ± 0.11	0.39 ± 0.06	0.62 ± 0.14	2.1 ± 0.5	0.59 ± 0.14
WZ + c - 2j	21 ± 5	5.6 ± 1.2	3.0 ± 0.7	2.0 ± 0.5	0.70 ± 0.20	0.30 ± 0.08
WZ + l - 2j	250 ± 60	5.7 ± 1.6	0.73 ± 0.53	0.31 ± 0.15	0.07 ± 0.06	0.01 ± 0.01
WZ - Other	13 ± 5	1.4 ± 0.4	0.42 ± 0.08	0.2 ± 0.01	0.30 ± 0.05	0.67 ± 0.15
Other VV	6.2 ± 0.6	0.92 ± 0.07	0.02 ± 0.01	0.01 ± 0.01	0.01 ± 0.01	0.01 ± 0.01
ZZ	346 ± 57	19 ± 5	4.3 ± 0.8	2.7 ± 0.5	2.4 ± 0.1	2.1 ± 0.6
t̄W	1.09 ± 0.21	0.2 ± 0.1	0.1 ± 0.1	0.4 ± 0.1	1.5 ± 0.3	0.1 ± 0.2
t̄Z	6.8 ± 1.2	1.4 ± 0.3	1.0 ± 0.2	1.2 ± 0.2	4.4 ± 0.7	3.2 ± 0.5
rare Top	0.14 ± 0.04	0.04 ± 0.02	0.04 ± 0.0	0.1 ± 0.03	0.14 ± 0.04	0.15 ± 0.05
t̄WW	0.04 ± 0.03	0.01 ± 0.02	0.01 ± 0.01	0.01 ± 0.01	0.01 ± 0.02	0.01 ± 0.01
Z + jets	169 ± 37	8.9 ± 1.9	3.7 ± 0.8	3.3 ± 0.7	3.2 ± 0.7	0.8 ± 0.2
W + jets	0.01 ± 0.01					
V + γ	46 ± 28	1.9 ± 2.4	0.1 ± 0.1	0.0 ± 0.2	1.0 ± 0.9	0.0 ± 0.0
tZ	31 ± 4	6.0 ± 1.0	5.3 ± 0.8	7.2 ± 1.0	11.8 ± 1.8	33.9 ± 4.5
tW	1.37 ± 0.82	0.18 ± 0.26	0.01 ± 0.12	0.67 ± 0.64	0.26 ± 0.42	0.39 ± 0.41
WtZ	2.3 ± 1.2	0.6 ± 0.3	0.3 ± 0.2	0.3 ± 0.2	1.1 ± 0.6	0.6 ± 0.3
VVV	12.4 ± 0.4	0.9 ± 0.1	0.4 ± 0.1	0.13 ± 0.02	0.14 ± 0.03	0.02 ± 0.01
VH	40 ± 6	2.6 ± 1.4	0.9 ± 0.8	0.7 ± 0.8	0.4 ± 0.6	0.01 ± 0.01
t̄t	12.1 ± 1.6	2.9 ± 0.6	2.5 ± 0.5	2.8 ± 0.5	11.2 ± 1.5	10.9 ± 1.4
t̄tH	0.24 ± 0.03	0.05 ± 0.01	0.04 ± 0.01	0.06 ± 0.01	0.20 ± 0.03	0.13 ± 0.02
Total	5100 ± 110	227 ± 12	87 ± 6	56.7 ± 4.4	76 ± 9	52.5 ± 4.2

Table 16: Post-fit yields in each of the 1-jet regions.

578 The impact of each NP is calculated by performing the fit with the parameter of interest held
 579 fixed, varied from its fitted value by its uncertainty, and calculating $\Delta\mu$ relative to the baseline
 580 fit. The impact of the most significant sources of systematic uncertainties on WZ + b with one
 581 associated jet is summarized in Table ??.

Uncertainty Source	$\Delta\mu$	
WZ + 1-jet light cross-section	0.13	-0.15
WZ + 1-jet charm cross-section	-0.10	0.12
Jet Energy Scale	0.1	-0.13
Other Diboson + b cross-section	-0.09	0.09
tZ cross-section	-0.08	0.08
WZ 1-jet/2-jet Migration	0.08	-0.07
Jet Energy Resolution	-0.07	0.08
Luminosity	-0.06	0.07
Flavor tagging	0.05	0.05
t <bar>t} cross-section</bar>	-0.05	0.05
Total Systematic Uncertainty	0.28	0.33

Table 17: Summary of the most significant sources of systematic uncertainty on the measurement of WZ + b with exactly one associated jet.

Uncertainty Source	$\Delta\sigma/\sigma_{\text{nominal}}$	
WZ + c 1j/2j migration	0.12	-0.09
Flavor Tagging	0.09	0.08
WZ + b, 1-jet cross-section	-0.04	0.05
Luminosity	-0.04	0.04
Jet Energy Resolution	0.04	0.04
WZ + b, 2-jet cross-section	0.04	-0.03
WZ cross-section - QCD scale	-0.04	0.04
Jet Energy Scaling	0.04	0.02
WZ cross-section - PDF	-0.03	0.03
WZ + light, 1-jet cross-section	0.03	-0.03
total	0.1879	0.1753

Table 18: Summary of the most significant sources of systematic uncertainty on the measurement of WZ + c with exactly one associated jet.

⁵⁸² The ranking and impact of those nuisance parameters with the largest contribution to the overall
⁵⁸³ uncertainty is shown in Figure ??.

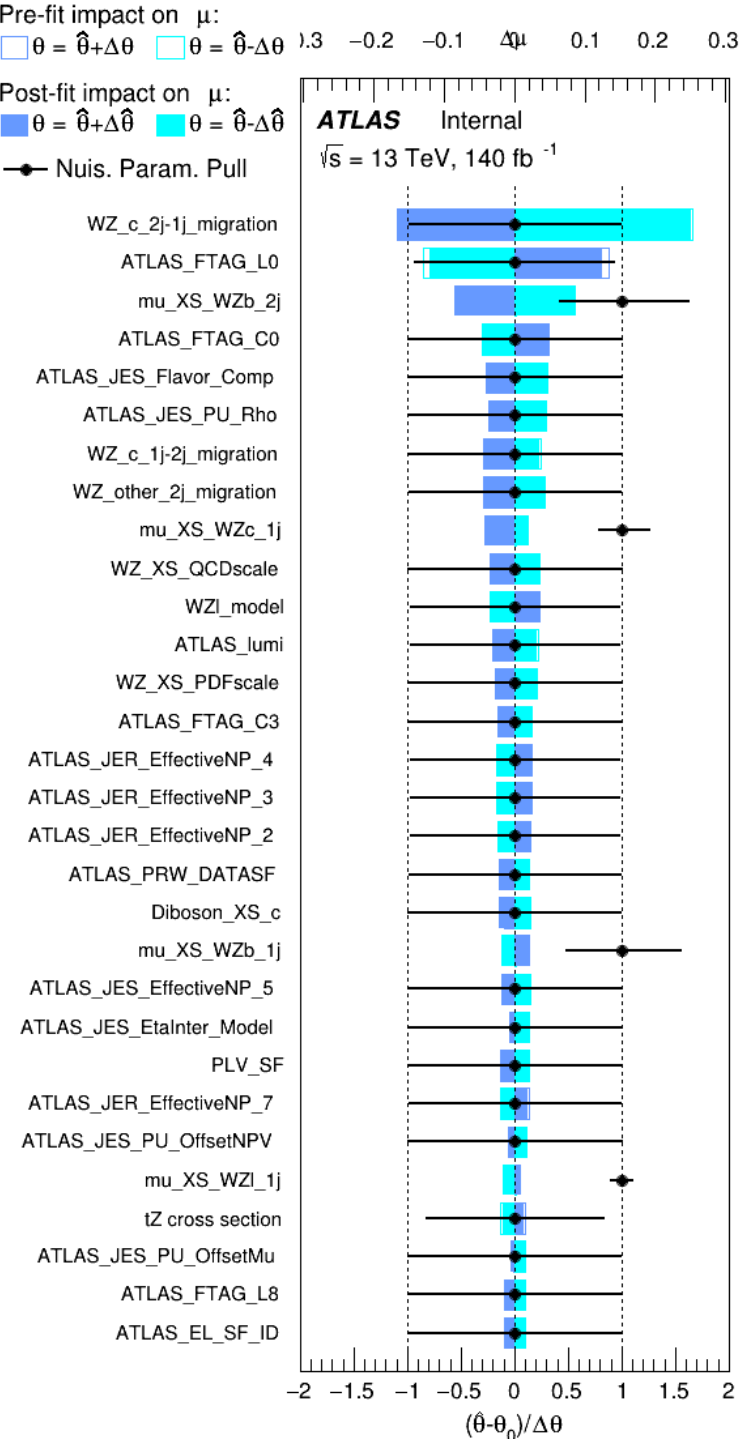


Figure 36: Impact of systematic uncertainties on the signal-strength of $WZ + b$ for events with exactly one jet

584 The large impact of the Jet Energy Scale and Jet Flavor Tagging is unsurprising, as the shape of
 585 the fit regions depends heavily on the modeling of the jets. The other major sources of uncertainty
 586 come from background modelling and cross-section uncertainty.

587 Pre-fit yields in each of the 2-jet fit are shown in Figure ??.

	2j, <85% WP	2j, 77%-85% WP	2j, 70%-77% WP	2j, 60%-70% WP	2j, >60% WP	tZ CR 2j
WZ + b - 2j	3.1 ± 1.6	6.7 ± 0.5	5.6 ± 0.4	8.0 ± 0.6	24 ± 2	5 ± 1
WZ + c - 2j	180 ± 20	54 ± 6	41 ± 3	24 ± 3	17 ± 2	7.0 ± 0.6
WZ + l - 2j	1250 ± 150	90 ± 14	18 ± 3	5.8 ± 1.4	1.4 ± 0.4	0.25 ± 0.15
WZ + b - 1j	3.4 ± 0.6	1.52 ± 0.35	1.58 ± 0.23	1.95 ± 0.39	7.8 ± 1.1	0.8 ± 0.6
WZ + c - 1j	56 ± 14	17.6 ± 4.0	8.6 ± 2.2	6.3 ± 1.8	3.0 ± 0.9	0.7 ± 0.2
WZ + l - 1j	427 ± 120	24 ± 7	4.7 ± 2.3	1.6 ± 0.7	0.3 ± 0.2	0.01 ± 0.01
WZ - Other	129 ± 29	6.1 ± 4.6	1.2 ± 0.3	0.3 ± 0.2	2.9 ± 0.5	3.6 ± 0.6
Other VV	7.63 ± 0.63	0.6 ± 0.5	0.16 ± 0.03	0.01 ± 0.01	0.1 ± 0.1	0.1 ± 0.1
ZZ	135 ± 20	14.1 ± 3.2	4.7 ± 0.8	4.0 ± 0.6	4.1 ± 0.7	3.1 ± 0.5
t̄W	0.8 ± 0.2	0.4 ± 0.1	0.5 ± 0.1	0.7 ± 0.2	4.3 ± 0.6	3.9 ± 0.6
t̄Z	14.7 ± 2.2	5.6 ± 0.8	4.5 ± 0.7	6.5 ± 1.1	25.4 ± 4.0	21.9 ± 3.4
rare Top	0.14 ± 0.04	0.07 ± 0.03	0.03 ± 0.02	0.09 ± 0.03	0.37 ± 0.07	0.6 ± 0.1
t̄WW	0.04 ± 0.03	0.02 ± 0.02	0.01 ± 0.01	0.01 ± 0.00	0.03 ± 0.03	0.01 ± 0.01
Z + jets	110.0 ± 22.9	9.6 ± 2.0	2.1 ± 0.50	1.6 ± 0.4	5.1 ± 1.1	1.5 ± 0.3
W + jets	0.0 ± 0.0	0.0 ± 0.0	0.0 ± 0.0	0.0 ± 0.0	0.0 ± 0.0	0.0 ± 0.0
V + γ	25 ± 18	0.5 ± 0.2	0.1 ± 0.1	0.1 ± 0.1	0.0 ± 0.02	0.05 ± 0.07
tZ	21.9 ± 2.9	9.6 ± 1.3	9.1 ± 1.0	10.0 ± 1.5	14.7 ± 3.2	60 ± 6
tW	0.9 ± 0.7	0.2 ± 0.3	0.0 ± 0.1	0.0 ± 0.0	0.8 ± 0.6	0.2 ± 0.2
WtZ	4.9 ± 2.5	1.5 ± 0.8	1.1 ± 0.6	1.3 ± 0.7	4.6 ± 2.4	3.3 ± 1.7
VVV	7.4 ± 0.3	1.0 ± 0.1	0.4 ± 0.1	0.2 ± 0.1	0.13 ± 0.03	0.04 ± 0.01
VH	19.5 ± 4.2	2.8 ± 1.6	0.7 ± 0.7	0.1 ± 0.2	0.0 ± 0.0	0.0 ± 0.0
t̄t	0.7 ± 0.4	0.1 ± 0.1	0.05 ± 0.06	0.15 ± 0.13	0.8 ± 0.5	2.3 ± 1.2
t̄t̄	6.8 ± 1.0	2.4 ± 0.5	1.8 ± 0.4	3.3 ± 0.6	8.4 ± 1.2	13.6 ± 1.7
t̄tH	0.4 ± 0.1	0.2 ± 0.1	0.16 ± 0.02	0.23 ± 0.03	0.94 ± 0.11	1.03 ± 0.12
Total	2580 ± 160	229 ± 24	89 ± 13	69 ± 11	120 ± 15	108 ± 11

Table 19: Pre-fit yields in each of the 2-jet regions.

588 The post-fit yields in each region are summarized in Figure ??.

	2j, <85% WP	2j, 77%-85% WP	2j, 70%-77% WP	2j, 60%-70% WP	2j, >60% WP	tZ CR 2j
WZ + b	13 ± 6	6.7 ± 2.9	5.8 ± 2.5	8.0 ± 3.5	31 ± 13	14 ± 5
WZ + c	260 ± 60	77 ± 15	41 ± 8	26 ± 5	10.9 ± 2.4	4.8 ± 1.1
WZ + l	1860 ± 90	90 ± 12	17.6 ± 2.8	5.8 ± 1.3	1.4 ± 0.4	0.3 ± 0.2
WZ + b - 1j	3.4 ± 0.6	1.52 ± 0.35	1.58 ± 0.23	1.95 ± 0.39	6.7 ± 1.1	1.9 ± 0.6
WZ + c - 1j	56 ± 14	17.6 ± 4.0	8.6 ± 2.2	6.3 ± 1.8	3.0 ± 0.9	0.7 ± 0.2
WZ + l - 1j	427 ± 120	24 ± 7	4.7 ± 2.3	1.6 ± 0.7	0.3 ± 0.2	0.01 ± 0.01
WZ - Other	129 ± 29	6.1 ± 4.6	1.2 ± 0.3	0.3 ± 0.2	2.9 ± 0.5	3.6 ± 0.6
Other VV	7.6 ± 0.6	0.3 ± 0.3	0.3 ± 0.1	0.1 ± 0.06	0.03 ± 0.02	0.1 ± 0.1
ZZ	145 ± 30	11.3 ± 4.4	2.7 ± 1.6	1.0 ± 0.3	4.0 ± 0.1	2.4 ± 0.1
t̄tW	0.8 ± 0.2	0.4 ± 0.1	0.54 ± 0.12	0.74 ± 0.15	4.3 ± 0.6	3.9 ± 0.6
t̄tZ	14.7 ± 2.2	5.6 ± 0.8	4.5 ± 0.7	6.5 ± 1.0	25.4 ± 3.9	21.9 ± 3.3
rare Top	0.14 ± 0.04	0.07 ± 0.03	0.03 ± 0.02	0.09 ± 0.03	0.4 ± 0.1	0.6 ± 0.1
t̄tWW	0.04 ± 0.03	0.02 ± 0.02	0.01 ± 0.01	0.01 ± 0.01	0.03 ± 0.03	0.01 ± 0.01
Z + jets	110 ± 23	9.6 ± 2.0	2.1 ± 0.5	1.6 ± 0.4	5.1 ± 1.1	1.5 ± 0.3
W + jets	0.0 ± 0.0					
V + γ	25 ± 19	0.5 ± 0.2	0.1 ± 0.1	0.13 ± 0.14	0.0 ± 0.02	0.05 ± 0.07
tZ	21.9 ± 2.7	9.6 ± 1.2	7.1 ± 0.9	10.0 ± 1.4	14.7 ± 3.0	60 ± 6
tW	0.1 ± 0.7	0.2 ± 0.3	0.0 ± 0.1	0.0 ± 0.0	0.8 ± 0.6	0.2 ± 0.2
WtZ	4.9 ± 2.5	1.5 ± 0.8	1.1 ± 0.6	1.3 ± 0.7	4.6 ± 2.3	3.3 ± 1.7
VVV	7.4 ± 0.3	1.0 ± 0.1	0.36 ± 0.03	0.19 ± 0.03	0.13 ± 0.03	0.04 ± 0.01
VH	19 ± 4	2.8 ± 1.6	0.7 ± 0.7	0.1 ± 0.2	0.0 ± 0.0	0.0 ± 0.0
t̄t	6.8 ± 1.0	2.4 ± 0.5	1.8 ± 0.4	3.3 ± 0.6	8.4 ± 1.2	13.6 ± 1.7
t̄tH	0.40 ± 0.05	0.19 ± 0.03	0.16 ± 0.02	0.23 ± 0.03	0.94 ± 0.11	1.03 ± 0.11
Total	2580 ± 60	229 ± 11	89 ± 6	69.1 ± 4.1	120 ± 10	108 ± 6

Table 20: Post-fit yields in each of the 2-jet regions.

589 The same set of systematic uncertainties consider for the 1-jet fit are included in the 2-jet fit as
 590 well. The impact of the most significant systematic uncertainties is summarized in Table ??.

Uncertainty Source	$\Delta\mu$	
WZ + c 2-jet cross-section	-0.13	0.16
WZ + l 2-jet cross-section	0.12	-0.09
ttZ cross-section - QCD scale	-0.10	0.13
WZ + b 1-jet cross-section	-0.11	0.10
Jet Energy Scale	-0.11	0.11
Luminosity	-0.11	0.12
tZ cross-section	-0.11	0.11
WtZ cross-section	-0.07	0.07
Flavor tagging	0.05	0.05
Other VV + b cross-section	-0.05	0.05
Total	0.35	0.37

Table 21: Summary of the most significant sources of systematic uncertainty on the measurement of WZ + b 2-jet events.

Uncertainty Source	$\Delta\sigma/\sigma_{\text{nominal}}$	
WZ + c 1j/2j migration	-0.17	0.25
Flavor Tagging	0.14	0.13
WZ + b, 1-jet cross-section	-0.09	0.09
Jet Energy Scale	0.06	0.08
Jet Energy Resolution	0.05	0.05
WZ $\geq 3j/2j$ migration	-0.04	0.04
WZ + c 2j/1j migration	-0.04	0.04
WZ cross-section - QCD scale	-0.04	0.04
WZ + light modelling	0.04	-0.03
Luminosity	-0.03	0.03
total	0.2694	0.3274

Table 22: Summary of the most significant sources of systematic uncertainty on the measurement of WZ + c with 2 associated jets.

⁵⁹¹ The ranking and impact of those nuisance parameters with the largest contribution to the overall
⁵⁹² uncertainty is shown in Figure ??.

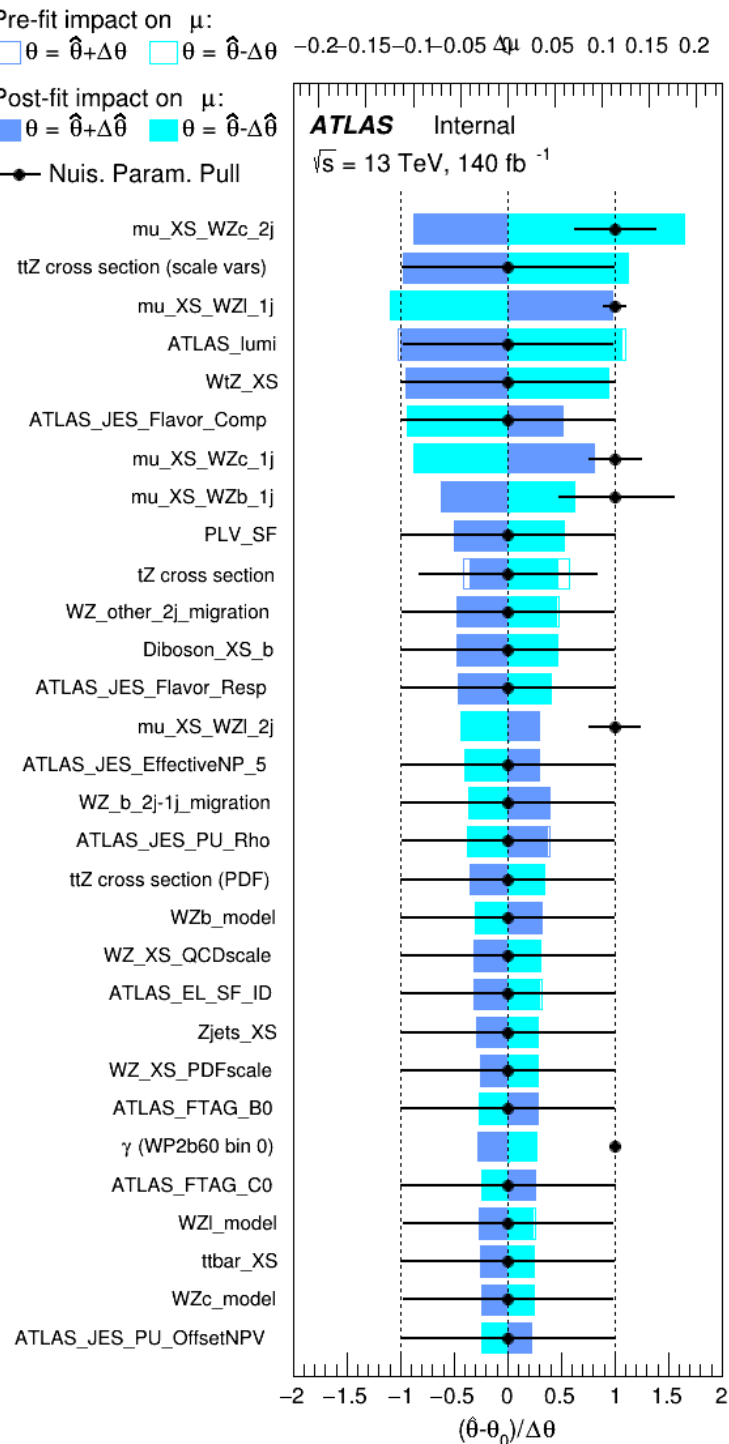


Figure 37: Impact of systematic uncertainties on the signal-strength of WZ + b in 2-jet events.

593 The large impact of the Jet Energy Scale and Jet Flavor Tagging is unsurprising, as the shape of
594 the fit regions depends heavily on the modeling of the jets. The other major sources of uncertainty
595 come from background modelling and cross-section uncertainty.

596 **8.3 Inclusive 1+2 Jet Fit**

597 An alternative fit is performed which combines the WZ + 1-jet and WZ + 2-jet samples rather than
598 fitting them independently. This is done primarily as a cross-check of the nominal analysis, to
599 see if measuring 1-jet and 2-jet events separately and combining them gives drastically different
600 results than measuring them together.

601 For this study, three signal templates, WZ + b, WZ + charm and WZ + light, are fit to data, and
602 the systematics accounting for migrations between 1-jet and 2-jet bins are removed. All other
603 background and nuisance parameters remain the same as the nominal fit.

604 The measured μ value for WZ + b is $\mu = 1.00^{+0.30}_{-0.29}(\text{stat})^{+0.25}_{-23}(\text{sys})$, with a significance of 2.8σ ,
605 and the uncertainty on WZ + charm is $\mu = 1.00 \pm 0.12(\text{stat}) \pm 0.13(\text{sys})$. This is compared to
606 combined uncertainty of $\mu = 1.00^{+0.32}_{-0.30}(\text{stat})^{+0.24}_{-23}(\text{sys})$ for WZ + b when 1-jet and 2-jet events
607 are measured separately and then combined.

608 A post-fit summary plot of the fit regions is shown in Figure 4:

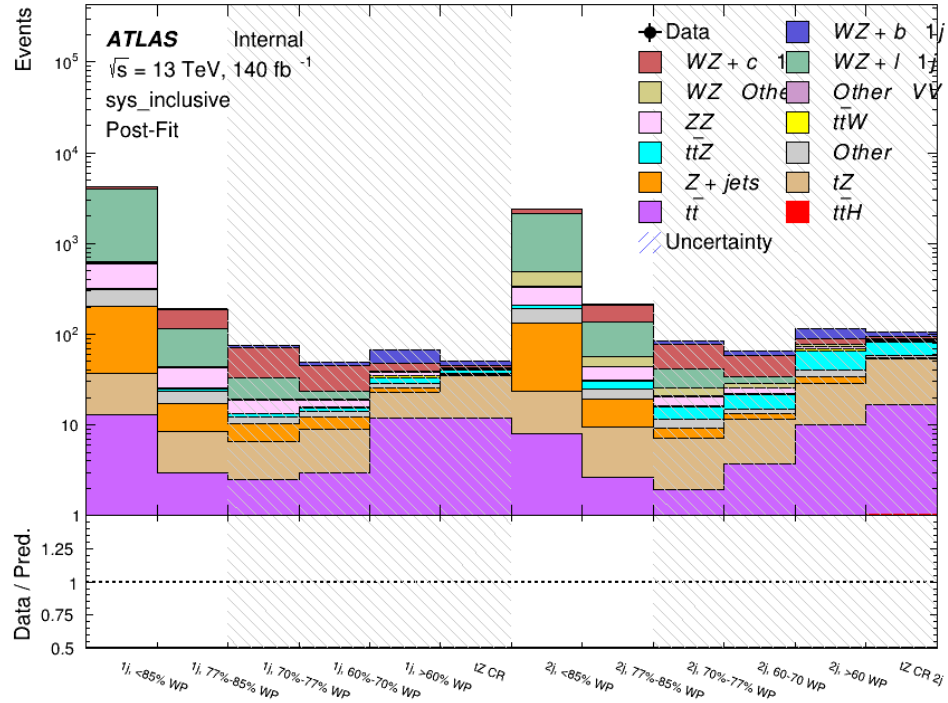


Figure 38: Post-fit summary of the 1-jet fit regions.

609 The impact of the most significant sources of systematic uncertainties on the measurement of
 610 WZ+b is summarized in Table 11.

Uncertainty Source	$\Delta\mu$	
WZ + light cross-section	0.13	-0.12
WZ + charm cross-section	-0.10	0.12
Jet Energy Scale	0.08	0.13
tZ cross-section	-0.10	0.10
Jet Energy Resolution	-0.10	0.10
Luminosity	-0.08	0.09
Other Diboson + b cross-section	-0.07	0.07
Flavor tagging	0.05	0.05
t̄t cross-section	-0.05	0.05
WZ cross-section - QCD scale	-0.04	0.03
Total Systematic Uncertainty	0.28	0.32

Table 23: Summary of the most significant sources of systematic uncertainty on the measurement of WZ + b with one or two associated jets.

₆₁₁ The ranking and impact of those nuisance parameters with the largest contribution to the overall
₆₁₂ uncertainty is shown in Figure ??.

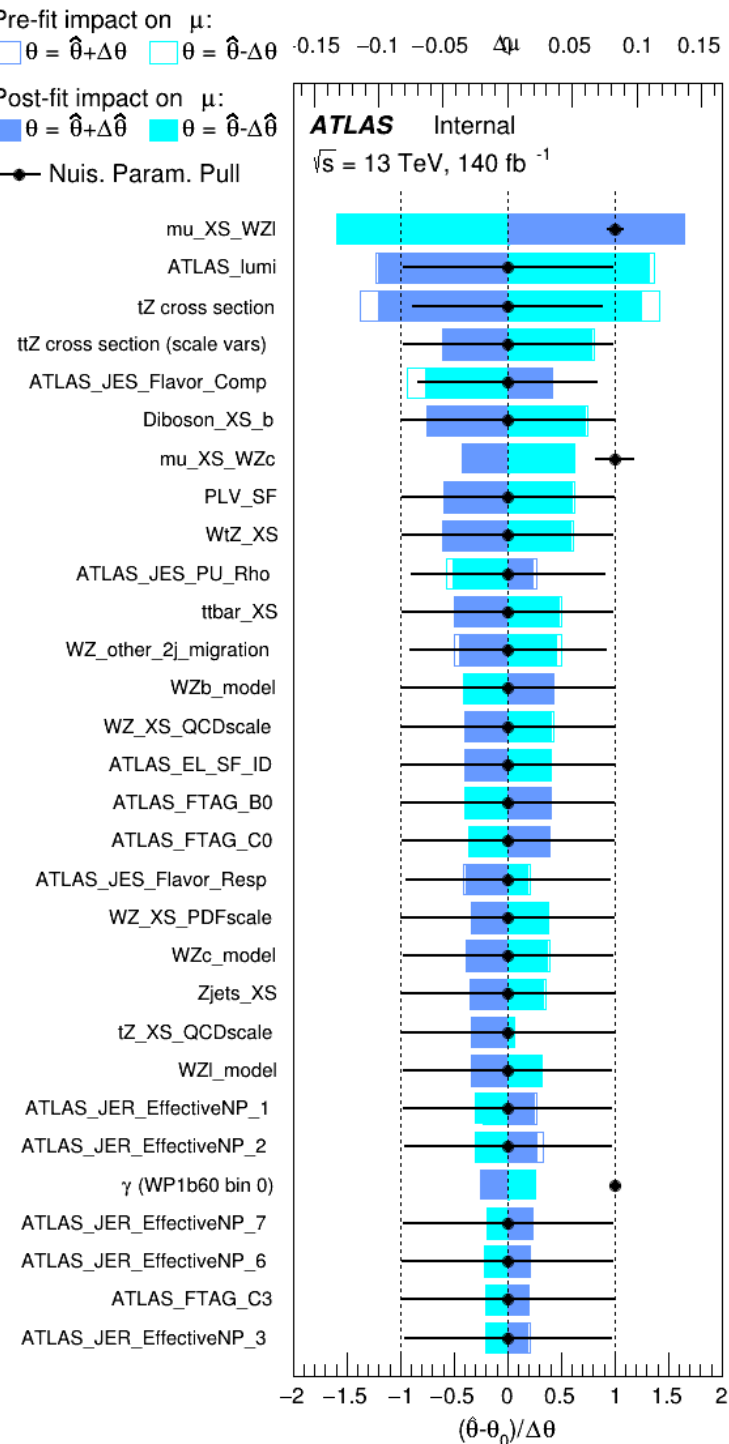


Figure 39: Impact of systematic uncertainties on the signal-strength of $WZ + b$ for events with one or two jets

613 **8.4 Alternate tZ Inclusive Fit**

614 **8.4.1 tZ Inclusive Fit**

615 While tZ is often considered as a distinct process from WZ + b, this could also be considered part
 616 of the signal. Alternate studies are performed where, using the same framework as the nominal
 617 analysis, a measurement of WZ + b is performed that includes tZ as part of WZ+b.

618 Because of this change, the tZ CR is no longer necessary, and only the five pseudo-continuous
 619 b-tag regions are used in the fit. Further, systematics related to the tZ cross-section are removed
 620 from the fit, as they are now encompassed by the normalization measurement of WZ + b. All
 621 other systematic uncertainties are carried over from the nominal analysis.

622 An expected WZ + b cross-section of $4.1^{+0.78}_{-0.74}(\text{stat})^{+0.53}_{-0.52}(\text{sys}) \text{ fb}$ is extracted from the fit, with
 623 an expected significance of 4.0σ .

624 The impact of the predominate systematics are summarized in Table 12.

Uncertainty Source	$\Delta\mu$	
WZ + light cross-section	0.08	-0.08
Jet Energy Scale	-0.06	0.08
Luminosity	-0.05	0.06
WZ + charm cross-section	-0.04	0.05
Other Diboson + b cross-section	-0.04	0.04
WZ cross-section - QCD scale	-0.04	0.03
t̄t cross-section	-0.03	0.03
Jet Energy Resolution	-0.03	0.03
Flavor tagging	-0.03	0.03
Z+jets cross section	-0.02	0.02
Total Systematic Uncertainty	-0.15	0.16

Table 24: Summary of the most significant sources of systematic uncertainty on the measurement of WZ + b with exactly one associated jet.

625 **8.4.2 Floating tZ**

626 In order to quantify the impact of the tZ uncertainty on the fit, an alternative fit strategy is
 627 used where the tZ normalization is allowed to float. This normalization factor replaces the
 628 cross-section uncertainty on tZ, and all other parameters of the fit remain the same.

629 An uncertainty of 17% on the normalization of tZ is extracted from the fit, compared to a theory
 630 uncertainty of 15% applied to the tZ cross-section. The measured uncertainties on WZ remain
 631 the same.

632 9 Conclusion

633 A measurement of WZ + heavy flavor is performed using 140 fb^{-1} of $\sqrt{s} = 13 \text{ TeV}$ proton-
 634 proton collision data collected by the ATLAS detector at the LHC. The expected cross-section
 635 of WZ+b with 1-jet is $1.74^{+0.82}_{-0.75}(\text{stat})^{+0.53}_{-0.48}(\text{sys}) \text{ fb}$, and $14.6 \pm 2.5(\text{stat}) \pm 2.3(\text{sys}) \text{ fb}$ for WZ
 636 + charm, with a correlation of -0.22 between them. An expected significance of 2.0 is observed
 637 for WZ + b in this region.

638 For the 2-jet regions, an expected significance of 1.7 is observed for WZ + b, with an ex-
 639 pected cross-section of $2.5^{+1.3}_{-1.3}(\text{stat})^{+0.95}_{-0.83}(\text{sys}) \text{ fb}$. For WZ + charm, a cross-section of
 640 $12.7 \pm 3.2(\text{stat}) \pm 2.7(\text{sys}) \text{ fb}$ is expected for 2-jet events. A correlation of -0.26 is observed
 641 for WZ+b and WZ + charm.

642 **This section will be include final results once unblinded.**

643 References

- 644 [1] ATLAS Collaboration. ‘Observation of electroweak $W^\pm Z$ boson pair production in asso-
 645 ciation with two jets in pp collisions at $\sqrt{s} = 13 \text{ TeV}$ with the ATLAS detector’. In: *Phys.*
 646 *Lett.* B793 (2019), pp. 469–492. doi: [10.1016/j.physletb.2019.05.012](https://doi.org/10.1016/j.physletb.2019.05.012). arXiv:
 647 [1812.09740 \[hep-ex\]](https://arxiv.org/abs/1812.09740).
- 648 [2] ATLAS Collaboration. ‘Luminosity determination in pp collisions at $\sqrt{s} = 7 \text{ TeV}$ using
 649 the ATLAS detector at the LHC’. In: *Eur. Phys. J. C* 71 (2011), p. 1630. doi: [10.1140/epjc/s10052-011-1630-5](https://doi.org/10.1140/epjc/s10052-011-1630-5). arXiv: [1101.2185 \[hep-ex\]](https://arxiv.org/abs/1101.2185).
- 651 [3] ATLAS Collaboration. ‘Performance of the ATLAS detector using first collision data’. In:
 652 *JHEP* 09 (2010), p. 056. doi: [10.1007/JHEP09\(2010\)056](https://doi.org/10.1007/JHEP09(2010)056). arXiv: [1005.5254 \[hep-ex\]](https://arxiv.org/abs/1005.5254).
- 654 [4] S. Agostinelli et al. ‘GEANT4: A Simulation toolkit’. In: *Nucl. Instrum. Meth.* A506
 655 (2003), pp. 250–303. doi: [10.1016/S0168-9002\(03\)01368-8](https://doi.org/10.1016/S0168-9002(03)01368-8).
- 656 [5] T. Gleisberg et al. ‘Event generation with SHERPA 1.1’. In: *JHEP* 02 (2009), p. 007. doi:
 657 [10.1088/1126-6708/2009/02/007](https://doi.org/10.1088/1126-6708/2009/02/007). arXiv: [0811.4622 \[hep-ph\]](https://arxiv.org/abs/0811.4622).
- 658 [6] H.-L. Lai et al. ‘New parton distributions for collider physics’. In: *Phys. Rev. D* 82 (2010),
 659 p. 074024. doi: [10.1103/PhysRevD.82.074024](https://doi.org/10.1103/PhysRevD.82.074024). arXiv: [1007.2241 \[hep-ph\]](https://arxiv.org/abs/1007.2241).
- 660 [7] J. Alwall et al. ‘The automated computation of tree-level and next-to-leading order dif-
 661 ferential cross sections, and their matching to parton shower simulations’. In: *JHEP* 07
 662 (2014), p. 079. doi: [10.1007/JHEP07\(2014\)079](https://doi.org/10.1007/JHEP07(2014)079). arXiv: [1405.0301 \[hep-ph\]](https://arxiv.org/abs/1405.0301).
- 663 [8] R. D. Ball et al. ‘Parton distributions for the LHC Run II’. In: *JHEP* 04 (2015), p. 040.
 664 doi: [10.1007/JHEP04\(2015\)040](https://doi.org/10.1007/JHEP04(2015)040). arXiv: [1410.8849 \[hep-ph\]](https://arxiv.org/abs/1410.8849).
- 665 [9] M. Bahr et al. ‘Herwig++ Physics and Manual’. In: *Eur. Phys. J. C* 58 (2008), p. 639. doi:
 666 [10.1140/epjc/s10052-008-0798-9](https://doi.org/10.1140/epjc/s10052-008-0798-9). arXiv: [0803.0883 \[hep-ph\]](https://arxiv.org/abs/0803.0883).

- 667 [10] R. D. Ball et al. ‘Parton distributions with LHC data’. In: *Nucl. Phys. B* 867 (2013), p. 244.
 668 doi: [10.1016/j.nuclphysb.2012.10.003](https://doi.org/10.1016/j.nuclphysb.2012.10.003). arXiv: [1207.1303 \[hep-ph\]](https://arxiv.org/abs/1207.1303).
- 669 [11] S. Frixione, G. Ridolfi and P. Nason. ‘A positive-weight next-to-leading-order Monte Carlo
 670 for heavy flavour hadroproduction’. In: *JHEP* 09 (2007), p. 126. doi: [10.1088/1126-
 671 6708/2007/09/126](https://doi.org/10.1088/1126-6708/2007/09/126). arXiv: [0707.3088 \[hep-ph\]](https://arxiv.org/abs/0707.3088).
- 672 [12] E. Re. ‘Single-top Wt-channel production matched with parton showers using the POWHEG
 673 method’. In: *Eur. Phys. J. C* 71 (2011), p. 1547. doi: [10.1140/epjc/s10052-011-
 674 1547-z](https://doi.org/10.1140/epjc/s10052-011-1547-z). arXiv: [1009.2450 \[hep-ph\]](https://arxiv.org/abs/1009.2450).
- 675 [13] ATLAS Collaboration. *Electron efficiency measurements with the ATLAS detector using
 676 the 2015 LHC proton–proton collision data*. ATLAS-CONF-2016-024. 2016. URL: <https://cds.cern.ch/record/2157687>.
- 678 [14] ATLAS Collaboration. ‘Measurement of the muon reconstruction performance of the
 679 ATLAS detector using 2011 and 2012 LHC proton–proton collision data’. In: *Eur. Phys.
 680 J. C* 74 (2014), p. 3130. doi: [10.1140/epjc/s10052-014-3130-x](https://doi.org/10.1140/epjc/s10052-014-3130-x). arXiv: [1407.3935
 681 \[hep-ex\]](https://arxiv.org/abs/1407.3935).
- 682 [15] R. Narayan et al. *Measurement of the total and differential cross sections of a top-quark-
 683 antiquark pair in association with a W boson in proton-proton collisions at a centre-of-
 684 mass energy of 13 TeV with ATLAS detector at the Large Hadron Collider*. Tech. rep.
 685 ATL-COM-PHYS-2020-217. Geneva: CERN, Mar. 2020. URL: <https://cds.cern.ch/record/2712986>.
- 687 [16] ATLAS Collaboration. *Jet Calibration and Systematic Uncertainties for Jets Reconstruc-
 688 ted in the ATLAS Detector at $\sqrt{s} = 13$ TeV*. ATL-PHYS-PUB-2015-015. 2015. URL:
 689 <https://cds.cern.ch/record/2037613>.
- 690 [17] ATLAS Collaboration. *Selection of jets produced in 13 TeV proton–proton collisions with
 691 the ATLAS detector*. ATLAS-CONF-2015-029. 2015. URL: <https://cds.cern.ch/record/2037702>.
- 693 [18] ATLAS Collaboration. ‘Performance of pile-up mitigation techniques for jets in pp col-
 694 lisions at $\sqrt{s} = 8$ TeV using the ATLAS detector’. In: *Eur. Phys. J. C* 76 (2016), p. 581.
 695 doi: [10.1140/epjc/s10052-016-4395-z](https://doi.org/10.1140/epjc/s10052-016-4395-z). arXiv: [1510.03823 \[hep-ex\]](https://arxiv.org/abs/1510.03823).
- 696 [19] ATLAS Collaboration. ‘Performance of missing transverse momentum reconstruction
 697 with the ATLAS detector using proton–proton collisions at $\sqrt{s} = 13$ TeV’. In: *The
 698 European Physical Journal C* 78.11 (Nov. 2018). ISSN: 1434-6052. doi: [10.1140/epjc/s10052-018-
 700 6288-9](https://doi.org/10.1140/epjc/s10052-018-6288-9). URL: [http://dx.doi.org/10.1140/epjc/s10052-018-
 6288-9](http://dx.doi.org/10.1140/epjc/s10052-018-6288-9).
- 701 [20] 2021. URL: https://twiki.cern.ch/twiki/bin/view/AtlasProtected/BTagCalibrationRecommendationsRelease21#Tools_for_Flavor_Tagging_Calibra.
- 704 [21] ATLAS Collaboration. ‘Measurement of the fiducial and differential cross-section of a top
 705 quark pair in association with a Z boson at 13 TeV with the ATLAS detector’. In: ATL-
 706 COM-PHYS-2019-334 (Apr. 2019). URL: <https://cds.cern.ch/record/2672207>.

- 707 [22] T. Chen and C. Guestrin. ‘XGBoost: A Scalable Tree Boosting System’. In: *Proceedings*
708 *of the 22nd ACM SIGKDD International Conference on Knowledge Discovery and Data*
709 *Mining*. KDD ’16. San Francisco, California, USA: ACM, 2016, pp. 785–794. ISBN: 978-
710 1-4503-4232-2. doi: [10.1145/2939672.2939785](https://doi.acm.org/10.1145/2939672.2939785). URL: <http://doi.acm.org/10.1145/2939672.2939785>.
- 712 [23] ‘Luminosity determination in pp collisions at $\sqrt{s} = 13$ TeV using the ATLAS detector at
713 the LHC’. In: (June 2019).
- 714 [24] ATLAS Collaboration. ‘The new LUCID-2 detector for luminosity measurement and
715 monitoring in ATLAS’. In: *JINST* 13.07 (2018), P07017. doi: [10.1088/1748-0221/13/07/P07017](https://doi.org/10.1088/1748-0221/13/07/P07017).
- 717 [25] ATLAS Collaboration. ‘Jet energy resolution in proton-proton collisions at $\sqrt{s} = 7$ TeV
718 recorded in 2010 with the ATLAS detector’. In: *The European Physical Journal C* 73.3
719 (Mar. 2013), p. 2306. ISSN: 1434-6052. doi: [10.1140/epjc/s10052-013-2306-0](https://doi.org/10.1140/epjc/s10052-013-2306-0).
720 URL: <https://doi.org/10.1140/epjc/s10052-013-2306-0>.
- 721 [26] ATLAS Collaboration. ‘Performance of b -jet identification in the ATLAS experiment’.
722 In: *Journal of Instrumentation* 11.04 (2016), P04008. URL: <http://stacks.iop.org/1748-0221/11/i=04/a=P04008>.
- 724 [27] ATLAS Collaboration. ‘Observation of the associated production of a top quark and a
725 Z boson in pp collisions at $\sqrt{s}= 13$ TeV with the ATLAS detector’. In: *Journal of High*
726 *Energy Physics* 2020.7 (July 2020). ISSN: 1029-8479. doi: [10.1007/jhep07\(2020\)124](https://doi.org/10.1007/jhep07(2020)124).
727 URL: [http://dx.doi.org/10.1007/JHEP07\(2020\)124](http://dx.doi.org/10.1007/JHEP07(2020)124).

728 **A Appendices**

729 **A.1 Non-prompt lepton MVA**

730 A lepton MVA has been developed to better reject non-prompt leptons than standard cut
 731 based selections based upon impact parameter, isolation and PID. The name of this MVA is
 732 `PromptLeptonIso`. The full set of studies and detailed explanation can be found in [15].

733 The decays of W and Z bosons are commonly selected by the identification of one or two electrons
 734 or muons. The negligible lifetimes of these bosons mean that the leptons produced in the decay
 735 originate from the interaction vertex and are thus labelled “prompt”. Analyses using these
 736 light leptons impose strict reconstruction quality, isolation and impact parameter requirements
 737 to remove “fake” leptons. A significant source of the fake light leptons are non-prompt leptons
 738 produced in decays of hadrons that contain bottom (b) or charm (c) quarks. Such hadrons
 739 typically have microscopically significant lifetimes that can be detected experimentally.

740 These non-prompt leptons can also pass the tight selection criteria. In analyses that involve top (t)
 741 quarks, which decay almost exclusively into a W boson and a b quark, non-prompt leptons from
 742 the semileptonic decay of bottom and charm hadrons can be a significant source of background
 743 events. This is particularly the case in the selection of same-sign dilepton and multilepton final
 744 states.

745 The main idea is to identify non-prompt light leptons using lifetime information associated with a
 746 track jet that matches the selected light lepton. This lifetime information is computed using tracks
 747 contained within the jet. Typically, lepton lifetime is determined using the impact parameter of the
 748 track reconstructed by the inner tracking detector which is matched to the reconstructed lepton.
 749 Using additional reconstructed charged particle tracks increases the precision of identifying the
 750 displaced decay vertex of bottom or charm hadrons that produced a non-prompt light lepton.
 751 The MVA also includes information related to the isolation of the lepton to reject non-prompt
 752 leptons.

753 `PromptLeptonIso` is a gradient boosted BDT. The training of the BDT is performed on leptons
 754 selected from the POWHEG+PYTHIA6 non-allhad t̄t MC sample. Eight variables are used to train
 755 the BDT in order to discriminate between prompt and non-prompt leptons. The track jets that
 756 are matched to the non-prompt leptons correspond to jets initiated by b or c quarks, and may
 757 contain a displaced vertex. Consequently, three of the selected variables are used to identify
 758 b-tag jets by standard ATLAS flavour tagging algorithms. Two variables use the relationship
 759 between the track jet and lepton: the ratio of the lepton p_T with respect to the track jet p_T and
 760 ΔR between the lepton and the track jet axis. Finally three additional variables test whether the
 761 reconstructed lepton is isolated: the number of tracks collected by the track jet and the lepton
 762 track and calorimeter isolation variables. Table ?? describes the variables used to train the BDT
 763 algorithm. The choice of input variables has been extensively discussed with Egamma, Muon,
 764 Tracking, and Flavour Tagging CP groups.

765 The output distribution of the BDT is shown in Figure ??.

Variable	Description
N_{track} in track jet	Number of tracks collected by the track jet
$\text{IP2 log}(P_b/P_{\text{light}})$	Log-likelihood ratio between the b and light jet hypotheses with the IP2D algorithm
$\text{IP3 log}(P_b/P_{\text{light}})$	Log-likelihood ratio between the b and light jet hypotheses with the IP3D algorithm
N_{TrkAtVtx} SV + JF	Number of tracks used in the secondary vertex found by the SV1 algorithm in addition to the number of tracks from secondary vertices found by the JetFitter algorithm with at least two tracks
$p_T^{\text{lepton}}/p_T^{\text{track jet}}$	The ratio of the lepton p_T and the track jet p_T
$\Delta R(\text{lepton}, \text{track jet})$	ΔR between the lepton and the track jet axis
$p_T^{\text{VarCone30}}/p_T$	Lepton track isolation, with track collecting radius of $\Delta R < 0.3$
$E_T^{\text{TopoCone30}}/p_T$	Lepton calorimeter isolation, with topological cluster collecting radius of $\Delta R < 0.3$

Table 25: A table of the variables used in the training of `PromptLeptonIso`.

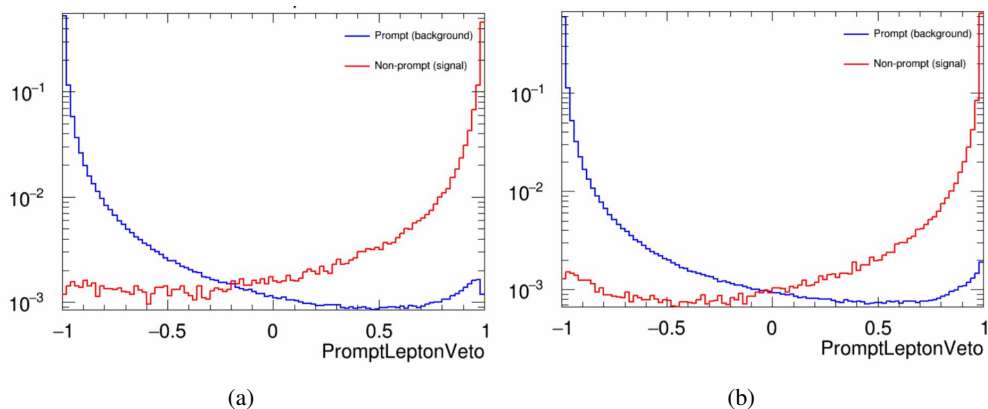


Figure 40: Distribution of the PLV BDT discriminant for (a) electrons and (b) muons

The ROC curve for the BDT response, compared to the standard `FixedCutTight` WP, is shown in figure ??, which shows a clear improvement when using this alternative training.

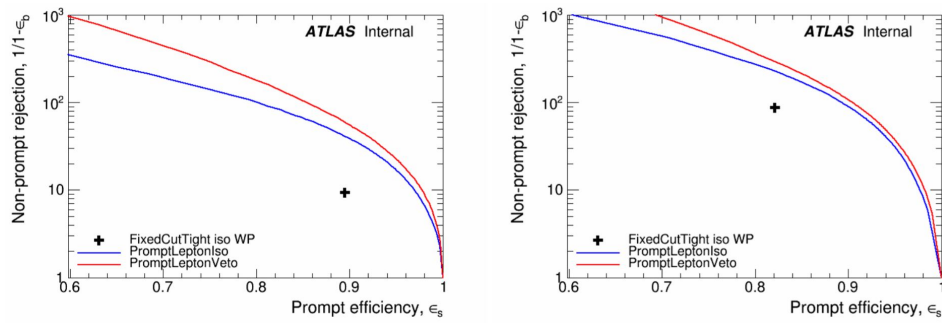


Figure 41: ROC curves for the PLV as well as the performance of the standard FixedCutTight WP for (left) electrons and (right) muons

768 A cutoff value of -0.7 for electrons and -0.5 for muons are chosen as the WPs for this MVA, based
769 on an optimisation of S/\sqrt{B} performed in the preselection regions of the $t\bar{t}H$ – ML analysis,
770 which have a signature similar to that of this analysis.

771 The efficiency of the tight PromptLeptonIso working point is measured using the tag and probe
772 method with $Z \rightarrow \ell^+\ell^-$ events. Such calibration are performed by analysers from this analysis
773 in communication with the Egamma and Muon combined performance groups. The scale factor
774 are approximately 0.92 for $10 < p_T < 15$ GeV, and averaging at 0.98 to 0.99 for higher p_T
775 leptons. An extra systematic is applied to muons within $\Delta R < 0.6$ of a calorimeter jet, since
776 there is a strong dependence on the scale factor due to the presence of these jets. For electrons,
777 the dominant systematics is coming from pile-up dependence. Overall the systematics are a
778 maximum of 3% at low p_T and decreasing at a function of p_T .

779 **A.2 Non-prompt CR Modelling**

780 In order to further validate the modeling in each of the non-prompt CRs, additional kinematic
781 plots are made in the Z+jets CR and $t\bar{t}$ CR in each of the continuous b-tag regions, after the
782 correction factors detailed in Section 7.3 have been applied.

783 In the case of the Z+jets CR, the p_T spectrum of the lepton originating from the W candidate is
784 shown, as this is the distribution used to extract the scale factor applied to Z+jets. These plots
785 are shown in Figures ?? and ??.

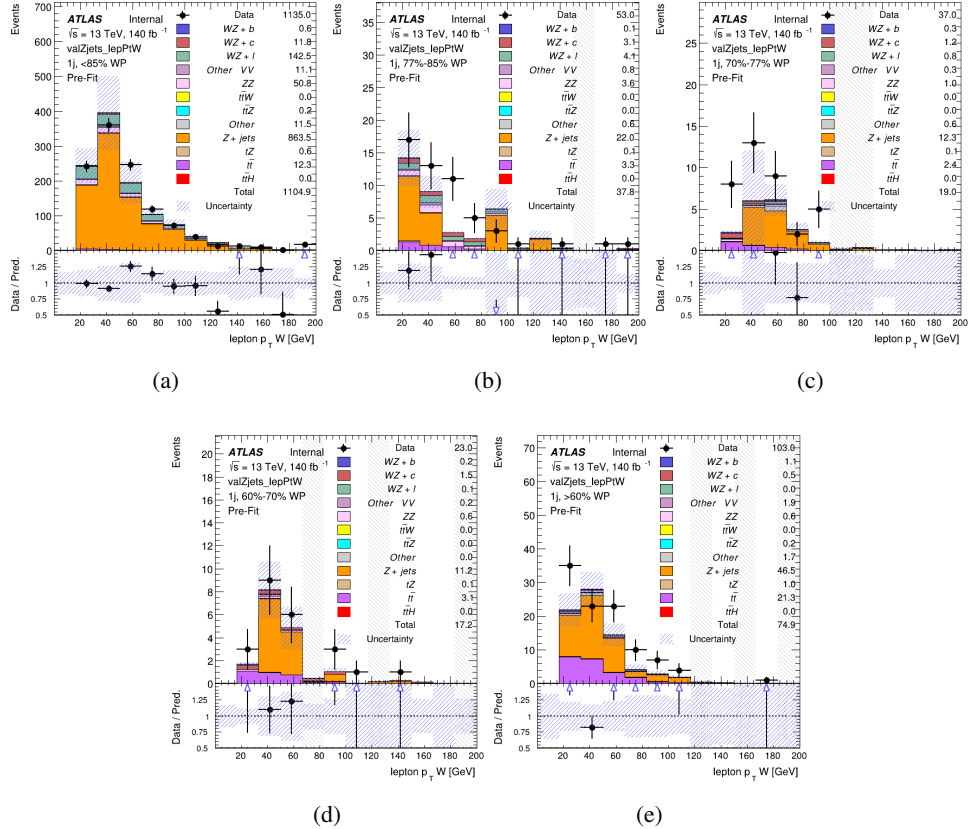


Figure 42: Comparisons between the data and MC distributions of the p_T of the lepton originating from the W-candidate in the Z+jets CR for each of the 1-jet b-tag working point regions

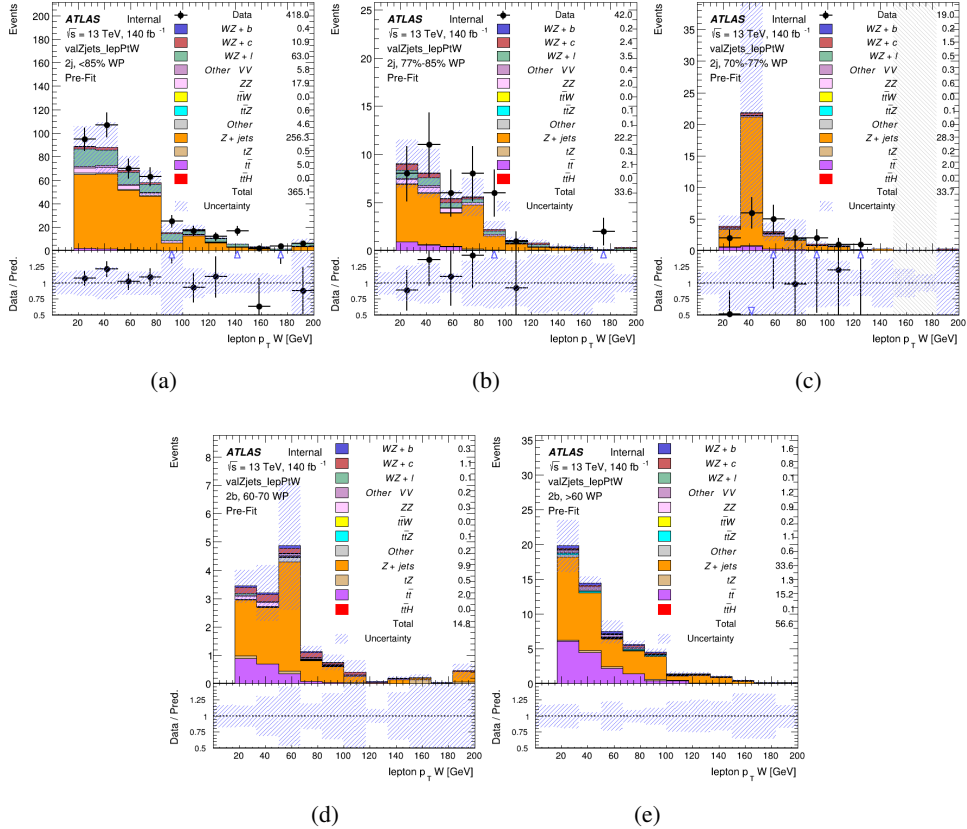


Figure 43: Comparisons between the data and MC distributions of the p_T of the lepton originating from the W-candidate in the Z+jets CR for each of the 2-jet b-tag working point regions

786 The same is shown for the $t\bar{t}$ CR, but the p_T of the OS lepton is used instead as a representation
 787 of the modeling, as the lepton from the W is not well defined for $t\bar{t}$ events. These plots are shown
 788 in Figures ?? and ??.

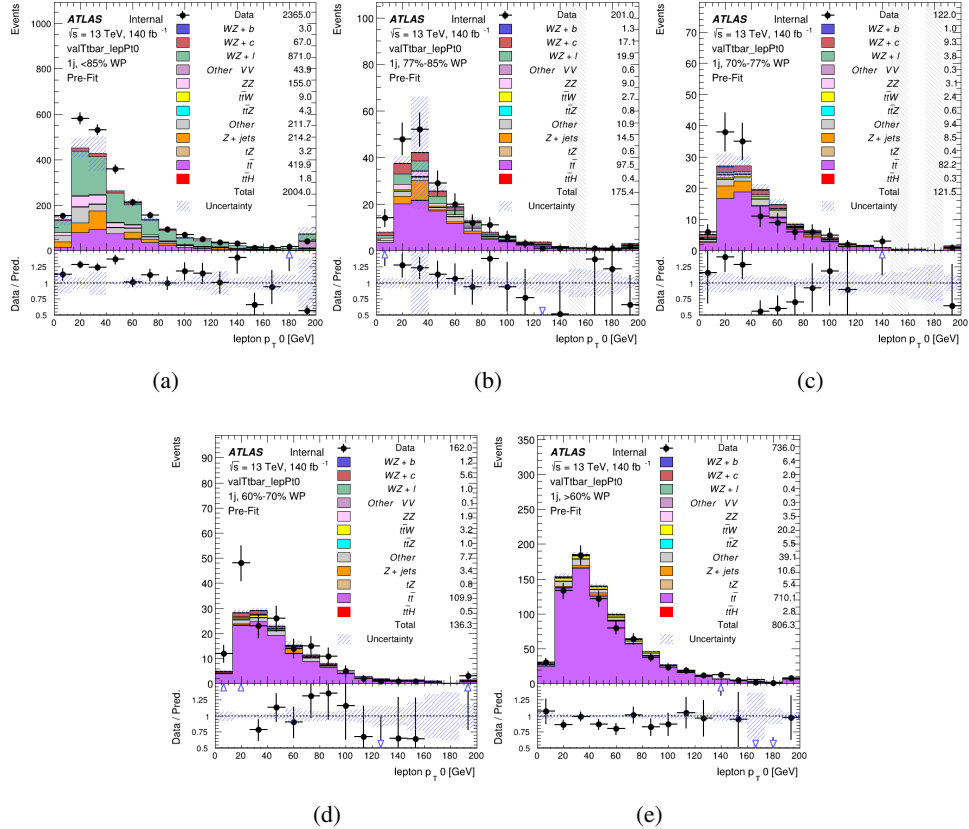


Figure 44: Comparisons between the data and MC distributions of the p_T of the OS lepton in the $t\bar{t}$ CR for each of the 1-jet b-tag working point regions

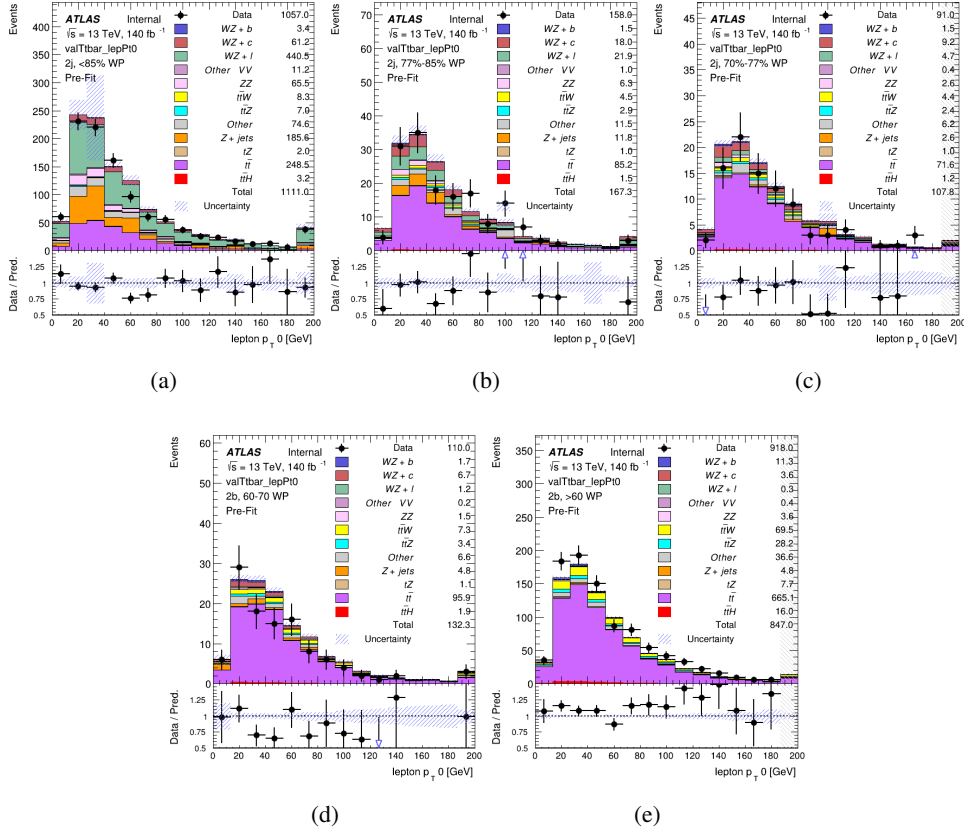


Figure 45: Comparisons between the data and MC distributions of the p_T of the OS lepton in the $t\bar{t}$ CR for each of the 2-jet b-tag working point regions

789 A.3 DSID list

Data:

```
data15_13TeV.AllYear.physics_Main.PhysCont.DAOD_HIGG8D1.grp15_v01_p4134
data16_13TeV.AllYear.physics_Main.PhysCont.DAOD_HIGG8D1.grp16_v01_p4134
data17_13TeV.AllYear.physics_Main.PhysCont.DAOD_HIGG8D1.grp17_v01_p4134
data18_13TeV.AllYear.physics_Main.PhysCont.DAOD_HIGG8D1.grp18_v01_p4134
```

mc16a:

```
mc16_13TeV.361603.PowhegPy8EG_CT10nloME_AZNLOCTEQ6L1_ZZllll_mll4.deriv.DAOD_HIGG8D1.e4475_s3126_r9364_r9315_p4133
mc16_13TeV.361602.PowhegPy8EG_CT10nloME_AZNLOCTEQ6L1_WZlvvv_mll4.deriv.DAOD_HIGG8D1.e4054_s3126_r9364_r9315_p4133
mc16_13TeV.361604.PowhegPy8EG_CT10nloME_AZNLOCTEQ6L1_ZZvvll_mll4.deriv.DAOD_HIGG8D1.e4475_s3126_r9364_r9315_p4133
mc16_13TeV.361600.PowhegPy8EG_CT10nloME_AZNLOCTEQ6L1_WWlvvv.deriv.DAOD_HIGG8D1.e4616_s3126_r9364_r9315_p4133
mc16_13TeV.361605.PowhegPy8EG_CT10nloME_AZNLOCTEQ6L1_ZZvvvv_mll4.deriv.DAOD_HIGG8D1.e4054_s3126_s3136_r9364_r9315_p4133
mc16_13TeV.361601.PowhegPy8EG_CT10nloME_AZNLOCTEQ6L1_WZlvvll_mll4.deriv.DAOD_HIGG8D1.e4475_s3126_r9364_r9315_p4133
mc16_13TeV.364286.Sherpa_222_NNPDF30NNLO_llvvjj_ss_EW4.deriv.DAOD_HIGG8D1.e6055_e5984_s3126_r9364_r9315_p3983 mc16_13TeV.364285.Sherpa_222_NNPDF30NNLO_llvvjj_ss_EW4.deriv.DAOD_HIGG8D1.e6055_e5984_s3126_r9364_r9315_p4133
mc16_13TeV.364740.MGPy8EG_NNPDF30NLO_A14NNPDF23LO_llvlij_EW6_OFPlus.deriv.DAOD_HIGG8D1.e7421_e5984_s3126_r9364_r9315_p4133
mc16_13TeV.364742.MGPy8EG_NNPDF30NLO_A14NNPDF23LO_llvlij_EW6_SFPlus.deriv.DAOD_HIGG8D1.e7421_e5984_s3126_r9364_r9315_p4133
mc16_13TeV.364253.Sherpa_222_NNPDF30NNLO_llvv.deriv.DAOD_HIGG8D1.e5916_s3126_r9364_r9315_p4133
mc16_13TeV.364250.Sherpa_222_NNPDF30NNLO_llll.deriv.DAOD_HIGG8D1.e5894_s3126_r9364_r9315_p4133
mc16_13TeV.364254.Sherpa_222_NNPDF30NNLO_llvv.deriv.DAOD_HIGG8D1.e5916_s3126_r9364_r9315_p4133
```

mc16_13TeV.364255.Sherpa_222_NNPDF30NNLO_lvyy.deriv.DAOD_HIGG8D1.e5916_s3126_r9364_r9315_p4133
 mc16_13TeV.410155.aMcAtNloPythia8EvtGen_MEN30NLO_A14N23LO_ttW.deriv.DAOD_HIGG8D1.e5070_s3126_r9364_r9315_p4133
 mc16_13TeV.410156.aMcAtNloPythia8EvtGen_MEN30NLO_A14N23LO_ttZnuu.deriv.DAOD_HIGG8D1.e5070_s3126_r9364_r9315_p4133
 mc16_13TeV.410157.aMcAtNloPythia8EvtGen_MEN30NLO_A14N23LO_ttZqq.deriv.DAOD_HIGG8D1.e5070_s3126_r9364_r9315_p4133
 mc16_13TeV.410218.aMcAtNloPythia8EvtGen_MEN30NLO_A14N23LO_ttee.deriv.DAOD_HIGG8D1.e5070_s3126_r9364_r9315_p4133
 mc16_13TeV.410219.aMcAtNloPythia8EvtGen_MEN30NLO_A14N23LO_ttmumu.deriv.DAOD_HIGG8D1.e5070_s3126_r9364_r9315_p4133
 mc16_13TeV.410220.aMcAtNloPythia8EvtGen_MEN30NLO_A14N23LO_ttautau.deriv.DAOD_HIGG8D1.e5070_s3126_r9364_r9315_p4133
 mc16_13TeV.412063.aMcAtNloPythia8EvtGen_tllq_NNPDF30_nf4_A4.deriv.DAOD_TOPQ1.e7054_e5984_s3126_r9364_r9315_p4174
 mc16_13TeV.410276.aMcAtNloPythia8EvtGen_MEN30NLO_A14N23LO_ttee_mll_1_5.deriv.DAOD_HIGG8D1.e6087_e5984_s3126_r9364_r9315_p4133
 mc16_13TeV.410277.aMcAtNloPythia8EvtGen_MEN30NLO_A14N23LO_ttmumu_mll_1_5.deriv.DAOD_HIGG8D1.e6087_e5984_s3126_r9364_r9315_p4133
 mc16_13TeV.410278.aMcAtNloPythia8EvtGen_MEN30NLO_A14N23LO_ttautau_mll_1_5.deriv.DAOD_HIGG8D1.e6087_e5984_s3126_r9364_r9315_p4133
 mc16_13TeV.410397.MadGraphPythia8EvtGen_ttbar_wbee_MEN30LO_A14N23LO.deriv.DAOD_HIGG8D1.e6086_e5984_s3126_r9364_r9315_p4133
 mc16_13TeV.410398.MadGraphPythia8EvtGen_ttbar_wbmumu_MEN30LO_A14N23LO.deriv.DAOD_HIGG8D1.e6086_e5984_s3126_r9364_r9315_p4133
 mc16_13TeV.410399.MadGraphPythia8EvtGen_ttbar_wbtautau_MEN30LO_A14N23LO.deriv.DAOD_HIGG8D1.e6086_e5984_s3126_r9364_r9315_p4133
 mc16_13TeV.410658.PhPy8EG_A14_tchan_BW50_lept_top.deriv.DAOD_HIGG8D1.e6671_e5984_s3126_r9364_r9315_p4133
 mc16_13TeV.410659.PhPy8EG_A14_tchan_BW50_lept_antitop.deriv.DAOD_HIGG8D1.e6671_e5984_s3126_r9364_r9315_p4133
 mc16_13TeV.410644.PowhegPythia8EvtGen_A14_singletop_schan_lept_top.deriv.DAOD_HIGG8D1.e6527_e5984_s3126_r9364_r9315_p4133
 mc16_13TeV.410645.PowhegPythia8EvtGen_A14_singletop_schan_lept_antitop.deriv.DAOD_HIGG8D1.e6527_e5984_s3126_r9364_r9315_p4133
 mc16_13TeV.304014.MadGraphPythia8EvtGen_A14NNPDF23_3top_SM.deriv.DAOD_HIGG8D1.e4324_s3126_r9364_r9315_p4133
 mc16_13TeV.410080.MadGraphPythia8EvtGen_A14NNPDF23_4topSM.deriv.DAOD_HIGG8D1.e4111_s3126_r9364_r9315_p4133
 mc16_13TeV.410081.MadGraphPythia8EvtGen_A14NNPDF23_ttbarWW.deriv.DAOD_HIGG8D1.e4111_s3126_r9364_r9315_p4133
 mc16_13TeV.364100.Sherpa_221_NNPDF30NNLO_Zmumu_MAXHTPTV0_70_CVetoBVeto.deriv.DAOD_HIGG8D1.e5271_s3126_r9364_r9315_p4133
 mc16_13TeV.364101.Sherpa_221_NNPDF30NNLO_Zmumu_MAXHTPTV0_70_CFilterBVeto.deriv.DAOD_HIGG8D1.e5271_s3126_r9364_r9315_p4133
 mc16_13TeV.364102.Sherpa_221_NNPDF30NNLO_Zmumu_MAXHTPTV0_70_BFilter.deriv.DAOD_HIGG8D1.e5271_s3126_r9364_r9315_p4133
 mc16_13TeV.364103.Sherpa_221_NNPDF30NNLO_Zmumu_MAXHTPTV70_140_CVetoBVeto.deriv.DAOD_HIGG8D1.e5271_s3126_r9364_r9315_p4133
 mc16_13TeV.364104.Sherpa_221_NNPDF30NNLO_Zmumu_MAXHTPTV70_140_CFilterBVeto.deriv.DAOD_HIGG8D1.e5271_s3126_r9364_r9315_p4133
 mc16_13TeV.364106.Sherpa_221_NNPDF30NNLO_Zmumu_MAXHTPTV140_280_CVetoBVeto.deriv.DAOD_HIGG8D1.e5271_s3126_r9364_r9315_p4133
 mc16_13TeV.364107.Sherpa_221_NNPDF30NNLO_Zmumu_MAXHTPTV140_280_CFilterBVeto.deriv.DAOD_HIGG8D1.e5271_s3126_r9364_r9315_p4133
 mc16_13TeV.364108.Sherpa_221_NNPDF30NNLO_Zmumu_MAXHTPTV140_280_BFilter.deriv.DAOD_HIGG8D1.e5271_s3126_r9364_r9315_p4133
 mc16_13TeV.364109.Sherpa_221_NNPDF30NNLO_Zmumu_MAXHTPTV280_500_CVetoBVeto.deriv.DAOD_HIGG8D1.e5271_s3126_r9364_r9315_p4133
 mc16_13TeV.364110.Sherpa_221_NNPDF30NNLO_Zmumu_MAXHTPTV280_500_CFilterBVeto.deriv.DAOD_HIGG8D1.e5271_s3126_r9364_r9315_p4133
 mc16_13TeV.364111.Sherpa_221_NNPDF30NNLO_Zmumu_MAXHTPTV280_500_BFilter.deriv.DAOD_HIGG8D1.e5271_e5984_s3126_r9364_r9315_p4133
 mc16_13TeV.364111.Sherpa_221_NNPDF30NNLO_Zmumu_MAXHTPTV280_500_BFilter.deriv.DAOD_HIGG8D1.e5271_s3126_r9364_r9315_p4133
 mc16_13TeV.364112.Sherpa_221_NNPDF30NNLO_Zmumu_MAXHTPTV500_1000.deriv.DAOD_HIGG8D1.e5271_s3126_r9364_r9315_p4133
 mc16_13TeV.364113.Sherpa_221_NNPDF30NNLO_Zmumu_MAXHTPTV1000_E_CMS.deriv.DAOD_HIGG8D1.e5271_s3126_r9364_r9315_p4133
 mc16_13TeV.364114.Sherpa_221_NNPDF30NNLO_Zee_MAXHTPTV0_70_CVetoBVeto.deriv.DAOD_HIGG8D1.e5299_s3126_r9364_r9315_p4133
 mc16_13TeV.364115.Sherpa_221_NNPDF30NNLO_Zee_MAXHTPTV0_70_CFilterBVeto.deriv.DAOD_HIGG8D1.e5299_s3126_r9364_r9315_p4133
 mc16_13TeV.364116.Sherpa_221_NNPDF30NNLO_Zee_MAXHTPTV0_70_BFilter.deriv.DAOD_HIGG8D1.e5299_s3126_r9364_r9315_p4133
 mc16_13TeV.364117.Sherpa_221_NNPDF30NNLO_Zee_MAXHTPTV70_140_CVetoBVeto.deriv.DAOD_HIGG8D1.e5299_s3126_r9364_r9315_p4133
 mc16_13TeV.364118.Sherpa_221_NNPDF30NNLO_Zee_MAXHTPTV70_140_CFilterBVeto.deriv.DAOD_HIGG8D1.e5299_s3126_r9364_r9315_p4133
 mc16_13TeV.364119.Sherpa_221_NNPDF30NNLO_Zee_MAXHTPTV70_140_BFilter.deriv.DAOD_HIGG8D1.e5299_s3126_r9364_r9315_p4133
 mc16_13TeV.364120.Sherpa_221_NNPDF30NNLO_Zee_MAXHTPTV140_280_CVetoBVeto.deriv.DAOD_HIGG8D1.e5299_s3126_r9364_r9315_p4133
 mc16_13TeV.364121.Sherpa_221_NNPDF30NNLO_Zee_MAXHTPTV140_280_CFilterBVeto.deriv.DAOD_HIGG8D1.e5299_s3126_r9364_r9315_p4133
 mc16_13TeV.364122.Sherpa_221_NNPDF30NNLO_Zee_MAXHTPTV140_280_BFilter.deriv.DAOD_HIGG8D1.e5299_s3126_r9364_r9315_p4133
 mc16_13TeV.364123.Sherpa_221_NNPDF30NNLO_Zee_MAXHTPTV280_500_CVetoBVeto.deriv.DAOD_HIGG8D1.e5299_s3126_r9364_r9315_p4133
 mc16_13TeV.364124.Sherpa_221_NNPDF30NNLO_Zee_MAXHTPTV280_500_CFilterBVeto.deriv.DAOD_HIGG8D1.e5299_s3126_r9364_r9315_p4133
 mc16_13TeV.364125.Sherpa_221_NNPDF30NNLO_Zee_MAXHTPTV280_500_BFilter.deriv.DAOD_HIGG8D1.e5299_s3126_r9364_r9315_p4133
 mc16_13TeV.364126.Sherpa_221_NNPDF30NNLO_Zee_MAXHTPTV280_500_BFilter.deriv.DAOD_HIGG8D1.e5299_s3126_r9364_r9315_p4133
 mc16_13TeV.364127.Sherpa_221_NNPDF30NNLO_Zee_MAXHTPTV1000_E_CMS.deriv.DAOD_HIGG8D1.e5299_s3126_r9364_r9315_p4133
 mc16_13TeV.364128.Sherpa_221_NNPDF30NNLO_Ztautau_MAXHTPTV0_70_CVetoBVeto.deriv.DAOD_HIGG8D1.e5307_s3126_r9364_r9315_p4133
 mc16_13TeV.364129.Sherpa_221_NNPDF30NNLO_Ztautau_MAXHTPTV0_70_CFilterBVeto.deriv.DAOD_HIGG8D1.e5307_s3126_r9364_r9315_p4133
 mc16_13TeV.364130.Sherpa_221_NNPDF30NNLO_Ztautau_MAXHTPTV0_70_BFilter.deriv.DAOD_HIGG8D1.e5307_s3126_r9364_r9315_p4133
 mc16_13TeV.364131.Sherpa_221_NNPDF30NNLO_Ztautau_MAXHTPTV70_140_CVetoBVeto.deriv.DAOD_HIGG8D1.e5307_s3126_r9364_r9315_p4133
 mc16_13TeV.364132.Sherpa_221_NNPDF30NNLO_Ztautau_MAXHTPTV70_140_CFilterBVeto.deriv.DAOD_HIGG8D1.e5307_s3126_r9364_r9315_p4133
 mc16_13TeV.364133.Sherpa_221_NNPDF30NNLO_Ztautau_MAXHTPTV70_140_BFilter.deriv.DAOD_HIGG8D1.e5307_s3126_r9364_r9315_p4133
 mc16_13TeV.364134.Sherpa_221_NNPDF30NNLO_Ztautau_MAXHTPTV140_280_CVetoBVeto.deriv.DAOD_HIGG8D1.e5307_s3126_r9364_r9315_p4133
 mc16_13TeV.364135.Sherpa_221_NNPDF30NNLO_Ztautau_MAXHTPTV140_280_CFilterBVeto.deriv.DAOD_HIGG8D1.e5307_s3126_r9364_r9315_p4133
 mc16_13TeV.364136.Sherpa_221_NNPDF30NNLO_Ztautau_MAXHTPTV140_280_BFilter.deriv.DAOD_HIGG8D1.e5307_s3126_r9364_r9315_p4133
 mc16_13TeV.364137.Sherpa_221_NNPDF30NNLO_Ztautau_MAXHTPTV280_500_CVetoBVeto.deriv.DAOD_HIGG8D1.e5307_e5984_s3126_r9364_r9315_p4133
 mc16_13TeV.364138.Sherpa_221_NNPDF30NNLO_Ztautau_MAXHTPTV280_500_CFilterBVeto.deriv.DAOD_HIGG8D1.e5313_s3126_r9364_r9315_p4133

mc16_13TeV.364189.Sherpa_221_NNPDF30NNLO_Wtaunu_MAXHTPTV70_140_BFilter.deriv.DAOD_HIGG8D1.e5340_s3126_r9364_r9315_p4133
 mc16_13TeV.364190.Sherpa_221_NNPDF30NNLO_Wtaunu_MAXHTPTV140_280_CVetoBVeto.deriv.DAOD_HIGG8D1.e5340_e5984_s3126_r9364_r9315_p4133
 mc16_13TeV.364190.Sherpa_221_NNPDF30NNLO_Wtaunu_MAXHTPTV140_280_CVetoBVeto.deriv.DAOD_HIGG8D1.e5340_s3126_r9364_r9315_p4133
 mc16_13TeV.364191.Sherpa_221_NNPDF30NNLO_Wtaunu_MAXHTPTV140_280_CFilterBVeto.deriv.DAOD_HIGG8D1.e5340_s3126_r9364_r9315_p4133
 mc16_13TeV.364191.Sherpa_221_NNPDF30NNLO_Wtaunu_MAXHTPTV140_280_CFilterBVeto.deriv.DAOD_HIGG8D1.e5340_e5984_s3126_s3136_r9364_r9315_p4133
 mc16_13TeV.364192.Sherpa_221_NNPDF30NNLO_Wtaunu_MAXHTPTV140_280_BFilter.deriv.DAOD_HIGG8D1.e5340_s3126_r9364_r9315_p4133
 mc16_13TeV.364193.Sherpa_221_NNPDF30NNLO_Wtaunu_MAXHTPTV280_500_CVetoBVeto.deriv.DAOD_HIGG8D1.e5340_s3126_r9364_r9315_p4133
 mc16_13TeV.364193.Sherpa_221_NNPDF30NNLO_Wtaunu_MAXHTPTV280_500_CVetoBVeto.deriv.DAOD_HIGG8D1.e5340_e5984_s3126_s3136_r9364_r9315_p4133
 mc16_13TeV.364194.Sherpa_221_NNPDF30NNLO_Wtaunu_MAXHTPTV280_500_CFilterBVeto.deriv.DAOD_HIGG8D1.e5340_s3126_r9364_r9315_p4133
 mc16_13TeV.364194.Sherpa_221_NNPDF30NNLO_Wtaunu_MAXHTPTV280_500_CFilterBVeto.deriv.DAOD_HIGG8D1.e5340_e5984_s3126_s3136_r9364_r9315_p4133
 mc16_13TeV.364195.Sherpa_221_NNPDF30NNLO_Wtaunu_MAXHTPTV280_500_BFilter.deriv.DAOD_HIGG8D1.e5340_s3126_r9364_r9315_p4133
 mc16_13TeV.364196.Sherpa_221_NNPDF30NNLO_Wtaunu_MAXHTPTV500_1000.deriv.DAOD_HIGG8D1.e5340_s3126_r9364_r9315_p4133
 mc16_13TeV.364197.Sherpa_221_NNPDF30NNLO_Wtaunu_MAXHTPTV1000_E_CMS.deriv.DAOD_HIGG8D1.e5340_s3126_r9364_r9315_p4133
 mc16_13TeV.364500.Sherpa_222_NNPDF30NNLO_eegamma_pty_7_15.deriv.DAOD_HIGG8D1.e5928_e5984_s3126_r9364_r9315_p4133
 mc16_13TeV.364501.Sherpa_222_NNPDF30NNLO_eegamma_pty_15_35.deriv.DAOD_HIGG8D1.e5928_e5984_s3126_r9364_r9315_p4133
 mc16_13TeV.364502.Sherpa_222_NNPDF30NNLO_eegamma_pty_35_70.deriv.DAOD_HIGG8D1.e5928_e5984_s3126_r9364_r9315_p4133
 mc16_13TeV.364503.Sherpa_222_NNPDF30NNLO_eegamma_pty_70_140.deriv.DAOD_HIGG8D1.e5928_e5984_s3126_r9364_r9315_p4133
 mc16_13TeV.364504.Sherpa_222_NNPDF30NNLO_eegamma_pty_140_E_CMS.deriv.DAOD_HIGG8D1.e5928_e5984_s3126_r9364_r9315_p4133
 mc16_13TeV.364505.Sherpa_222_NNPDF30NNLO_mumugamma_pty_7_15.deriv.DAOD_HIGG8D1.e5928_e5984_s3126_r9364_r9315_p4133
 mc16_13TeV.364506.Sherpa_222_NNPDF30NNLO_mumugamma_pty_15_35.deriv.DAOD_HIGG8D1.e5988_e5984_s3126_r9364_r9315_p4133
 mc16_13TeV.364507.Sherpa_222_NNPDF30NNLO_mumugamma_pty_35_70.deriv.DAOD_HIGG8D1.e5928_e5984_s3126_r9364_r9315_p4133
 mc16_13TeV.364508.Sherpa_222_NNPDF30NNLO_mumugamma_pty_70_140.deriv.DAOD_HIGG8D1.e5928_e5984_s3126_r9364_r9315_p4133
 mc16_13TeV.364509.Sherpa_222_NNPDF30NNLO_mumugamma_pty_140_E_CMS.deriv.DAOD_HIGG8D1.e5928_e5984_s3126_r9364_r9315_p4133
 mc16_13TeV.364510.Sherpa_222_NNPDF30NNLO_tautaugamma_pty_7_15.deriv.DAOD_HIGG8D1.e5928_s3126_r9364_r9315_p4133
 mc16_13TeV.364511.Sherpa_222_NNPDF30NNLO_tautaugamma_pty_15_35.deriv.DAOD_HIGG8D1.e5928_s3126_r9364_r9315_p4133
 mc16_13TeV.364512.Sherpa_222_NNPDF30NNLO_tautaugamma_pty_35_70.deriv.DAOD_HIGG8D1.e5928_s3126_r9364_r9315_p4133
 mc16_13TeV.364513.Sherpa_222_NNPDF30NNLO_tautaugamma_pty_70_140.deriv.DAOD_HIGG8D1.e5982_s3126_r9364_r9315_p4133
 mc16_13TeV.364514.Sherpa_222_NNPDF30NNLO_tautaugamma_pty_140_E_CMS.deriv.DAOD_HIGG8D1.e5928_s3126_r9364_r9315_p4133
 mc16_13TeV.364521.Sherpa_222_NNPDF30NNLO_enugamma_pty_7_15.deriv.DAOD_HIGG8D1.e5928_s3126_r9364_r9315_p4133
 mc16_13TeV.364522.Sherpa_222_NNPDF30NNLO_enugamma_pty_15_35.deriv.DAOD_HIGG8D1.e5928_s3126_r9364_r9315_p4133
 mc16_13TeV.364523.Sherpa_222_NNPDF30NNLO_enugamma_pty_35_70.deriv.DAOD_HIGG8D1.e5928_s3126_r9364_r9315_p4133
 mc16_13TeV.364524.Sherpa_222_NNPDF30NNLO_enugamma_pty_70_140.deriv.DAOD_HIGG8D1.e5928_s3126_r9364_r9315_p4133
 mc16_13TeV.364525.Sherpa_222_NNPDF30NNLO_enugamma_pty_140_E_CMS.deriv.DAOD_HIGG8D1.e5928_s3126_r9364_r9315_p4133
 mc16_13TeV.364525.Sherpa_222_NNPDF30NNLO_enugamma_pty_140_E_CMS.deriv.DAOD_HIGG8D1.e5928_e5984_s3126_r9364_r9315_p4133
 mc16_13TeV.364526.Sherpa_222_NNPDF30NNLO_munugamma_pty_7_15.deriv.DAOD_HIGG8D1.e5928_s3126_r9364_r9315_p4133
 mc16_13TeV.364527.Sherpa_222_NNPDF30NNLO_munugamma_pty_15_35.deriv.DAOD_HIGG8D1.e5928_s3126_r9364_r9315_p4133
 mc16_13TeV.364528.Sherpa_222_NNPDF30NNLO_munugamma_pty_35_70.deriv.DAOD_HIGG8D1.e5928_s3126_r9364_r9315_p4133
 mc16_13TeV.364529.Sherpa_222_NNPDF30NNLO_munugamma_pty_70_140.deriv.DAOD_HIGG8D1.e5928_s3126_r9364_r9315_p4133
 mc16_13TeV.364530.Sherpa_222_NNPDF30NNLO_munugamma_pty_140_E_CMS.deriv.DAOD_HIGG8D1.e5928_s3126_r9364_r9315_p4133
 mc16_13TeV.364530.Sherpa_222_NNPDF30NNLO_munugamma_pty_140_E_CMS.deriv.DAOD_HIGG8D1.e5928_e5984_s3126_r9364_r9315_p4133
 mc16_13TeV.364531.Sherpa_222_NNPDF30NNLO_taunugamma_pty_7_15.deriv.DAOD_HIGG8D1.e5928_s3126_r9364_r9315_p4133
 mc16_13TeV.364532.Sherpa_222_NNPDF30NNLO_taunugamma_pty_15_35.deriv.DAOD_HIGG8D1.e5928_s3126_r9364_r9315_p4133
 mc16_13TeV.364533.Sherpa_222_NNPDF30NNLO_taunugamma_pty_35_70.deriv.DAOD_HIGG8D1.e5928_s3126_r9364_r9315_p4133
 mc16_13TeV.364534.Sherpa_222_NNPDF30NNLO_taunugamma_pty_70_140.deriv.DAOD_HIGG8D1.e5928_s3126_r9364_r9315_p4133
 mc16_13TeV.364535.Sherpa_222_NNPDF30NNLO_taunugamma_pty_140_E_CMS.deriv.DAOD_HIGG8D1.e5928_s3126_r9364_r9315_p4133
 mc16_13TeV.364535.Sherpa_222_NNPDF30NNLO_taunugamma_pty_140_E_CMS.deriv.DAOD_HIGG8D1.e5928_e5984_s3126_r9364_r9315_p4133
 mc16_13TeV.410560.MadGraphPythia8EvtGen_A14_Z_4fl_tchan_noAllHad.deriv.DAOD_HIGG8D1.e5803_s3126_r9364_r9315_p4133
 mc16_13TeV.410013.PowhegPythiaEvtGen_P2012_Wt_inclusive_top.deriv.DAOD_HIGG8D1.e3753_s3126_r9364_r9315_p4133
 mc16_13TeV.410014.PowhegPythiaEvtGen_P2012_Wt_inclusive_antitop.deriv.DAOD_HIGG8D1.e3753_s3126_r9364_r9315_p4133
 mc16_13TeV.410408.aMcAtNloPythia8EvtGen_tWZ_Tzoll_minDR1.deriv.DAOD_HIGG8D1.e6423_e5984_s3126_r9364_r9315_p4133
 mc16_13TeV.364242.Sherpa_222_NNPDF30NNLO_WWW_31v_EW6.deriv.DAOD_HIGG8D1.e5887_s3126_r9364_r9315_p4133
 mc16_13TeV.364243.Sherpa_222_NNPDF30NNLO_WWW_412v_EW6.deriv.DAOD_HIGG8D1.e5887_s3126_r9364_r9315_p4133
 mc16_13TeV.364244.Sherpa_222_NNPDF30NNLO_WWW_214v_EW6.deriv.DAOD_HIGG8D1.e5887_s3126_r9364_r9315_p4133
 mc16_13TeV.364245.Sherpa_222_NNPDF30NNLO_WZZ_51v_EW6.deriv.DAOD_HIGG8D1.e5887_s3126_r9364_r9315_p4133
 mc16_13TeV.364246.Sherpa_222_NNPDF30NNLO_WZZ_313v_EW6.deriv.DAOD_HIGG8D1.e5887_s3126_r9364_r9315_p4133
 mc16_13TeV.364247.Sherpa_222_NNPDF30NNLO_ZZZ_610v_EW6.deriv.DAOD_HIGG8D1.e5887_s3126_r9364_r9315_p4133
 mc16_13TeV.364248.Sherpa_222_NNPDF30NNLO_ZZZ_412v_EW6.deriv.DAOD_HIGG8D1.e5887_s3126_r9364_r9315_p4133
 mc16_13TeV.364249.Sherpa_222_NNPDF30NNLO_ZZZ_214v_EW6.deriv.DAOD_HIGG8D1.e5887_s3126_r9364_r9315_p4133
 mc16_13TeV.342284.Pythia8EvtGen_A14NNPDF23LO_WH125_inc.deriv.DAOD_HIGG8D1.e4246_s3126_r9364_r9315_p4133
 mc16_13TeV.342285.Pythia8EvtGen_A14NNPDF23LO_ZH125_inc.deriv.DAOD_HIGG8D1.e4246_s3126_r9364_r9315_p4133
 mc16_13TeV.341998.aMcAtNloHppEG_UEEE5_CTEQ6L1_CT10ME_tWH125_gamgam_yt_plus1.deriv.DAOD_HIGG8D1.e4394_e5984_s3126_r9364_r9315_p4133
 mc16_13TeV.410389.MadGraphPythia8EvtGen_A14NNPDF23_ttgamma_nonallhadronic.deriv.DAOD_HIGG8D1.e6155_e5984_s3126_r9364_r9315_p4133

mc16_13TeV.410470.PhPy8EG_A14_ttbar_hdamp258p75_nonallhad.deriv.DAOD_HIGG8D1.e6337_e5984_s3126_r9364_r9315_p4133
 mc16_13TeV.410472.PhPy8EG_A14_ttbar_hdamp258p75_dil.deriv.DAOD_HIGG8D1.e6348_e5984_s3126_r9364_r9315_p4133
 mc16_13TeV.346343.PhPy8EG_A14NNPDF23_NNPDF30ME_ttH125_allhad.deriv.DAOD_HIGG8D1.e7148_e5984_s3126_r9364_r9315_p4133
 mc16_13TeV.346344.PhPy8EG_A14NNPDF23_NNPDF30ME_ttH125_semilep.deriv.DAOD_HIGG8D1.e7148_e5984_s3126_r9364_r9315_p4133
 mc16_13TeV.346345.PhPy8EG_A14NNPDF23_NNPDF30ME_ttH125_dilep.deriv.DAOD_HIGG8D1.e7148_e5984_s3126_r9364_r9315_p4133

 mc16d:
 mc16_13TeV.364253.Sherpa_222_NNPDF30NNLO_lllv.deriv.DAOD_HIGG8D1.e5916_e5984_s3126_r10201_r10210_p4133
 mc16_13TeV.364250.Sherpa_222_NNPDF30NNLO_llll.deriv.DAOD_HIGG8D1.e5894_e5984_s3126_r10201_r10210_p4133
 mc16_13TeV.364254.Sherpa_222_NNPDF30NNLO_llvv.deriv.DAOD_HIGG8D1.e5916_e5984_s3126_r10201_r10210_p4133
 mc16_13TeV.364255.Sherpa_222_NNPDF30NNLO_lvvv.deriv.DAOD_HIGG8D1.e5916_e5984_s3126_r10201_r10210_p4133
 mc16_13TeV.410155.aMcAtNloPythia8EvtGen_MEN30NLO_A14N23LO_ttW.deriv.DAOD_HIGG8D1.e5070_e5984_s3126_r10201_r10210_p4133
 mc16_13TeV.410156.aMcAtNloPythia8EvtGen_MEN30NLO_A14N23LO_ttZnunu.deriv.DAOD_HIGG8D1.e5070_e5984_s3126_r10201_r10210_p4133
 mc16_13TeV.410157.aMcAtNloPythia8EvtGen_MEN30NLO_A14N23LO_ttZqq.deriv.DAOD_HIGG8D1.e5070_e5984_s3126_r10201_r10210_p4133
 mc16_13TeV.410218.aMcAtNloPythia8EvtGen_MEN30NLO_A14N23LO_ttee.deriv.DAOD_HIGG8D1.e5070_e5984_s3126_r10201_r10210_p4133
 mc16_13TeV.410219.aMcAtNloPythia8EvtGen_MEN30NLO_A14N23LO_ttmumu.deriv.DAOD_HIGG8D1.e5070_e5984_s3126_r10201_r10210_p4133
 mc16_13TeV.410220.aMcAtNloPythia8EvtGen_MEN30NLO_A14N23LO_ttautau.deriv.DAOD_HIGG8D1.e5070_e5984_s3126_r10201_r10210_p4133
 mc16_13TeV.410276.aMcAtNloPythia8EvtGen_MEN30NLO_A14N23LO_ttautau_mll_1_5.deriv.DAOD_HIGG8D1.e6087_e5984_s3126_r10201_r10210_p4133
 mc16_13TeV.410277.aMcAtNloPythia8EvtGen_MEN30NLO_A14N23LO_ttautau_mll_1_5.deriv.DAOD_HIGG8D1.e6087_e5984_s3126_r10201_r10210_p4133
 mc16_13TeV.410278.aMcAtNloPythia8EvtGen_MEN30NLO_A14N23LO_ttautau_mll_1_5.deriv.DAOD_HIGG8D1.e6087_e5984_s3126_r10201_r10210_p4133
 mc16_13TeV.410397.MadGraphPythia8EvtGen_ttbar_wbee_MEN30LO_A14N23LO.deriv.DAOD_HIGG8D1.e6086_e5984_s3126_r10201_r10210_p4133
 mc16_13TeV.410398.MadGraphPythia8EvtGen_ttbar_wbmumu_MEN30LO_A14N23LO.deriv.DAOD_HIGG8D1.e6086_e5984_s3126_r10201_r10210_p4133
 mc16_13TeV.410399.MadGraphPythia8EvtGen_ttbar_wbtautau_MEN30LO_A14N23LO.deriv.DAOD_HIGG8D1.e6086_e5984_s3126_r10201_r10210_p4133
 mc16_13TeV.410658.PhPy8EG_A14_tchan_BW50_lept_top.deriv.DAOD_HIGG8D1.e6671_e5984_s3126_r10201_r10210_p4133
 mc16_13TeV.410659.PhPy8EG_A14_tchan_BW50_lept_antitop.deriv.DAOD_HIGG8D1.e6671_e5984_s3126_r10201_r10210_p4133
 mc16_13TeV.410644.PowhegPythia8EvtGen_A14_singleton_schan_lept_top.deriv.DAOD_HIGG8D1.e6527_e5984_s3126_r10201_r10210_p4133
 mc16_13TeV.410645.PowhegPythia8EvtGen_A14_singleton_schan_lept_antitop.deriv.DAOD_HIGG8D1.e6527_s3126_r10201_r10210_p4133
 mc16_13TeV.412063.aMcAtNloPythia8EvtGen_tllq_NNPDF30_nf4_A14.deriv.DAOD_TOPQ1.e7054_e5984_s3126_r10201_r10210_p4174
 mc16_13TeV.304014.MadGraphPythia8EvtGen_A14NNPDF23_3top_SM.deriv.DAOD_HIGG8D1.e4324_e5984_s3126_r10201_r10210_p4133
 mc16_13TeV.410080.MadGraphPythia8EvtGen_A14NNPDF23_4topSM.deriv.DAOD_HIGG8D1.e4111_e5984_s3126_r10201_r10210_p4133
 mc16_13TeV.410081.MadGraphPythia8EvtGen_A14NNPDF23_ttbarWW.deriv.DAOD_HIGG8D1.e4111_e5984_s3126_r10201_r10210_p4133
 mc16_13TeV.364100.Sherpa_221_NNPDF30NNLO_Zmumu_MAXHTPTV0_70_CVetoBVeto.deriv.DAOD_HIGG8D1.e5271_s3126_r10201_r10210_p4133
 mc16_13TeV.364101.Sherpa_221_NNPDF30NNLO_Zmumu_MAXHTPTV0_70_CFilterBVeto.deriv.DAOD_HIGG8D1.e5271_s3126_r10201_r10210_p4133
 mc16_13TeV.364101.Sherpa_221_NNPDF30NNLO_Zmumu_MAXHTPTV0_70_CFilterBVeto.deriv.DAOD_HIGG8D1.e5271_s3126_r10201_r10210_p4133
 mc16_13TeV.364102.Sherpa_221_NNPDF30NNLO_Zmumu_MAXHTPTV0_70_BFilter.deriv.DAOD_HIGG8D1.e5271_s3126_r10201_r10210_p4133
 mc16_13TeV.364103.Sherpa_221_NNPDF30NNLO_Zmumu_MAXHTPTV70_140_CVetoBVeto.deriv.DAOD_HIGG8D1.e5271_s3126_r10201_r10210_p4133
 mc16_13TeV.364104.Sherpa_221_NNPDF30NNLO_Zmumu_MAXHTPTV70_140_CFilterBVeto.deriv.DAOD_HIGG8D1.e5271_s3126_r10201_r10210_p4133
 mc16_13TeV.364106.Sherpa_221_NNPDF30NNLO_Zmumu_MAXHTPTV140_280_CVetoBVeto.deriv.DAOD_HIGG8D1.e5271_s3126_r10201_r10210_p4133
 mc16_13TeV.364107.Sherpa_221_NNPDF30NNLO_Zmumu_MAXHTPTV140_280_CFilterBVeto.deriv.DAOD_HIGG8D1.e5271_s3126_r10201_r10210_p4133
 mc16_13TeV.364108.Sherpa_221_NNPDF30NNLO_Zmumu_MAXHTPTV140_280_BFilter.deriv.DAOD_HIGG8D1.e5271_s3126_r10201_r10210_p4133
 mc16_13TeV.364108.Sherpa_221_NNPDF30NNLO_Zmumu_MAXHTPTV140_280_BFilter.deriv.DAOD_HIGG8D1.e5271_s3126_r10201_r10210_p4133
 mc16_13TeV.364109.Sherpa_221_NNPDF30NNLO_Zmumu_MAXHTPTV280_500_CVetoBVeto.deriv.DAOD_HIGG8D1.e5271_s3126_r10201_r10210_p4133
 mc16_13TeV.364109.Sherpa_221_NNPDF30NNLO_Zmumu_MAXHTPTV280_500_CVetoBVeto.deriv.DAOD_HIGG8D1.e5271_s3126_r10201_r10210_p4133
 mc16_13TeV.364110.Sherpa_221_NNPDF30NNLO_Zmumu_MAXHTPTV280_500_CFilterBVeto.deriv.DAOD_HIGG8D1.e5271_s3126_r10201_r10210_p4133
 mc16_13TeV.364111.Sherpa_221_NNPDF30NNLO_Zmumu_MAXHTPTV280_500_BFilter.deriv.DAOD_HIGG8D1.e5271_s3126_r10201_r10210_p4133
 mc16_13TeV.364112.Sherpa_221_NNPDF30NNLO_Zmumu_MAXHTPTV280_500_BFilter.deriv.DAOD_HIGG8D1.e5271_s3126_r10201_r10210_p4133
 mc16_13TeV.364112.Sherpa_221_NNPDF30NNLO_Zmumu_MAXHTPTV500_1000.deriv.DAOD_HIGG8D1.e5271_s3126_r10201_r10210_p4133
 mc16_13TeV.364113.Sherpa_221_NNPDF30NNLO_Zmumu_MAXHTPTV1000_E_CMS.deriv.DAOD_HIGG8D1.e5271_s3126_r10201_r10210_p4133
 mc16_13TeV.364114.Sherpa_221_NNPDF30NNLO_Zee_MAXHTPTV0_70_CVetoBVeto.deriv.DAOD_HIGG8D1.e5299_s3126_r10201_r10210_p4133
 mc16_13TeV.364115.Sherpa_221_NNPDF30NNLO_Zee_MAXHTPTV0_70_CFilterBVeto.deriv.DAOD_HIGG8D1.e5299_e5984_s3126_r10201_r10210_p4133
 mc16_13TeV.364116.Sherpa_221_NNPDF30NNLO_Zee_MAXHTPTV0_70_BFilter.deriv.DAOD_HIGG8D1.e5299_e5984_s3126_r10201_r10210_p4133
 mc16_13TeV.364117.Sherpa_221_NNPDF30NNLO_Zee_MAXHTPTV70_140_CVetoBVeto.deriv.DAOD_HIGG8D1.e5299_e5984_s3126_r10201_r10210_p4133
 mc16_13TeV.364118.Sherpa_221_NNPDF30NNLO_Zee_MAXHTPTV70_140_CFilterBVeto.deriv.DAOD_HIGG8D1.e5299_e5984_s3126_r10201_r10210_p4133
 mc16_13TeV.364119.Sherpa_221_NNPDF30NNLO_Zee_MAXHTPTV70_140_BFilter.deriv.DAOD_HIGG8D1.e5299_e5984_s3126_r10201_r10210_p4133
 mc16_13TeV.364120.Sherpa_221_NNPDF30NNLO_Zee_MAXHTPTV140_280_CVetoBVeto.deriv.DAOD_HIGG8D1.e5299_e5984_s3126_r10201_r10210_p4133
 mc16_13TeV.364121.Sherpa_221_NNPDF30NNLO_Zee_MAXHTPTV140_280_CFilterBVeto.deriv.DAOD_HIGG8D1.e5299_e5984_s3126_r10201_r10210_p4133
 mc16_13TeV.364122.Sherpa_221_NNPDF30NNLO_Zee_MAXHTPTV140_280_BFilter.deriv.DAOD_HIGG8D1.e5299_e5984_s3126_r10201_r10210_p4133
 mc16_13TeV.364123.Sherpa_221_NNPDF30NNLO_Zee_MAXHTPTV280_500_CVetoBVeto.deriv.DAOD_HIGG8D1.e5299_e5984_s3126_r10201_r10210_p4133
 mc16_13TeV.364124.Sherpa_221_NNPDF30NNLO_Zee_MAXHTPTV280_500_CFilterBVeto.deriv.DAOD_HIGG8D1.e5299_e5984_s3126_r10201_r10210_p4133
 mc16_13TeV.364125.Sherpa_221_NNPDF30NNLO_Zee_MAXHTPTV280_500_BFilter.deriv.DAOD_HIGG8D1.e5299_e5984_s3126_r10201_r10210_p4133
 mc16_13TeV.364126.Sherpa_221_NNPDF30NNLO_Zee_MAXHTPTV500_1000.deriv.DAOD_HIGG8D1.e5299_e5984_s3126_r10201_r10210_p4133

mc16_13TeV.364506.Sherpa_222_NNPDF30NNLO_mumugamma_pty_15_35.deriv.DAOD_HIGG8D1.e5928_e5984_s3126_r10201_r10210_p4133
mc16_13TeV.364507.Sherpa_222_NNPDF30NNLO_mumugamma_pty_35_70.deriv.DAOD_HIGG8D1.e5928_e5984_s3126_r10201_r10210_p4133
mc16_13TeV.364508.Sherpa_222_NNPDF30NNLO_mumugamma_pty_70_140.deriv.DAOD_HIGG8D1.e5928_e5984_s3126_r10201_r10210_p4133
mc16_13TeV.364509.Sherpa_222_NNPDF30NNLO_mumugamma_pty_140_E_CMS.deriv.DAOD_HIGG8D1.e5928_e5984_s3126_r10201_r10210_p4133
mc16_13TeV.364510.Sherpa_222_NNPDF30NNLO_tautaugamma_pty_7_15.deriv.DAOD_HIGG8D1.e5928_e5984_s3126_r10201_r10210_p4133
mc16_13TeV.364511.Sherpa_222_NNPDF30NNLO_tautaugamma_pty_15_35.deriv.DAOD_HIGG8D1.e5928_e5984_s3126_r10201_r10210_p4133
mc16_13TeV.364512.Sherpa_222_NNPDF30NNLO_tautaugamma_pty_35_70.deriv.DAOD_HIGG8D1.e5928_e5984_s3126_r10201_r10210_p4133
mc16_13TeV.364513.Sherpa_222_NNPDF30NNLO_tautaugamma_pty_70_140.deriv.DAOD_HIGG8D1.e5928_e5984_s3126_r10201_r10210_p4133
mc16_13TeV.364513.Sherpa_222_NNPDF30NNLO_tautaugamma_pty_70_140.deriv.DAOD_HIGG8D1.e5928_e5984_s3126_r10201_r10210_p4133
mc16_13TeV.364514.Sherpa_222_NNPDF30NNLO_tautaugamma_pty_140_E_CMS.deriv.DAOD_HIGG8D1.e5928_e5984_s3126_r10201_r10210_p4133
mc16_13TeV.364521.Sherpa_222_NNPDF30NNLO_enugamma_pty_7_15.deriv.DAOD_HIGG8D1.e5928_e5984_s3126_r10201_r10210_p4133
mc16_13TeV.364522.Sherpa_222_NNPDF30NNLO_enugamma_pty_15_35.deriv.DAOD_HIGG8D1.e5928_e5984_s3126_r10201_r10210_p4133
mc16_13TeV.364523.Sherpa_222_NNPDF30NNLO_enugamma_pty_35_70.deriv.DAOD_HIGG8D1.e5928_e5984_s3126_r10201_r10210_p4133
mc16_13TeV.364524.Sherpa_222_NNPDF30NNLO_enugamma_pty_70_140.deriv.DAOD_HIGG8D1.e5928_e5984_s3126_r10201_r10210_p4133
mc16_13TeV.364525.Sherpa_222_NNPDF30NNLO_enugamma_pty_140_E_CMS.deriv.DAOD_HIGG8D1.e5928_e5984_s3126_r10201_r10210_p4133
mc16_13TeV.364526.Sherpa_222_NNPDF30NNLO_munugamma_pty_7_15.deriv.DAOD_HIGG8D1.e5928_e5984_s3126_r10201_r10210_p4133
mc16_13TeV.364527.Sherpa_222_NNPDF30NNLO_munugamma_pty_15_35.deriv.DAOD_HIGG8D1.e5928_e5984_s3126_r10201_r10210_p4133
mc16_13TeV.364528.Sherpa_222_NNPDF30NNLO_munugamma_pty_35_70.deriv.DAOD_HIGG8D1.e5928_e5984_s3126_r10201_r10210_p4133
mc16_13TeV.364529.Sherpa_222_NNPDF30NNLO_munugamma_pty_70_140.deriv.DAOD_HIGG8D1.e5928_e5984_s3126_r10201_r10210_p4133
mc16_13TeV.364530.Sherpa_222_NNPDF30NNLO_munugamma_pty_140_E_CMS.deriv.DAOD_HIGG8D1.e5928_e5984_s3126_r10201_r10210_p4133
mc16_13TeV.364531.Sherpa_222_NNPDF30NNLO_taunugamma_pty_7_15.deriv.DAOD_HIGG8D1.e5928_e5984_s3126_r10201_r10210_p4133
mc16_13TeV.364532.Sherpa_222_NNPDF30NNLO_taunugamma_pty_15_35.deriv.DAOD_HIGG8D1.e5928_e5984_s3126_r10201_r10210_p4133
mc16_13TeV.364533.Sherpa_222_NNPDF30NNLO_taunugamma_pty_35_70.deriv.DAOD_HIGG8D1.e5928_e5984_s3126_r10201_r10210_p4133
mc16_13TeV.364534.Sherpa_222_NNPDF30NNLO_taunugamma_pty_70_140.deriv.DAOD_HIGG8D1.e5928_e5984_s3126_r10201_r10210_p4133
mc16_13TeV.364535.Sherpa_222_NNPDF30NNLO_taunugamma_pty_140_E_CMS.deriv.DAOD_HIGG8D1.e5928_e5984_s3126_r10201_r10210_p4133
mc16_13TeV.410056.MadGraphPythiaEvtGen_A14_iZ_4fl_tchan_noAllHad.deriv.DAOD_HIGG8D1.e5803_e5984_s3126_r10201_r10210_p4133
mc16_13TeV.410013.PowhegPythiaEvtGen_P2012_Wt_inclusive_top.deriv.DAOD_HIGG8D1.e3753_s3126_r10201_r10210_p4133
mc16_13TeV.410014.PowhegPythiaEvtGen_P2012_Wt_inclusive_antitop.deriv.DAOD_HIGG8D1.e3753_s3126_r10201_r10210_p4133
mc16_13TeV.410408.aMcAtNloPythia8EvtGen_tWZ_Ztoll_minDR1.deriv.DAOD_HIGG8D1.e6423_e5984_s3126_r10201_r10210_p4133
mc16_13TeV.364242.Sherpa_222_NNPDF30NNLO_WWW_313v_EW6.deriv.DAOD_HIGG8D1.e5887_e5984_s3126_r10201_r10210_p4133
mc16_13TeV.364243.Sherpa_222_NNPDF30NNLO_WWZ_412v_EW6.deriv.DAOD_HIGG8D1.e5887_e5984_s3126_r10201_r10210_p4133
mc16_13TeV.364244.Sherpa_222_NNPDF30NNLO_WWZ_214v_EW6.deriv.DAOD_HIGG8D1.e5887_e5984_s3126_r10201_r10210_p4133
mc16_13TeV.364245.Sherpa_222_NNPDF30NNLO_WZZ_511v_EW6.deriv.DAOD_HIGG8D1.e5887_e5984_s3126_r10201_r10210_p4133
mc16_13TeV.364246.Sherpa_222_NNPDF30NNLO_WZZ_313v_EW6.deriv.DAOD_HIGG8D1.e5887_e5984_s3126_r10201_r10210_p4133
mc16_13TeV.364247.Sherpa_222_NNPDF30NNLO_ZZZ_610v_EW6.deriv.DAOD_HIGG8D1.e5887_e5984_s3126_r10201_r10210_p4133
mc16_13TeV.364248.Sherpa_222_NNPDF30NNLO_ZZZ_412v_EW6.deriv.DAOD_HIGG8D1.e5887_e5984_s3126_r10201_r10210_p4133
mc16_13TeV.364249.Sherpa_222_NNPDF30NNLO_ZZZ_214v_EW6.deriv.DAOD_HIGG8D1.e5887_e5984_s3126_r10201_r10210_p4133
mc16_13TeV.342284.Pythia8EvtGen_A14NNPDF23LO_WH125_inc.deriv.DAOD_HIGG8D1.e4246_e5984_s3126_r10201_r10210_p4133
mc16_13TeV.342285.Pythia8EvtGen_A14NNPDF23LO_ZH125_inc.deriv.DAOD_HIGG8D1.e4246_e5984_s3126_r10201_r10210_p4133
mc16_13TeV.341998.aMcAtNloHppEG_UEEE5_CTEQ6L1_CT10ME_tWH125_gamgam_yt_plus1.deriv.DAOD_HIGG8D1.e4394_e5984_s3126_r10201_r10210_p4133
mc16_13TeV.410470.PhPy8EG_A14_ttbar_hdamp258p75_nonallhad.deriv.DAOD_HIGG8D1.e6337_e5984_s3126_r10201_r10210_p4133
mc16_13TeV.410472.PhPy8EG_A14_ttbar_hdamp258p75_dil.deriv.DAOD_HIGG8D1.e6348_e5984_s3126_r10201_r10210_p4133
mc16_13TeV.346343.PhPy8EG_A14NNPDF23_NNPDF30ME_ttH125_allhad.deriv.DAOD_HIGG8D1.e7148_e5984_s3126_r10201_r10210_p4133
mc16_13TeV.346344.PhPy8EG_A14NNPDF23_NNPDF30ME_ttH125_semilep.deriv.DAOD_HIGG8D1.e7148_e5984_a875_r10201_r10210_p4133
mc16_13TeV.346345.PhPy8EG_A14NNPDF23_NNPDF30ME_ttH125_dilep.deriv.DAOD_HIGG8D1.e7148_e5984_a875_r10201_r10210_p4133

mc16e:

mc16_13TeV.361605.PowhegPy8EG_CT10nloME_AZNLOCTEQ6L1_ZZvvvv_mll4.deriv.DAOD_HIGG8D1.e4054_e5984_s3126_r10724_r10726_p4133
mc16_13TeV.361602.PowhegPy8EG_CT10nloME_AZNLOCTEQ6L1_WZlvvv_mll4.deriv.DAOD_HIGG8D1.e4054_e5984_s3126_r10724_r10726_p4133
mc16_13TeV.361601.PowhegPy8EG_CT10nloME_AZNLOCTEQ6L1_WZlavl_mll4.deriv.DAOD_HIGG8D1.e4475_e5984_s3126_r10724_r10726_p4133
mc16_13TeV.361600.PowhegPy8EG_CT10nloME_AZNLOCTEQ6L1_WWlvlv.deriv.DAOD_HIGG8D1.e4616_e5984_s3126_r10724_r10726_p4133
mc16_13TeV.361603.PowhegPy8EG_CT10nloME_AZNLOCTEQ6L1_ZZllll_mll4.deriv.DAOD_HIGG8D1.e4475_e5984_s3126_r10724_r10726_p4133
mc16_13TeV.361604.PowhegPy8EG_CT10nloME_AZNLOCTEQ6L1_ZZvvll_mll4.deriv.DAOD_HIGG8D1.e4475_e5984_s3126_r10724_r10726_p4133
mc16_13TeV.364288.Sherpa_222_NNPDF30NNLO_llll_lowMllPtComplement.deriv.DAOD_HIGG8D1.e6096_s3126_r10724_p3983 mc16_13TeV.364287.Sherpa_222_NNPDF30NNLO_llll_lowMllPtComplement.deriv.DAOD_HIGG8D1.e6096_s3126_r10724_p3983
mc16_13TeV.364285.Sherpa_222_NNPDF30NNLO_llvjj_EW6.deriv.DAOD_HIGG8D1.e6055_s3126_r10724_p3983
mc16_13TeV.364284.Sherpa_222_NNPDF30NNLO_llvjj_EW6.deriv.DAOD_HIGG8D1.e6055_s3126_r10724_p3983
mc16_13TeV.364283.Sherpa_222_NNPDF30NNLO_lllijj_EW6.deriv.DAOD_HIGG8D1.e6055_s3126_r10724_p3983
mc16_13TeV.364739.MGPy8EG_NNPDF30NLO_A14NNPDF23LO_lvjlljjEW6_OFMinus.deriv.DAOD_HIGG8D1.e7421_e5984_s3126_r10724_r10726_p4133
mc16_13TeV.364742.MGPy8EG_NNPDF30NLO_A14NNPDF23LO_lvjlljjEW6_SFPlus.deriv.DAOD_HIGG8D1.e7421_e5984_s3126_r10724_r10726_p4133
mc16_13TeV.364740.MGPy8EG_NNPDF30NLO_A14NNPDF23LO_lvjlljjEW6_OFPlus.deriv.DAOD_HIGG8D1.e7421_e5984_s3126_r10724_r10726_p4133
mc16_13TeV.364741.MGPy8EG_NNPDF30NLO_A14NNPDF23LO_lvjlljjEW6_SFMinus.deriv.DAOD_HIGG8D1.e7421_e5984_s3126_r10724_r10726_p4133
mc16_13TeV.364253.Sherpa_222_NNPDF30NNLO_llv.deriv.DAOD_HIGG8D1.e5916_e5984_s3126_r10724_r10726_p4133

mc16_13TeV.364250.Sherpa_222_NNPDF30NNLO_llll.deriv.DAOD_HIGG8D1.e5894_e5984_s3126_r10724_r10726_p4133
 mc16_13TeV.364254.Sherpa_222_NNPDF30NNLO_llvv.deriv.DAOD_HIGG8D1.e5916_e5984_s3126_r10724_r10726_p4133
 mc16_13TeV.364255.Sherpa_222_NNPDF30NNLO_lvvv.deriv.DAOD_HIGG8D1.e5916_e5984_s3126_r10724_r10726_p4133
 mc16_13TeV.410155.aMcAtNloPythia8EvtGen_MEN30NLO_A14N23LO_ttW.deriv.DAOD_HIGG8D1.e5070_e5984_s3126_r10724_r10726_p4133
 mc16_13TeV.410156.aMcAtNloPythia8EvtGen_MEN30NLO_A14N23LO_ttZnunu.deriv.DAOD_HIGG8D1.e5070_e5984_s3126_r10724_r10726_p4133
 mc16_13TeV.410157.aMcAtNloPythia8EvtGen_MEN30NLO_A14N23LO_ttZqq.deriv.DAOD_HIGG8D1.e5070_e5984_s3126_r10724_r10726_p4133
 mc16_13TeV.410218.aMcAtNloPythia8EvtGen_MEN30NLO_A14N23LO_ttee.deriv.DAOD_HIGG8D1.e5070_e5984_s3126_r10724_r10726_p4133
 mc16_13TeV.410219.aMcAtNloPythia8EvtGen_MEN30NLO_A14N23LO_ttmumu.deriv.DAOD_HIGG8D1.e5070_e5984_s3126_r10724_r10726_p4133
 mc16_13TeV.410220.aMcAtNloPythia8EvtGen_MEN30NLO_A14N23LO_ttautau.deriv.DAOD_HIGG8D1.e5070_e5984_s3126_r10724_r10726_p4133
 mc16_13TeV.410276.aMcAtNloPythia8EvtGen_MEN30NLO_A14N23LO_ttee_mll_1_5.deriv.DAOD_HIGG8D1.e6087_e5984_s3126_r10724_r10726_p4133
 mc16_13TeV.410277.aMcAtNloPythia8EvtGen_MEN30NLO_A14N23LO_ttmumu_mll_1_5.deriv.DAOD_HIGG8D1.e6087_e5984_s3126_r10724_r10726_p4133
 mc16_13TeV.410278.aMcAtNloPythia8EvtGen_MEN30NLO_A14N23LO_ttautau_mll_1_5.deriv.DAOD_HIGG8D1.e6087_e5984_s3126_r10724_r10726_p4133
 mc16_13TeV.410397.MadGraphPythia8EvtGen_ttbar_wbee_MEN30NLO_A14N23LO.deriv.DAOD_HIGG8D1.e6086_e5984_s3126_r10724_r10726_p4133
 mc16_13TeV.410398.MadGraphPythia8EvtGen_ttbar_wbmumu_MEN30NLO_A14N23LO.deriv.DAOD_HIGG8D1.e6086_e5984_s3126_r10724_r10726_p4133
 mc16_13TeV.410399.MadGraphPythia8EvtGen_ttbar_wbtautau_MEN30NLO_A14N23LO.deriv.DAOD_HIGG8D1.e6086_e5984_s3126_r10724_r10726_p4133
 mc16_13TeV.410658.PhPy8EG_A14_tchan_BW50_lept_top.deriv.DAOD_HIGG8D1.e6671_e5984_s3126_s3136_r10724_r10726_p4133
 mc16_13TeV.410659.PhPy8EG_A14_tchan_BW50_lept_antitop.deriv.DAOD_HIGG8D1.e6671_e5984_s3126_s3136_r10724_r10726_p4133
 mc16_13TeV.410644.PowhegPythia8EvtGen_A14_singletop_schan_lept_top.deriv.DAOD_HIGG8D1.e6527_e5984_s3126_r10724_r10726_p4133
 mc16_13TeV.410645.PowhegPythia8EvtGen_A14_singletop_schan_lept_antitop.deriv.DAOD_HIGG8D1.e6527_e5984_s3126_r10724_r10726_p4133
 mc16_13TeV.412063.aMcAtNloPythia8EvtGen_tllq_NNPDF30_nf4_A14.deriv.DAOD_TOPQ1.e7054_e5984_s3126_r10724_r10726_p4174
 mc16_13TeV.304014.MadGraphPythia8EvtGen_A14NNPDF23_3top_SM.deriv.DAOD_HIGG8D1.e4324_e5984_s3126_r10724_r10726_p4133
 mc16_13TeV.410080.MadGraphPythia8EvtGen_A14NNPDF23_4topSM.deriv.DAOD_HIGG8D1.e4111_e5984_s3126_r10724_r10726_p4133
 mc16_13TeV.410081.MadGraphPythia8EvtGen_A14NNPDF23_ttbarWW.deriv.DAOD_HIGG8D1.e4111_e5984_s3126_r10724_r10726_p4133
 mc16_13TeV.364100.Sherpa_221_NNPDF30NNLO_Zmumu_MAXHPTV0_70_CVetoBVeto.deriv.DAOD_HIGG8D1.e5271_e5984_s3126_s3136_r10724_r10726_p4133
 mc16_13TeV.364100.Sherpa_221_NNPDF30NNLO_Zmumu_MAXHPTV0_70_CVetoBVeto.deriv.DAOD_HIGG8D1.e5271_e5984_s3126_r10724_r10726_p4133
 mc16_13TeV.364101.Sherpa_221_NNPDF30NNLO_Zmumu_MAXHPTV0_70_CFilterBVeto.deriv.DAOD_HIGG8D1.e5271_e5984_s3126_r10724_r10726_p4133
 mc16_13TeV.364102.Sherpa_221_NNPDF30NNLO_Zmumu_MAXHPTV0_70_BFilter.deriv.DAOD_HIGG8D1.e5271_e5984_s3126_s3136_r10724_r10726_p4133
 mc16_13TeV.364102.Sherpa_221_NNPDF30NNLO_Zmumu_MAXHPTV0_70_BFilter.deriv.DAOD_HIGG8D1.e5271_e5984_s3126_r10724_r10726_p4133
 mc16_13TeV.364103.Sherpa_221_NNPDF30NNLO_Zmumu_MAXHPTV70_140_CVetoBVeto.deriv.DAOD_HIGG8D1.e5271_e5984_s3126_r10724_r10726_p4133
 mc16_13TeV.364103.Sherpa_221_NNPDF30NNLO_Zmumu_MAXHPTV70_140_CVetoBVeto.deriv.DAOD_HIGG8D1.e5271_e5984_s3126_s3136_r10724_r10726_p4133
 mc16_13TeV.364104.Sherpa_221_NNPDF30NNLO_Zmumu_MAXHPTV70_140_CFilterBVeto.deriv.DAOD_HIGG8D1.e5271_e5984_s3126_r10724_r10726_p4133
 mc16_13TeV.364104.Sherpa_221_NNPDF30NNLO_Zmumu_MAXHPTV70_140_CFilterBVeto.deriv.DAOD_HIGG8D1.e5271_e5984_s3126_s3136_r10724_r10726_p4133
 mc16_13TeV.364106.Sherpa_221_NNPDF30NNLO_Zmumu_MAXHPTV140_280_CVetoBVeto.deriv.DAOD_HIGG8D1.e5271_e5984_s3126_s3136_r10724_r10726_p4133
 mc16_13TeV.364106.Sherpa_221_NNPDF30NNLO_Zmumu_MAXHPTV140_280_CVetoBVeto.deriv.DAOD_HIGG8D1.e5271_e5984_s3126_r10724_r10726_p4133
 mc16_13TeV.364107.Sherpa_221_NNPDF30NNLO_Zmumu_MAXHPTV140_280_CFilterBVeto.deriv.DAOD_HIGG8D1.e5271_e5984_s3126_r10724_r10726_p4133
 mc16_13TeV.364107.Sherpa_221_NNPDF30NNLO_Zmumu_MAXHPTV140_280_CFilterBVeto.deriv.DAOD_HIGG8D1.e5271_e5984_s3126_s3136_r10724_r10726_p4133
 mc16_13TeV.364108.Sherpa_221_NNPDF30NNLO_Zmumu_MAXHPTV140_280_BFilter.deriv.DAOD_HIGG8D1.e5271_e5984_s3126_r10724_r10726_p4133
 mc16_13TeV.364109.Sherpa_221_NNPDF30NNLO_Zmumu_MAXHPTV280_500_CVetoBVeto.deriv.DAOD_HIGG8D1.e5271_e5984_s3126_r10724_r10726_p4133
 mc16_13TeV.364110.Sherpa_221_NNPDF30NNLO_Zmumu_MAXHPTV280_500_CFilterBVeto.deriv.DAOD_HIGG8D1.e5271_e5984_s3126_r10724_r10726_p4133
 mc16_13TeV.364110.Sherpa_221_NNPDF30NNLO_Zmumu_MAXHPTV280_500_CFilterBVeto.deriv.DAOD_HIGG8D1.e5271_e5984_s3126_s3136_r10724_r10726_p4133
 mc16_13TeV.364111.Sherpa_221_NNPDF30NNLO_Zmumu_MAXHPTV280_500_BFilter.deriv.DAOD_HIGG8D1.e5271_e5984_s3126_s3136_r10724_r10726_p4133
 mc16_13TeV.364111.Sherpa_221_NNPDF30NNLO_Zmumu_MAXHPTV280_500_BFilter.deriv.DAOD_HIGG8D1.e5271_e5984_s3126_r10724_r10726_p4133
 mc16_13TeV.364112.Sherpa_221_NNPDF30NNLO_Zmumu_MAXHPTV500_1000.deriv.DAOD_HIGG8D1.e5271_e5984_s3126_r10724_r10726_p4133
 mc16_13TeV.364113.Sherpa_221_NNPDF30NNLO_Zmumu_MAXHPTV1000_E_CMS.deriv.DAOD_HIGG8D1.e5271_e5984_s3126_r10724_r10726_p4133
 mc16_13TeV.364113.Sherpa_221_NNPDF30NNLO_Zmumu_MAXHPTV1000_E_CMS.deriv.DAOD_HIGG8D1.e5271_e5984_s3126_s3136_r10724_r10726_p4133
 mc16_13TeV.364114.Sherpa_221_NNPDF30NNLO_Zee_MAXHPTV0_70_CVetoBVeto.deriv.DAOD_HIGG8D1.e5299_e5984_s3126_s3136_r10724_r10726_p4133
 mc16_13TeV.364114.Sherpa_221_NNPDF30NNLO_Zee_MAXHPTV0_70_CVetoBVeto.deriv.DAOD_HIGG8D1.e5299_e5984_s3126_r10724_r10726_p4133
 mc16_13TeV.364115.Sherpa_221_NNPDF30NNLO_Zee_MAXHPTV0_70_CFilterBVeto.deriv.DAOD_HIGG8D1.e5299_e5984_s3126_s3136_r10724_r10726_p4133
 mc16_13TeV.364115.Sherpa_221_NNPDF30NNLO_Zee_MAXHPTV0_70_CFilterBVeto.deriv.DAOD_HIGG8D1.e5299_e5984_s3126_r10724_r10726_p4133
 mc16_13TeV.364116.Sherpa_221_NNPDF30NNLO_Zee_MAXHPTV0_70_BFilter.deriv.DAOD_HIGG8D1.e5299_e5984_s3126_r10724_r10726_p4133
 mc16_13TeV.364117.Sherpa_221_NNPDF30NNLO_Zee_MAXHPTV70_140_CVetoBVeto.deriv.DAOD_HIGG8D1.e5299_e5984_s3126_s3136_r10724_r10726_p4133
 mc16_13TeV.364117.Sherpa_221_NNPDF30NNLO_Zee_MAXHPTV70_140_CVetoBVeto.deriv.DAOD_HIGG8D1.e5299_e5984_s3126_r10724_r10726_p4133
 mc16_13TeV.364118.Sherpa_221_NNPDF30NNLO_Zee_MAXHPTV70_140_CFilterBVeto.deriv.DAOD_HIGG8D1.e5299_e5984_s3126_s3136_r10724_r10726_p4133
 mc16_13TeV.364118.Sherpa_221_NNPDF30NNLO_Zee_MAXHPTV70_140_CFilterBVeto.deriv.DAOD_HIGG8D1.e5299_e5984_s3126_r10724_r10726_p4133
 mc16_13TeV.364119.Sherpa_221_NNPDF30NNLO_Zee_MAXHPTV70_140_BFilter.deriv.DAOD_HIGG8D1.e5299_e5984_s3126_r10724_r10726_p4133
 mc16_13TeV.364120.Sherpa_221_NNPDF30NNLO_Zee_MAXHPTV140_280_CVetoBVeto.deriv.DAOD_HIGG8D1.e5299_e5984_s3126_r10724_r10726_p4133
 mc16_13TeV.364121.Sherpa_221_NNPDF30NNLO_Zee_MAXHPTV140_280_CFilterBVeto.deriv.DAOD_HIGG8D1.e5299_e5984_s3126_r10724_r10726_p4133
 mc16_13TeV.364122.Sherpa_221_NNPDF30NNLO_Zee_MAXHPTV140_280_BFilter.deriv.DAOD_HIGG8D1.e5299_e5984_s3126_s3136_r10724_r10726_p4133
 mc16_13TeV.364122.Sherpa_221_NNPDF30NNLO_Zee_MAXHPTV140_280_BFilter.deriv.DAOD_HIGG8D1.e5299_e5984_s3126_r10724_r10726_p4133
 mc16_13TeV.364123.Sherpa_221_NNPDF30NNLO_Zee_MAXHPTV280_500_CVetoBVeto.deriv.DAOD_HIGG8D1.e5299_e5984_s3126_r10724_r10726_p4133
 mc16_13TeV.364124.Sherpa_221_NNPDF30NNLO_Zee_MAXHPTV280_500_CFilterBVeto.deriv.DAOD_HIGG8D1.e5299_e5984_s3126_r10724_r10726_p4133
 mc16_13TeV.364125.Sherpa_221_NNPDF30NNLO_Zee_MAXHPTV280_500_BFilter.deriv.DAOD_HIGG8D1.e5299_e5984_s3126_s3136_r10724_r10726_p4133

mc16_13TeV.364513.Sherpa_222_NNPDF30NNLO_tautaugamma_pty_70_140.deriv.DAOD_HIGG8D1.e5982_e5984_s3126_r10724_r10726_p4133
 mc16_13TeV.364514.Sherpa_222_NNPDF30NNLO_tautaugamma_pty_140_E_CMS.deriv.DAOD_HIGG8D1.e5928_e5984_s3126_r10724_r10726_p4133
 mc16_13TeV.364522.Sherpa_222_NNPDF30NNLO_enugamma_pty_15_35.deriv.DAOD_HIGG8D1.e5928_e5984_s3126_r10724_r10726_p4133
 mc16_13TeV.364523.Sherpa_222_NNPDF30NNLO_enugamma_pty_35_70.deriv.DAOD_HIGG8D1.e5928_e5984_s3126_r10724_r10726_p4133
 mc16_13TeV.364524.Sherpa_222_NNPDF30NNLO_enugamma_pty_70_140.deriv.DAOD_HIGG8D1.e5928_e5984_s3126_r10724_r10726_p4133
 mc16_13TeV.364525.Sherpa_222_NNPDF30NNLO_enugamma_pty_140_E_CMS.deriv.DAOD_HIGG8D1.e5928_e5984_s3126_r10724_r10726_p4133
 mc16_13TeV.364527.Sherpa_222_NNPDF30NNLO_munugamma_pty_15_35.deriv.DAOD_HIGG8D1.e5928_e5984_s3126_r10724_r10726_p4133
 mc16_13TeV.364528.Sherpa_222_NNPDF30NNLO_munugamma_pty_35_70.deriv.DAOD_HIGG8D1.e5928_e5984_s3126_r10724_r10726_p4133
 mc16_13TeV.364529.Sherpa_222_NNPDF30NNLO_munugamma_pty_70_140.deriv.DAOD_HIGG8D1.e5928_e5984_s3126_r10724_r10726_p4133
 mc16_13TeV.364530.Sherpa_222_NNPDF30NNLO_munugamma_pty_140_E_CMS.deriv.DAOD_HIGG8D1.e5928_e5984_s3126_r10724_r10726_p4133
 mc16_13TeV.364532.Sherpa_222_NNPDF30NNLO_taunugamma_pty_15_35.deriv.DAOD_HIGG8D1.e5928_e5984_s3126_r10724_r10726_p4133
 mc16_13TeV.364533.Sherpa_222_NNPDF30NNLO_taunugamma_pty_35_70.deriv.DAOD_HIGG8D1.e5928_e5984_s3126_r10724_r10726_p4133
 mc16_13TeV.364534.Sherpa_222_NNPDF30NNLO_taunugamma_pty_70_140.deriv.DAOD_HIGG8D1.e5928_e5984_s3126_r10724_r10726_p4133
 mc16_13TeV.364535.Sherpa_222_NNPDF30NNLO_taunugamma_pty_140_E_CMS.deriv.DAOD_HIGG8D1.e5928_e5984_s3126_r10724_r10726_p4133
 mc16_13TeV.410560.MadGraphPythia8EvtGen_A14_tZ_4fl_tchan_noAllHad.deriv.DAOD_HIGG8D1.e5803_e5984_s3126_r10724_r10726_p4133
 mc16_13TeV.410408.aMcAtNloPythia8EvtGen_tWZ_Ztoll_minDR1.deriv.DAOD_HIGG8D1.e6423_e5984_s3126_r10724_r10726_p4133
 mc16_13TeV.364242.Sherpa_222_NNPDF30NNLO_WWW_3l3v_EW6.deriv.DAOD_HIGG8D1.e5887_e5984_s3126_r10724_r10726_p4133
 mc16_13TeV.364243.Sherpa_222_NNPDF30NNLO_WWZ_4l2v_EW6.deriv.DAOD_HIGG8D1.e5887_e5984_s3126_r10724_r10726_p4133
 mc16_13TeV.364244.Sherpa_222_NNPDF30NNLO_WWZ_2l4v_EW6.deriv.DAOD_HIGG8D1.e5887_e5984_s3126_r10724_r10726_p4133
 mc16_13TeV.364245.Sherpa_222_NNPDF30NNLO_WZZ_5l1v_EW6.deriv.DAOD_HIGG8D1.e5887_e5984_s3126_r10724_r10726_p4133
 mc16_13TeV.364246.Sherpa_222_NNPDF30NNLO_WZZ_3l3v_EW6.deriv.DAOD_HIGG8D1.e5887_e5984_s3126_r10724_r10726_p4133
 mc16_13TeV.364247.Sherpa_222_NNPDF30NNLO_ZZZ_6l0v_EW6.deriv.DAOD_HIGG8D1.e5887_e5984_s3126_r10724_r10726_p4133
 mc16_13TeV.364248.Sherpa_222_NNPDF30NNLO_ZZZ_4l2v_EW6.deriv.DAOD_HIGG8D1.e5887_e5984_s3126_r10724_r10726_p4133
 mc16_13TeV.364249.Sherpa_222_NNPDF30NNLO_ZZZ_2l4v_EW6.deriv.DAOD_HIGG8D1.e5887_e5984_s3126_r10724_r10726_p4133
 mc16_13TeV.342284.Pythia8EvtGen_A14NNPDF23LO_WH125_inc.deriv.DAOD_HIGG8D1.e4246_e5984_s3126_r10724_r10726_p4133
 mc16_13TeV.342285.Pythia8EvtGen_A14NNPDF23LO_ZH125_inc.deriv.DAOD_HIGG8D1.e4246_e5984_s3126_r10724_r10726_p4133
 mc16_13TeV.341998.aMcAtNloHppEG_UEEE5_CTEQ6L1_CT10ME_tWH125_gamgam_yt_plus1.deriv.DAOD_HIGG8D1.e4394_e5984_s3126_r10724_r10726_p4133
 mc16_13TeV.410389.MadGraphPythia8EvtGen_A14NNPDF23_ttgamma_nonallhadronic.deriv.DAOD_HIGG8D1.e6155_e5984_s3126_r10724_r10726_p4133
 mc16_13TeV.410470.PhPy8EG_A14_ttbar_hdamp258p75_nonallhad.deriv.DAOD_HIGG8D1.e6337_e5984_s3126_r10724_r10726_p4133
 mc16_13TeV.410472.PhPy8EG_A14_ttbar_hdamp258p75_dil.deriv.DAOD_HIGG8D1.e6348_e5984_s3126_r10724_r10726_p4133
 mc16_13TeV.346343.PhPy8EG_A14NNPDF23_NNPDF30ME_ttH125_allhad.deriv.DAOD_HIGG8D1.e7148_e5984_s3126_r10724_r10726_p4133
 mc16_13TeV.346343.PhPy8EG_A14NNPDF23_NNPDF30ME_ttH125_allhad.deriv.DAOD_HIGG8D1.e7148_e5984_a875_r10724_r10726_p4133
 mc16_13TeV.346344.PhPy8EG_A14NNPDF23_NNPDF30ME_ttH125_semilep.deriv.DAOD_HIGG8D1.e7148_e5984_a875_r10724_r10726_p4133
 mc16_13TeV.346344.PhPy8EG_A14NNPDF23_NNPDF30ME_ttH125_semilep.deriv.DAOD_HIGG8D1.e7148_e5984_s3126_r10724_r10726_p4133
 mc16_13TeV.346345.PhPy8EG_A14NNPDF23_NNPDF30ME_ttH125_dilep.deriv.DAOD_HIGG8D1.e7148_e5984_a875_r10724_r10726_p4133
 mc16_13TeV.346345.PhPy8EG_A14NNPDF23_NNPDF30ME_ttH125_dilep.deriv.DAOD_HIGG8D1.e7148_e5984_s3126_r10724_r10726_p4133